NASA/CR—2016-218485

Relating FTS Catalyst Properties to Performance

Wenping Ma, Venkat Ramana Rao Pendyala, Pei Gao, Thani Jermwongratanachai, Gary Jacobs, and Burtron H. Davis
University of Kentucky, Lexington, Kentucky

June 2016

NASA STI Program . . . in Profile

Since its founding, NASA has been dedicated to the advancement of aeronautics and space science. The NASA Scientific and Technical Information (STI) Program plays a key part in helping NASA maintain this important role.

The NASA STI Program operates under the auspices of the Agency Chief Information Officer. It collects, organizes, provides for archiving, and disseminates NASA's STI. The NASA STI Program provides access to the NASA Technical Report Server—Registered (NTRS Reg) and NASA Technical Report Server—Public (NTRS) thus providing one of the largest collections of aeronautical and space science STI in the world. Results are published in both non-NASA channels and by NASA in the NASA STI Report Series, which includes the following report types:

- TECHNICAL PUBLICATION. Reports of completed research or a major significant phase of research that present the results of NASA programs and include extensive data or theoretical analysis. Includes compilations of significant scientific and technical data and information deemed to be of continuing reference value. NASA counter-part of peer-reviewed formal professional papers, but has less stringent limitations on manuscript length and extent of graphic presentations.

- TECHNICAL MEMORANDUM. Scientific and technical findings that are preliminary or of specialized interest, e.g., "quick-release" reports, working papers, and bibliographies that contain minimal annotation. Does not contain extensive analysis.

- CONTRACTOR REPORT. Scientific and technical findings by NASA-sponsored contractors and grantees.

- CONFERENCE PUBLICATION. Collected papers from scientific and technical conferences, symposia, seminars, or other meetings sponsored or co-sponsored by NASA.

- SPECIAL PUBLICATION. Scientific, technical, or historical information from NASA programs, projects, and missions, often concerned with subjects having substantial public interest.

- TECHNICAL TRANSLATION. English-language translations of foreign scientific and technical material pertinent to NASA's mission.

For more information about the NASA STI program, see the following:

- Access the NASA STI program home page at http://www.sti.nasa.gov

- E-mail your question to help@sti.nasa.gov

- Fax your question to the NASA STI Information Desk at 757-864-6500

- Telephone the NASA STI Information Desk at 757-864-9658

- Write to:
  NASA STI Program
  Mail Stop 148
  NASA Langley Research Center
  Hampton, VA 23681-2199

NASA/CR—2016-218485

Relating FTS Catalyst Properties to Performance

Wenping Ma, Venkat Ramana Rao Pendyala, Pei Gao, Thani Jermwongratanachai, Gary Jacobs, and Burtron H. Davis
University of Kentucky, Lexington, Kentucky

Prepared under Grant NNX11AI75A

National Aeronautics and
Space Administration

Glenn Research Center
Cleveland, Ohio 44135

June 2016

Acknowledgments

CAER work was supported by a NASA grant (Relating FTS catalyst properties to performance No. NNX11AI75A) and by the Commonwealth of Kentucky. Argonne's research was supported in part by the U.S. DOE, Office of Fossil Energy, NETL. The use of the APS was supported by the U.S. DOE, Office of Science, Office of Basic Energy Sciences, under Contract No. DE-AC02-06CH11357. MRCAT operations are supported by the DOE and the MRCAT member institutions. This research was also carried out, in part, at the National Synchroton Light Source, Brookhaven National Laboratory, which is supported by the U.S. DOE, Division of Materials Science and Chemical Science. We are also grateful to the Fulbright-TRF scholarship program for financial support for Mr. Thani Jermwongratanachai.

Available from

NASA STI Program
Mail Stop 148
NASA Langley Research Center
Hampton, VA 23681-2199

National Technical Information Service
5285 Port Royal Road
Springfield, VA 22161
703-605-6000

This report is available in electronic form at http://www.sti.nasa.gov/ and http://ntrs.nasa.gov/

Relating FTS Catalyst Properties to Performance

Wenping Ma, Venkat Ramana Rao Pendyala, Pei Gao,
Thani Jermwongratanachai, Gary Jacobs, and Burtron H. Davis
University of Kentucky
Lexington, Kentucky 40506

Executive Summary

During the reporting period June 23, 2011 to August 31, 2013, CAER researchers carried out research in two areas of fundamental importance to the topic of cobalt-based Fischer-Tropsch Synthesis (FTS): promoters and stability. The first area was research into possible substitute promoters that might be used to replace the expensive promoters (e.g., Pt, Re, and Ru) that are commonly used. To that end, three separate investigations were carried out.

Due to the strong support interaction of γ-Al_2O_3 with cobalt, metal promoters are commonly added to commercial FTS catalysts to facilitate the reduction of cobalt oxides and thereby boost active surface cobalt metal sites. To date, the metal promoters examined have been those up to and including Group 11. Because two Group 11 promoters (i.e., Ag and Au) were identified to exhibit positive impacts on conversion, selectivity, or both, research was undertaken to explore metals in Groups 12 – 14. The three metals selected for this purpose were Cd, In, and Sn. At a higher loading of 25%Co on alumina, 1% addition of Cd, In, or Sn was found to—on average—facilitate reduction by promoting a heterogeneous distribution of cobalt consisting of larger lesser interacting cobalt clusters and smaller strongly interacting cobalt species. The lesser interacting species were identified in TPR profiles, where a sharp low temperature peak occurred for the reduction of larger, weakly interacting, CoO species. In XANES, the Cd, In, and Sn promoters were found to exist as oxides, whereas typical promoters (e.g., Re, Ru, Pt) were previously determined to exist in an metallic state in atomic coordination with cobalt. The larger cobalt clusters significantly decreased the active site density relative to the unpromoted 25%Co/Al_2O_3 catalyst. Decreasing the cobalt loading to 15%Co eliminated the large non-interacting species. The TPR peak for reduction of strongly interacting CoO in the Cd promoted catalyst occurred at a measurably lower temperature than in the unpromoted catalyst. Nevertheless, the Co clusters remained slightly larger, on average, in comparison with the unpromoted 15%Co/Al_2O_3 reference catalyst. None of the promoted catalysts (i.e., with Cd, In, or Sn) exhibited surface Co^0 site densities higher than that of the unpromoted catalyst. In activity testing, the activities were even much lower than what was expected from the H_2-TPD results. Two possible explanations were proposed: (1) the promoters may be located on the surfaces of cobalt particles, blocking surface Co^0 but being able to desorb hydrogen or (2) the promoters may facilitate Co oxidation during FTS, as previously observed by Huffman and coworkers when K was added to cobalt catalysts.

Continuing on the subject of reduction promoters for cobalt catalysts, it was identified in previous work by CAER researchers that Ag addition to Co/alumina catalysts provided significant benefits in terms of both CO conversion and selectivity (i.e., inhibiting light gas selectivity and promoting C_5+ selectivity), while maintaining stability. However, the structure of the catalyst remained unknown and the optimization of Ag promoter level had not been previously investigated. Therefore, to better understand the structure-function relationships, a series of Ag-promoted 25%Co/Al_2O_3 research catalysts and a series of Pt-promoted 25%Co/Al_2O_3 reference catalysts were prepared and the loading of promoter varied. The Ag catalysts were prepared to be atomically equivalent to 0.5, 1, 2, 3, 4, and 5% by weight Pt. Catalysts characterized not only by standard methods (e.g., BET, TPR, hydrogen chemisorption / pulse reoxidation, and XRD), but also by temperature programmed XANES/EXAFS at the Ag K edge and Pt L_3 edges, respectively (conducted at the Advance Photon Source at Argonne National Laboratory at Argonne, Illinois). This research was submitted as a manuscript to Applied Catalysis A in March of 2013, and is already published (Appl. Catal. 264-265 (2013) 165-180). While it is known that Pt in Co/Al_2O_3 catalyst is in intimate contact at the atomic level with cobalt clusters, with Pt-Co bonds being readily observed, this work demonstrates that this holds true even at very high promoter loadings. Ag promoter can also interact with Co to form Ag-Co bond in Ag promoted Co/Al_2O_3

catalysts. However, unlike Pt promoter, Ag promoter also displays coordination to other Ag atoms and a peak for Ag-Ag first shell coordination after complete activation in H_2 is evident. Moreover, the fraction of Ag in coordination with Co decreases as a function of Ag promoter loading, revealing that the interaction of Ag with Co is not as high as in the case of Pt. While either Pt-Co bonds or Ag-Co bonds formed in Co/Al_2O_3 can significantly facilitate the reduction of cobalt oxides, the fundamentally different atomic structure of the Ag promoter relative to Pt plays a different role in product selectivity of the FTS reaction. Pt promoter increases CH_4 and CO_2, at the expense of C_5+. The greater the amount of Pt, the higher the CH_4 and CO_2 selectivities. Interestingly, compared to both Pt promoted and unpromoted catalysts, Ag promoter at all loadings decreases CH_4 and CO_2 and benefits C_5+ selectivity. However, increasing Ag does not improve selectivity but rather worsens it relative to lower loadings, which may be attributed losses in Ag-Co bonding that inhibits excessive hydrogenation and/or WGS.

The final investigation into promoters was to examine how a support modifier—zirconia—influences both the structure (e.g., size, location), reducibility, and in turn, active site densities, of cobalt particles when applied to both narrow (Catalox 150 support) and wide (Puralox HP14/150) γ-alumina supported 25%Co catalysts prepared by slurry impregnation of cobalt. To determine size, chemisorption and XRD methods were applied, whereas pulse reoxidation and TPR were employed to assess the reducibility. Finally, synchrotron methods were used to directly compare differences in local atomic structure (e.g., Co-Co metal and Co-O coordination) by EXAFS, and electronic structure by analyzing the white line intensity in XANES spectroscopy. Both factors figured into the final active site density as determined by chemisorption, and as reflected in the steady state reaction testing data. Zr-doping is a complex subject. The method of preparation, cobalt loading, support type, and support porosity all play key factors in determining whether or not Zr doping improves Co site densities resulting in enhanced catalyst performance. When added to a weakly interacting support like SiO_2, Zr-doping can enhance the support interaction to stabilize a smaller cobalt cluster size. If Zr is added within narrow pore alumina, a strongly interacting support, as we previously observed utilizing the IWI method and lower cobalt loadings, very small strongly interacting cobalt oxides are formed which are difficult to reduce, resulting in lower cobalt site density relative to the unpromoted catalyst.

When the slurry method is used on a narrow pore support, larger cobalt clusters are formed, and the size suggests these are located at the mouth of pores and possibly external to pores. Zr-doping exacerbates this effect. The slightly larger species formed are marginally more reducible, and slight increase in site density results.

However, with wide pore alumina, the effect is very different. The cobalt is situated within pores, and Zr addition slightly narrows the pore to generate smaller, somewhat more interacting cobalt species. Because a significant fraction remains reducible, there is an important increase in the cobalt site density. The result was a catalyst with improved productivity, lower methane selectivity, and higher C_5+ selectivity.

The second topic of importance was catalyst stability. In this area of research, an investigation was carried out with the aim of shedding light on catalyst aging over supported cobalt catalysts as a function of particle size. For example, one question is whether internal pore filling by heavy wax contributes to catalyst deactivation. To that end, a large 2 kg batch of $0.5\%Pt\text{-}25\%Co/Al_2O_3$ was prepared and sieved to four sieving ranges (20 to 63 μm, 63 to 106 μm, 106 to 180 μm, and 180 to 355 μm). With the 3 larger particle size ranges, the catalyst displayed a greater initial decline in CO conversion as a function of catalyst particle size. The result correlates well with the hypothesis that gradual internal filling of the catalyst pores with wax increases diffusional resistances, such that only the exterior (i.e., egg-shell layer) of the catalyst remains active once steady state conversion is achieved. The results for the smallest particle size range remain enigmatic. While it was expected that the smallest particle sizes would essentially be “virtually all egg-shell”, the catalyst consistently displayed a significant slow decline in activity as a function of time on-stream. Additional studies are planned with the aim of understanding this apparent anomaly.

A separate investigation into the issue of catalyst deactivation was also carried out, this time to examine the effect of water partial pressure on the stability of cobalt catalysts as a function of cobalt cluster size. CoO formed at the onset of FTS by oxidation of tiny Co crystallites was proposed as one possible culprit in catalyst deactivation. CoO formation is undesirable because it can contribute to a complex reduction/sintering mechanism as a function of time on-stream, or form difficult-to-reduce cobalt aluminate species by reaction with Al_2O_3. In this work, freshly H_2-

reduced catalyst samples and FTS catalyst samples (i.e., freshly reduced and immediately exposed to the onset of FTS conditions mimicking 50% CO conversion) were prepared for the purpose of comparison. XAS was utilized as an effective tool for investigating the oxidation state of cobalt. A clear trend was obtained that revealed direct experimental evidence in support of the view that tiny cobalt crystallites do indeed undergo oxidation at the onset, and that catalysts should be designed with sizes above this threshold limit.

Contents

1.0 Promoter Study for Cobalt Fischer-Tropsch Synthesis Catalysts

1.1 Investigation Into Group 12 – 14 Metals as Possible Promoters

1.1.1 Experimental

1.1.1.1 Catalyst Preparation

All cobalt catalysts were prepared by either one of two methods—the incipient wetness impregnation (IWI) method or the slurry phase impregnation (SPI) method, for the addition of cobalt (Ref. 1). Note that promoters were always added by IWI after cobalt addition. Note that all catalysts were calcined under flowing UHP air for 4 h at 350 °C. The flow rate was ~250 cc/min for 35 g of cobalt nitrate/alumina. The ramp rate was 1 °C/min. Decomposition products were collected in a sidearm flask for disposal.

Incipient Wetness impregnation (IWI).—In the IWI method, loading solutions containing a precursor salt (e.g., cobalt nitrate) are prepared to just fill the pores of the support, with the pore volume being first determined by the BET method. To achieve loadings of 15 or 25% cobalt by weight, multiple impregnation and drying steps were required, due to the solubility limit of cobalt nitrate in water (Ref. 1).

Slurry Phase impregnation (SPI).—The SPI method differs from the IWI method only in the amount of liquid utilized in the loading solution, which was 2.5 times the pore volume.

1.1.1.1.1 Catalyst Samples

An opportunity arose for CAER researchers to investigate Cd, In, and Sn additives to Co/Al_2O_3 catalysts at Brookhaven National Laboratory for XANES. Thus, the first series prepared consisted of $25\%CoAl_2O_3$ promoted to the 1% by weight level of Cd, In, or Sn. The SPI method was used to add cobalt (Ref. 1). The precursors for the Cd and In catalysts were the corresponding nitrates, while $SnCl_2$ was used to add the Sn. The unpromoted reference catalyst was labeled EXAFS1, while the Cd, In, and Sn promoted were labeled EXAFS2, 3, and 4, respectively. The γ-Al_2O_3 support surface area was 150 m^2/g.

Because the first loading led to heterogeneity in the sample, with a peak developing in TPR corresponding to larger cobalt clusters in addition to those in interaction with the support, a second series using a lower cobalt loading of 15%Co was prepared. The cobalt was again added by the SPI method, while promoters were added in the same manner as carried out previously. The unpromoted reference catalyst was labeled NASA100, while the 1%Cd, 1%In, and 1%Sn promoted samples were labeled NASA101, 102, and 103, respectively. Again, the γ-Al_2O_3 support surface area was 150 m^2/g. The effect of Cd loading was also to be examined at the 1% (NASA101), 2% (NASA111), and 5% (NASA112) levels and catalysts were prepared. An unpromoted $15\%Co/Al_2O_3$ catalyst was also prepared using the SPI method as a reference (NASA110) for that series. However, after preliminary reaction testing results demonstrated no benefit in Cd addition, no characterization or reaction tests are planned for these samples.

The second series did not lead to increases in the active site density, despite increases in extent of cobalt oxide reduction. This was likely due to in part to an increase in average cobalt metal cluster size. Nevertheless, there was interest in possibly using Cd to try to increase the Co cluster size in cases where the clusters are small enough to be deemed unstable. Such a case arises when a noble metal promoter (e.g., Pt, Re, Ru) is added to $15\%Co/Al_2O_3$ catalysts prepared by IWI and whereby the support surface area is higher - 200 m^2/g. So, a third series was prepared where the reference catalysts were $15\%Co/Al_2O_3$ and $0.5\%Pt\text{-}15\%Co/Al_2O_3$ prepared by IWI using 200 m^2/g Al_2O_3. These were labeled NASA106 and NASA104, respectively. Cd was then added to make $0.5\%Pt\text{-}1\%Cd\text{-}15\%Co/Al_2O_3$ (NASA105) and $0.5\%Pt\text{-}3\%Cd\text{-}15\%Co/Al_2O_3$ (NASA115) catalysts in order to (a) determine if a systematic increase in cobalt cluster size occurred and (b) to determine if the increase in cobalt cluster size led to any improvement in catalyst stability during reaction tests. A third reference sample without Pt but containing $1\%Cd\text{-}15\%Co/Al_2O_3$ was also prepared (NASA114).

1.1.1.2 Characterization

1.1.1.2.1 BET Measurements

The surface area, pore volume, and average pore radius of the supports and catalysts were measured by BET using a Micromeritics Tri-Star 3000 gas adsorption analyzer system. Approximately 0.35 g of sample was weighed out and loaded into a 3/8 in. sample tube. Nitrogen was used as the adsorption gas and sample analysis was performed at the boiling temperature of liquid nitrogen. Prior to the measurement, the sample was slowly ramped to 433 K and evacuated overnight to approximately 6.7 Pa. Supports and catalysts were also quantified by the Barrett, Joyner, Halenda (BJH) desorption model, which provides a relationship where the amount of adsorbate lost during a desorption step gives the average size of the pore emptied during that desorption step. Single point pore volumes and pore radii from the BJH method as applied to adsorption and desorption branches are provided.

1.1.1.2.2 Temperature Programmed Reduction

Temperature programmed reduction (TPR) profiles of fresh catalyst samples were obtained using a Zeton Altamira AMI-200 unit. Calcined fresh samples were first heated and purged in flowing argon to remove traces of water. TPR was performed using 30 cc/min 10%H_2/Ar mixture referenced to argon. The ramp was 5 °C/min from 50 to 1100 °C, and the sample was held at 1100 °C for 30 min.

1.1.1.2.3 Hydrogen Chemisorption / Pulse Reoxidation

Hydrogen chemisorption measurements were performed using a Zeton Altamira AMI-200 unit, which incorporates a thermal conductivity detector (TCD). The sample weight was always ~0.220 g. The catalyst was activated at 350 °C for 10 hr using a flow of 30 ccm of 33%H_2 in He and then cooled under flowing hydrogen to 100 °C. The sample was then exposed at 100 °C to flowing argon to prevent physisorption of weakly bound species prior to increasing the temperature slowly to the activation temperature. At that temperature, the catalyst was held under flowing argon to desorb the remaining chemisorbed hydrogen so that the TCD signal returned to the baseline. The TPD spectrum was integrated and the number of moles of desorbed hydrogen was determined by comparing to the areas of calibrated hydrogen pulses. Prior to experiments, the sample loop was calibrated with pulses of nitrogen in helium flow and compared against a calibration line produced from gas tight syringe injections of nitrogen under helium flow.

After TPD of hydrogen, the sample was reoxidized at the activation temperature by injecting pulses of pure oxygen in helium referenced to helium gas (Ref. 1). After oxidation of the cobalt metal clusters, the number of moles of oxygen consumed was determined, and the percentage reduction calculated assuming that the Co^0 reoxidized to Co_3O_4. While the uncorrected dispersions are based on the assumption of complete reduction, the corrected dispersions reported include the percentage of reduced cobalt as follows.

$$\%D_c = (\text{\# of } Co^0 \text{ atoms on surface} \times 100\%)/(\text{total \# } Co^0 \text{ atoms})$$

$$\%D_c = (\text{\# of } Co^0 \text{ atoms on surface} \times 100\%)/[(\text{total \# Co atoms})(\text{fraction reduced})]$$

1.1.1.2.4 X-Ray Diffraction

Powder diffractograms of calcined catalysts were recorded using a Philips X'Pert diffractometer. First, short times were used over a long range to assess crystalline phases present. The conditions were as follows: scan rate of 0.02°/step, scan time of 5 s/step over a 2θ range of 15° to 80°. Then, long times were used over a short range in order to quantify average Co_3O_4 domain sizes using line broadening analysis for the peak at 2θ= 36.8° representing (3 1 1). The conditions employed for the latter were a scan rate of 0.01°/step and a scan time of 30 s/step over a 2θ range of 30° to 45°.

1.1.1.2.5 X-ray Absorption Near Edge Spectroscopy (XANES)

XANES spectra were recorded in transmission mode near the Cd, In, and Sn K-edges at the National Synchrotron Light Source (NSLS) at Brookhaven National Laboratory, Upton, New York, Beamline X18-b. The beamline was equipped with a Si (111) channel-cut monochromator. A crystal detuning procedure was used to help remove harmonic content from the beam and make the relative response of the incident and transmission detectors more linear. The x-ray flux for the beamline was on the order of 1 E 10 photons per second at 100 mA and 2.8 GeV, and the usable energy range at X-18b is from 5.8 to 40 keV. A sample thickness was determined by calculating the amount in grams per square centimeter of sample, w_D, by utilizing the thickness equation:

$$w_D = \ln(I_0/I_t)/\Sigma\{(m/r)_j w_j\}$$

where m/r is the total cross section (absorption coefficient/density) of element j in the sample at the absorption edge of the element under study in cm^2/g, w_j is the weight fraction of element j in the sample, and $\ln(I_0/I_t)$ was taken over a typical range of 1 to 2.5. An average value of w_D from inputting both values was employed. Based on the calculation for w_D, and the cross-sectional area of the pellet, the grams were calculated. The catalysts were prepared in the same manner as a reaction test. However, following the H_2-posttreatment step, the catalyst was cooled down and solidified in the startup Polywax. Samples were cut and pressed to make self-supporting wafers. XANES data reduction were carried out using the WinXAS program (Ref. 2). XANES spectra were compared qualitatively following normalization.

1.1.1.3 Reaction Testing

Cobalt catalysts were activated using a gas mixture of H_2/He with a molar ratio of 1:3 in an external plug flow reactor (10-in. long and 1-in. diameter) at 350 °C and 1 atm pressure using a flow of 1 Nl/min for 15 hr. The amount of catalyst used was 12 to 18 g.

The ex-situ reduced catalyst was transferred pneumatically under the protection of helium to the CSTR which contained 315 g of melted Polywax-3000 (polyethylene fraction with an average molecular weight of 3000). To facilitate the transfer, the fixed bed reactor was connected to the CSTR using a transfer tube fitted with a ball valve. The fixed bed reactor was pressurized with argon forcing the catalyst powder out of the reactor through the valve. The reactor was weighed before and after the transfer of the catalyst to ensure that all the catalyst powder was transferred to the CSTR. The catalyst was then reduced in-situ with hydrogen at a flow rate of 30 SL/h at atmospheric pressure. With the temperature controller programmed in a ramp/soak mode, the reactor temperature was ramped up to 230 °C at a rate of 1 °C /min and held at 230 °C for 10 hr.

After the activation period, the reactor temperature was decreased to 180 °C, synthesis gas (H_2:CO = 2.0:1) was introduced to the reactor and the pressure was increased to the desired value. The reactor temperature was increased to the reaction temperature at a rate of 1 °C /min. The reaction products were continuously removed from the vapor space of the reactor and passed through two traps, a warm trap maintained at 100 °C and a cold trap held at 0 °C, to condense out the liquid products. The uncondensed vapor stream was reduced to atmospheric pressure through a letdown valve. The outlet flow was measured using a wet test meter and analyzed by an online GC. High molecular weight hydrocarbons (e.g., wax at room temperature) were withdrawn from the CSTR through a porous 2 μm metal filter during routine daily sampling.

1.1.2 Results and Discussion

CAER researchers examined Cd, In, and Sn additives to Co/Al_2O_3 catalysts at Brookhaven National Laboratory for XANES. The series prepared consisted of 25%$CoAl_2O_3$ promoted to the 1% by weight level of Cd, In, or Sn. As mentioned previously, the SPI method was used to add cobalt and the γ-Al_2O_3 support surface area was 150 m^2/g. BET results are presented in Table 1.1. TPR profiles are presented in Figure 1.1. The profiles may be interpreted based on

earlier investigations by our group. In TPR-EXAFS/XANES work (previous work, Figure 1.2), CAER and Argonne researchers found that the reduction of cobalt oxides proceeds in two steps (Ref. 3):

$$Co_3O_4 + H_2 \rightarrow 3CoO + H_2O \quad (1)$$

$$3CoO + 3H_2 \rightarrow 3Co^0 + 3H_2O \quad (2)$$

Thus, on this basis, standard TPR profiles can be interpreted, as the second broad peak is typically 3 times as large as the first sharper peak (Ref. 1). In an earlier work (Ref. 1), where the IWI procedure was used, an interesting trend was noted as the support interaction was weakened by either (a) moving to higher cobalt loadings or (b) moving to lower support surface areas to generate larger Co_3O_4 clusters. At lower loadings the peaks were completely separated and a broad peak for CoO to Co^0 reduction was observed for the reduction of CoO strongly interacting with the γ-Al_2O_3 support. However, at higher loadings, the reduction of CoO was split into two components, including (a) a higher temperature broad peak for CoO interacting with the support and (b) a lower temperature peak which emerges as a shoulder on the high temperature side of the peak for Co_3O_4 to CoO reduction at moderate loadings, and then increases at higher loadings. This latter peak matches well with the second peak of bulk Co_3O_4 reduction and is likely assigned to the reduction of larger CoO species that are not in close interaction with γ-Al_2O_3.

Returning to Figure 1.1, it appears that the same scenario applies. There is the broad high temperature peak for the reduction of CoO in interaction with the support; however, there is also a sharper low temperature peak on the high temperature side of the peak for reduction of Co_3O_4 to CoO. It is likely due to the reduction of larger CoO species in weak interaction with the support. The primary interest is in what happens to the broad peak. In moving along Row 5 of the Periodic Table of Elements, the reduction peak for Cd is significantly shifted to lower temperature relative to the unpromoted 25%Co/Al_2O_3 catalyst, but as the atomic number of the promoter is increased, the broad high temperature peak moves to higher temperatures. There are three possibilities for shifts in the reduction temperature: (a) a direct chemical promotion (e.g., electronic effect, alloying, etc.) due to promoter coordination of a metal with cobalt; (b) reduction of the promoter at lower temperature, such that hydrogen dissociation and spillover can aid in the reduction of cobalt oxides; or (c) a geometric effect (e.g., pore blocking) that leads to the growth of cobalt clusters that are—on average—less interacting with the support. Either (a) or (b) can explain the promoting impact of typical promoters such as Pt (Ref. 2), Ru (Ref. 4), and Re (Ref. 5), as CAER researchers have observed direct promoter-cobalt coordination in EXAFS spectroscopy with no evidence of promoter-promoter coordination (i.e., intimate contact of the promoter with cobalt at the atomic level). Moreover, the typical promoters were found to be in the metallic state rather than the oxidized state (e.g., by XANES (Refs. 2 and 4), EXAFS (Refs. 2 and 4), and/or TPR (Ref. 1)).

TABLE 1.1.—CATALYST CHARACTERISTICS, BET SURFACE AREA, AND POROSITY RESULTS FOR THE SERIES OF Cd, In, AND Sn PROMOTED CATALYSTS PREPARED FOR XANES ANALYSIS AND HAVING 25%Co LOADING, IN COMPARISON WITH THE UNPROMOTED CATALYST

Catalyst ID	Support/catalyst	Preparation method/support surface area, m^2/g/batch size	BET SA, m^2/g	Pore volume,[a] cm^3/g	Average pore radius,[a] nm	Pore volume[b]	Pore volume[c]	Average pore radius,[b] nm	Average pore radius,[c] nm
EXAFS1	Unpromoted 25%Co/Al_2O_3	SPI, 150 m^2/g 10 g	104.4	0.2237	4.28	0.2301	0.2290	4.34	3.97
EXAFS1 duplicate	Unpromoted 25%Co/Al_2O_3	SPI, 150 m^2/g 10 g	102.1	0.2190	4.29	0.2248	0.2238	4.33	3.98
EXAFS2	1%Cd-25%Co/Al_2O_3	SPI, 150 m^2/g 10 g	94.8	0.2609	5.51	0.2691	0.2683	5.1	4.55
EXAFS3	1%In-25%Co/Al_2O_3	SPI, 150 m^2/g 10 g	102.0	0.2747	5.38	0.2793	0.2784	5.01	4.52
EXAFS4	1%Sn-25%Co/Al_2O_3	SPI, 150 m^2/g 10 g	107.3	0.2553	5.2	0.2624	0.2616	4.89	4.44

[a] Single point
[b] BJH adsorp
[c] BJH desorp

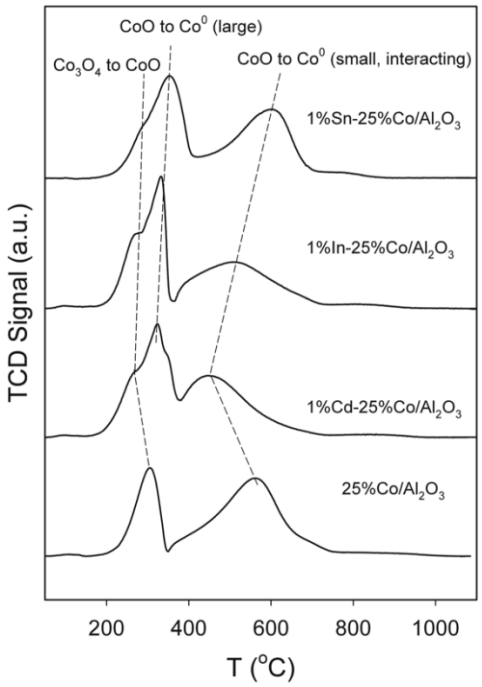

Figure 1.1.—TPR profiles of, moving upward, 25%Co/Al_2O_3, 1%Cd-25%Co/Al_2O_3, 1%In-25%Co/Al_2O_3, and 1%Sn-25%Co/Al_2O_3. Catalysts prepared by SPI using 150 m^2/g γ-Al_2O_3.

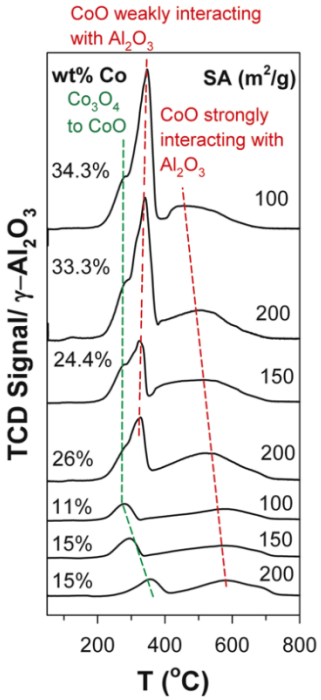

Figure 1.2.—TPR profiles of Co/Al_2O_3 catalysts as a function of (left side) loading and (right side) support surface area in m^2/g. (Reprinted with permission from G. Jacobs, T.K. Das, Y. Zhang, J. Li, G. Racoillet, B.H. Davis, Appl. Catal. 233 (2002) 263. Copyright (2002) Elsevier).

TABLE 1.2.—RESULTS OF HYDROGEN CHEMISORPTION/PULSE REOXIDATION OF Cd, In, AND Sn PROMOTED CATALYSTS PREPARED FOR XANES ANALYSIS AND HAVING 25%Co LOADING, IN COMPARISON WITH THE UNPROMOTED CATALYST

Catalyst ID	Catalyst	Preparation/amount made	H_2 desorbed, µmol/$g_{catalyst}$	Uncorrected percentage dispersion	Uncorrected average diameter, nm	O_2 pulsed, µmol/g	Percentage reduction	Corrected percentage dispersion	Corrected average diameter, nm
EXAFS1	Unpromoted 25%Co/Al_2O_3	SPI, 150 m^2/g 10 g	81.9	3.86	26.7	1371.1	48.5	7.96	13.0
EXAFS2	1%Cd-25%Co/Al_2O_3	SPI, 150 m^2/g 10 g	52.6	2.48	41.6	1641.3	58.0	4.27	24.2
EXAFS2 duplicate	1%Cd-25%Co/Al_2O_3	SPI, 150 m^2/g 10 g	54.4	2.56	40.3	1640.5	58.0	4.42	23.4
EXAFS3	1%In-25%Co/Al_2O_3	SPI, 150 m^2/g 10 g	60.0	2.83	36.5	1596.6	56.5	5.01	20.6
EXAFS4	1%Sn-25%Co/Al_2O_3	SPI, 150 m^2/g 10 g	53.6	2.53	40.9	1468	51.9	4.87	21.2

With Cd, In, and Sn, however, XANES spectra of catalysts retrieved from the reactor solidified in the wax product (i.e., in the in-situ state following activation) reveal that the promoter elements were in all cases oxidized (Figure 1.3 to Figure 1.5 for Cd, In, and Sn, respectively). Thus, it seems unlikely that the promoting effect came from either (a) chemical promotion or (b) hydrogen dissociation and spillover, although we cannot rule out some partial reduction of the promoter. That leaves case (c), an impact on the cobalt oxide cluster size, perhaps by pore blocking.

Assuming that the desorption of hydrogen is only from the surface Co^0 atoms, hydrogen chemisorption / pulse reoxidation results (Table 1.2) show that the site densities were considerably lower (i.e., see H_2 TPD results) than that of the unpromoted catalyst. Extents of reduction were on average higher for all of the catalysts. This is due to in part to the presence of non-interacting CoO in each sample as confirmed by TPR. Assuming that the desorption of hydrogen comes only from surface Co^0, the average cluster size was significantly higher for the promoted catalysts (21.2 nm+ compared to 13.0 nm). However, one cannot rule out at the present time whether the promoter is also present on the surface of the cobalt metal clusters.

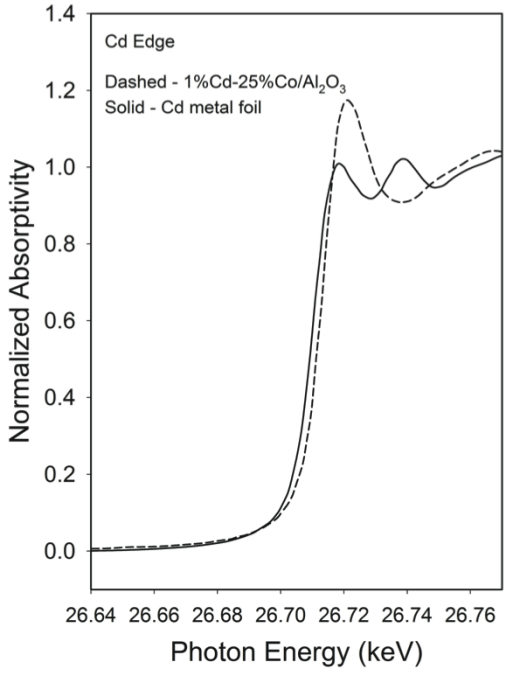

w

Figure 1.3.—XANES spectra of (dashed) 1%Cd-25%Co/Al_2O_3 compared to the (solid) reference Cd metal foil.

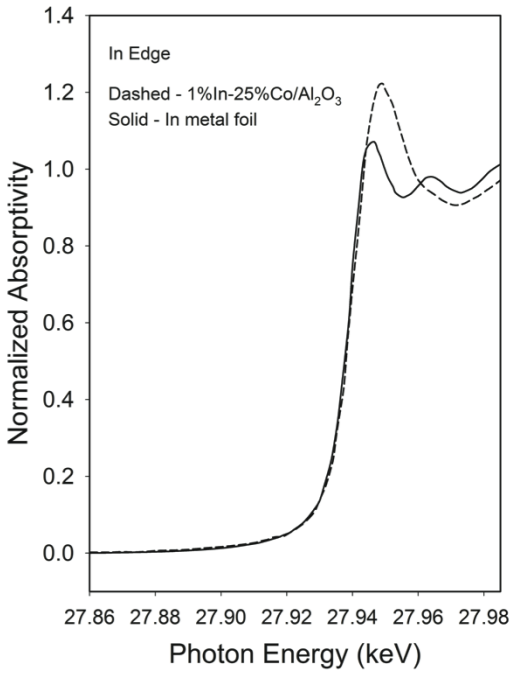

Figure 1.4.—XANES spectra of (dashed) 1%In-25%Co/Al_2O_3 compared to the (solid) reference In metal foil.

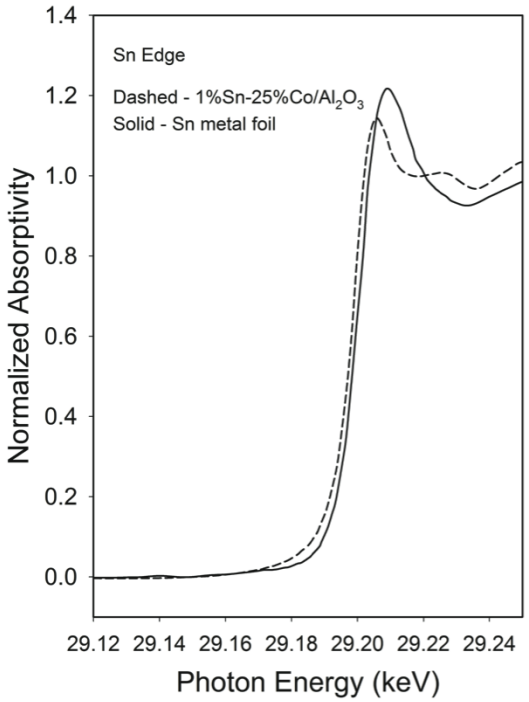

Figure 1.5.—XANES spectra of (dashed) 1%Sn-25%Co/Al_2O_3 compared to the (solid) reference Sn metal foil.

The next step was to decrease the loading of cobalt for the promoted catalysts in order to determine if the low temperature reduction peak for non-interacting CoO could be eliminated from the TPR profiles. The loading was decreased to 15%Co and BET and porosity characteristics of the samples are reported in Table 1.3. TPR profiles of the second series of catalysts are depicted in Figure 1.6. Decreasing the loading removed the sharp feature representing the reduction of CoO in weak interaction with the support and only the peaks for Co_3O_4 to CoO and the broad peak for CoO in interaction with the support are observed. Again, the broad peak for reduction of CoO in interaction with the support decreases in the case of Cd promotion, but as the promoter atomic number is increased (i.e., moving to In and Sn), the temperature of the peak shifts to higher temperatures. In examining the hydrogen chemisorption / pulse reoxidation results, there were only increases in extent of reduction for the cases of Cd and In. Despite any improvement in extent of reduction, the site densities as measured by H_2 TPD (again, assuming that all of the hydrogen desorbed from the surface of metallic cobalt) were less than that of the unpromoted catalyst for all cases (i.e., Cd, In, and Sn promotion). With the assumption that the hydrogen desorbed came only from the surface of metallic cobalt, the cluster sizes were found to be somewhat higher than the unpromoted catalyst in all cases, though to a much lesser degree than observed with 25%Co loading.

TABLE 1.3.—CATALYST CHARACTERISTICS, BET SURFACE AREA, AND POROSITY RESULTS FOR THE SERIES OF Cd, In, AND Sn PROMOTED CATALYSTS, INCLUDING A COMPARISON WITH THE UNPROMOTED CATALYST, CONTAINING A LOADING OF 15%Co

Catalyst ID	Support/catalyst	Preparation method/ support surface area, m^2/g/ batch size	BET SA, m^2/g	Pore volume,[a] cm^3/g	Average pore radius,[a] nm	Pore volume[b]	Pore volume[c]	Average pore radius,[b] nm	Average pore radius,[c] nm
NASA100	Unpromoted 15%Co/Al_2O_3	Slurry, 150 m^2/g 50 g	116.2	0.3040	5.23	0.3096	0.3088	4.72	4.28
NASA101	1%Cd-15%Co/Al_2O_3	Slurry, 150 m^2/g 50 g	110.1	0.2975	5.40	0.3024	0.3016	4.75	4.27
NASA102	1%In- 15%Co/Al_2O_3	Slurry, 150 m^2/g 50 g	111.6	0.3007	5.39	0.3053	0.3046	4.73	4.26
NASA103	1%Sn-15%Co/Al_2O_3	Slurry, 150 m^2/g 50 g	115.0	0.3004	5.23	0.3051	0.3043	4.68	4.25

[a] Single point
[b] BJH adsorp
[c] BJH desorp

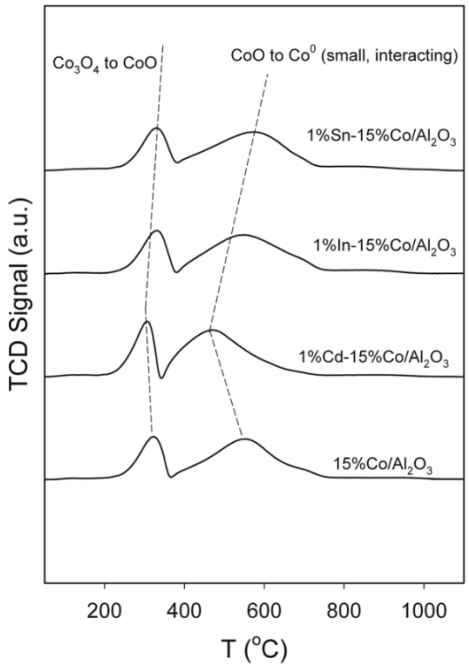

Figure 1.6.—TPR profiles of, moving upward, 15%Co/Al_2O_3, 1%Cd-15%Co/Al_2O_3, 1%In-15%Co/Al_2O_3, and 1%Sn-15%Co/Al_2O_3. Catalysts prepared by SPI using 150 m^2/g γ-Al_2O_3.

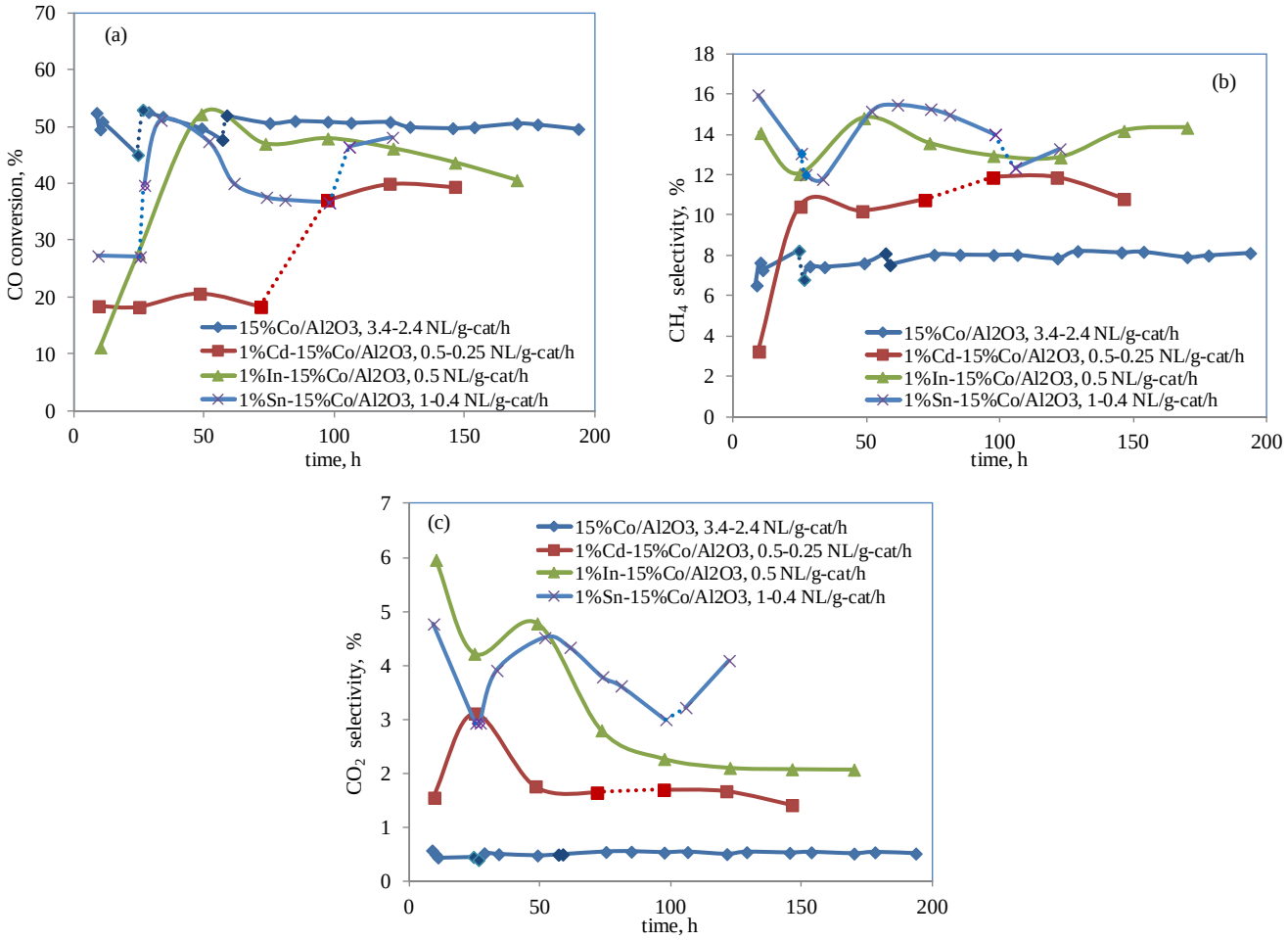

Figure 1.7.—Change of (a) CO conversion, (b) CH_4 selectivity, and (c) CO_2 selectivity with time over unpromoted, 1%Cd-, 1%In- and 1%Sn- promoted 15%Co/Al_2O_3 catalysts. Ex-situ reduction: 350 °C, 1 atm, H_2/He=3, 60 Nl/h; In-situ reduction: 230 °C, 1 atm, H_2/He=3, 30 Nl/h; FTS reaction conditions: 220 °C, 300 psig, H_2/CO = 2.1.

Figure 1.7(a) to (c) shows the change of CO conversion, CH_4 selectivity, CO_2 selectivity with time over unpromoted, 1%Cd, 1%In and 1%Sn promoted 15%Co/Al_2O_3 catalysts. To achieve 40 to 50% CO conversion, the space velocity (SV) was adjusted to 3.4-2.4 for the unpromoted 15%Co/Al_2O_3 during about 200 h of testing, while it was adjusted to much lower SV values, i.e., 0.5-0.25, 0.5, 1.0-0.4 Nl/$g_{catalyst}$/h for the Cd-, In- and Sn-promoted 15%Co/Al_2O_3 catalysts, respectively (Figure 1.1(a)). The addition of Cd, In or Sn promoter to the Co/Al_2O_3 catalyst significantly decreased the catalyst activity on a per g catalyst basis. From Figure 1.1(a), the unpromoted 15%Co/Al_2O_3 displayed better stability than the ones containing promoters, suggesting that the Cd, In or Sn promoters also reduced catalyst stability. The results suggest that decoration of Co with Cd, In, or Sn occurred either during or prior to FTS reaction testing. In re-examining the hydrogen chemisorption results (Table 1.4), the assumption is made that the H:Co ratio is 1:1 (Ref. 1), where "Co" refers to surface Co^0 atoms. For unpromoted catalysts and those promoted with Pt, Re, and Ru, where atomic coordination of the promoter to Co occurs, the H_2-TPD has in the past provided excellent indication of what the catalyst activity should be on a per g of catalyst basis. However, in the case of Cd, In, and Sn promoted catalysts, the reactor testing data demonstrate that this is not the case. That is, the activity on a per g of catalyst basis is even lower than what would be expected based on the albeit lower site densities from H_2-TPD measurements. This is not a new phenomenon. During an investigation of Group 11 promoters (Ref. 6) (i.e., the coinage metals—Cu, Ag, and Au), while all the promoters facilitated cobalt oxide reduction, only the Ag and Au promoters increased the catalyst activity on a per g of catalyst basis. All of the catalysts had higher metal site densities

TABLE 1.4.—HYDROGEN CHEMISORPTION/PULSE REOXIDATION OF C Cd, In, AND Sn PROMOTED CATALYSTS HAVING 15%Co LOADING, IN COMPARISON WITH THE UNPROMOTED CATALYST

Catalyst ID	Catalyst description	Preparation/amount made	H_2 desorbed, $\mu mol/g_{catalyst}$	Uncorrected percentage dispersion	Uncorrected average diameter, nm	O_2 pulsed, μmol/g	Percentage reduction	Corrected percentage dispersion	Corrected average diameter, nm
NASA100	Unpromoted 15%Co/Al_2O_3	Slurry, 150 m^2/g 50 g	57.3	4.50	22.9	823.1	48.5	9.28	11.1
NASA101	1%Cd-15%Co/Al_2O_3	Slurry, 150 m^2/g 50 g	52.6	4.14	25	997.6	58.8	7.19	14.3
NASA102	1%In-15%Co/Al_2O_3	Slurry, 150 m^2/g 50 g	45.6	3.59	28.8	959.9	56.6	6.34	16.3
NASA103	1%Sn-15%Co/Al_2O_3	Slurry, 150 m^2/g 50 g	36.6	2.87	35.9	783.1	46.2	6.23	13.8

by H_2-TPD relative to the unpromoted 15%Co/Al_2O_3 catalyst, but Cu decreased catalyst activity. Thus, it is important to remember that H_2-TPD only reports metal site density, and thus it was suggested that in the case of Cu, Cu^0 was likely on the surface of the cobalt particles so that, while it on the one hand promoted reduction of cobalt oxides, it decreased the cobalt surface site density by blocking sites on the surface (Ref. 6). The lower than expected activity of Cd, In, and Sn promoted catalysts may be due to the same problem. Another possibility, however, is that the catalysts have the active site density after activation, but that the site density is decreased due to reoxidation once FTS is started. There is precedence for this. For example, in Co catalysts tested in an in-situ EXAFS/XANES flow cell, Huffman et al. (Ref. 7) found that Co catalysts promoted with K were much more susceptible to reoxidation (i.e., even at low conversion) compared to catalysts having no K, which only oxidized at high conversion where the H_2O partial pressures were high.

CH_4 selectivity for the unpromoted 15%Co/Al_2O_3 catalyst was about 8% at 50% CO conversion, but it was increased to about 10% for the 1%Cd promoted catalyst, and to the 14 to 16% range for the 1%In and 1%Sn promoted Co catalysts (Figure 1.1(b)). Figure 1.1(c) also suggested that adding 1%Cd, 1%In or 1%Sn promoter to the Co catalyst led to significantly increased CO_2 selectivity (0.5 to 2-5%). The significant changes in catalyst selectivity are also indicators that species other than metallic Co are present in the catalyst, since metallic cobalt does not possess intrinsic water-gas shift (WGS) activity (Ref. 8). Note that higher WGS leads to higher methane selectivity, since WGS promotes the formation of hydrogen.

During the characterization phase of the project, it was noted that Cd was the best of the three elements to facilitate cobalt reduction and that an increase in cobalt size occurred, attention was paid to attempting to increase the cobalt size for a certain classification of research catalysts. In the past, catalysts prepared by the IWI method at relatively low loadings of cobalt of 15%Co were found to possess an average cluster size of ~5 to 6 nm (Ref. 1) when a 200 m^2/g support was used. Moreover, by adding a typical reduction promoter (i.e., Pt, Re, Ru), the site densities of surface Co^0 essentially doubled relative to the unpromoted catalyst (Ref. 1). However, the cluster size was found to be more sensitive to reoxidation in water co-feeding studies (Ref. 9). Moving to a higher loading of 25%Co, using the SPI method, and a somewhat lower support surface area of 150 m^2/g, cobalt clusters slightly higher than 10 nm were formed and the catalysts were more stable as a function of water partial pressure (Ref. 10). Thus, it was of interest to find out if Cd addition to a noble metal promoted 15%Co/Al_2O_3 catalyst (IWI, 200 m^2/g support), i.e., the one with smaller Co clusters—might promote stability against the water effect by increasing the cobalt cluster size. BET results are reported in Table 1.5. TPR profiles, depicted in Figure 1.8, show that, as expected, addition of 0.5% significantly shifts the peaks for both cobalt oxide reduction steps to lower temperatures. Addition of 1%Cd does not measurably impact the reduction temperature, although adding 3%Cd led to a shift to a slightly higher temperature for the CoO to Co^0 reduction step. Nevertheless, all of the catalysts displayed high extents of reduction in hydrogen chemisorption / pulse reoxidation tests (Table 1.6). Pt addition significantly boosted the active site density of the unpromoted 15%Co/Al_2O_3 catalyst. However, as with the previous catalysts that did not contain Pt, Cd addition to the catalysts containing Pt lowered the active site density. As before, this appears to be due to an increase in Co cluster size.

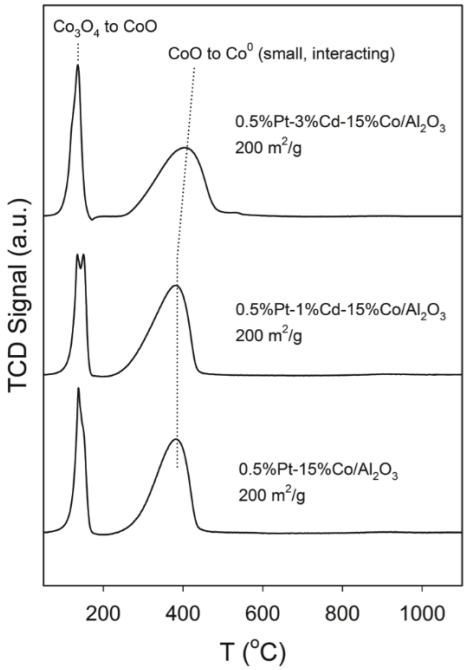

Figure 1.8.—TPR profiles of promoted 15%Co/Al_2O_3 catalysts prepared by IWI using 200 m^2/g Al_2O_3 and containing 0.5%Pt and, moving upward, (a) 0% Cd, (b) 1% Cd, and (c) 3% Cd.

TABLE 1.5.—CATALYST CHARACTERISTICS, BET SURFACE AREA, AND POROSITY RESULTS FOR A SERIES OF Pt AND Cd PROMOTED CATALYSTS PREPARED ON 15%Co/Al_2O_3 USING THE IWI METHOD AND A 200 m^2/g SUPPORT, ALONG WITH REFERENCE CATALYSTS

Catalyst ID	Support/catalyst	Preparation method/ support surface area, m^2/g/ batch size	BET SA, m^2/g	Pore volume,[a] cm^3/g	Average pore radius,[a] nm	Pore volume[b]	Pore volume[c]	Average pore radius,[b] nm	Average pore radius,[c] nm
NASA106	Unpromoted 15%Co/Al_2O_3	IWI, 200 m^2/g 50 g	165.0	0.3275	3.97	0.3363	0.3353	3.42	3.09
NASA104	0.5%Pt 15%Co/Al_2O_3	IWI, 200 m^2/g 200 g	168.8	0.3279	3.89	0.3372	0.336	3.44	3.12
NASA105	0.5%Pt+1%Cd 15%Co/Al_2O_3	IWI, 200 m^2/g 250g	167.5	0.3209	3.83	0.3293	0.3281	3.42	3.09
NASA115	0.5%Pt+3%Cd 15%Co/Al_2O_3	IWI, 200 m^2/g 50 g	165.3	0.3115	3.77	0.3192	0.3180	3.38	3.05

[a] Single point
[b] BJH adsorp
[c] BJH desorp

TABLE 1.6.—RESULTS OF HYDROGEN CHEMISORPTION/PULSE REOXIDATION OF A SERIES OF Pt AND Cd PROMOTED CATALYSTS PREPARED ON 15%Co/Al_2O_3 USING THE IWI METHOD AND A 200 m^2/g SUPPORT, ALONG WITH REFERENCE CATALYSTS

Catalyst ID	Catalyst description	Preparation/ amount made	H_2 desorbed, $\mu mol/g_{catalyst}$	Uncorrected percentage dispersion	Uncorrected average diameter, nm	O_2 pulsed, µmol/g	Percentage reduction	Corrected percentage dispersion	Corrected average diameter, nm
NASA106	Unpromoted 15%Co/Al_2O_3	IWI, 200 m^2/g 50 g	In progress	In progress	In progress	-	In progress	In progress	In progress
NASA104	0.5%Pt 15%Co/Al_2O_3	IWI, 200 m^2/g 200 g	135.6	10.65	9.7	1090.6	64.3	16.57	6.2
NASA105	0.5%Pt+1%Cd 15%Co/Al_2O_3	IWI, 200 m^2/g 250 g	115.2	9.05	11.4	1123.4	66.2	13.67	7.5
NASA115	0.5%Pt+3%Cd 15%Co/Al_2O_3	IWI, 200 m^2/g 50 g	97.3	7.65	13.5	1175.2	69.3	11.04	9.3

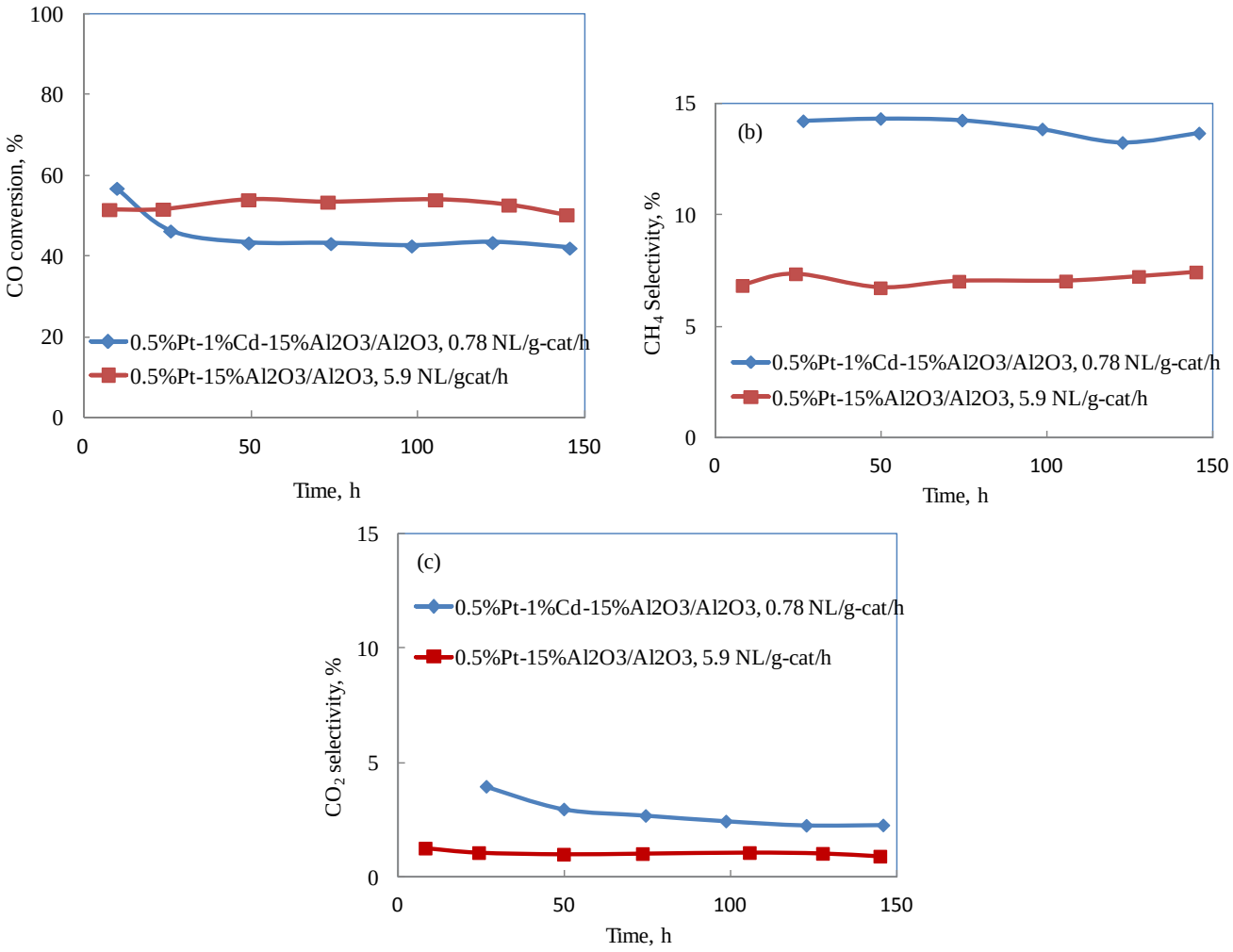

Figure 1.9.—Change of (a) CO conversion, (b) CH_4 selectivity, (C) CO_2 selectivity with time over 0.5%Pt-1%Cd-15%Co/Al_2O_3 and 0.5%Pt-15%Co/Al_2O_3 catalysts. Ex-situ reduction: 350 °C, 1 atm, H_2/He=3, 60 Nl/h; In-situ reduction: 230 °C, 1 atm, H_2/He = 3, 30 Nl/h; FTS reaction conditions: 220 °C, 300 psig, H_2/CO = 2.1.

Figure 1.9(a) to (c) shows the change of CO conversion, CH_4 selectivity, CO_2 selectivity with time over 0.5%Pt-1%Cd-15%Co/Al_2O_3 and 0.5%Pt 15%Co/Al_2O_3 catalysts. As expected from the hydrogen chemisorption / pulse reoxidation results, the 0.5%Pt 15%Co/Al_2O_3 catalyst displayed high activity, indicated by high space velocity (5.9 NL/$g_{catalyst}$/h) used at 50% CO conversion level. The catalyst was quite stable during 144 h of testing. However, the addition of 1%Cd to the Pt promoted Co catalyst, significantly decreased catalyst activity on a per g of catalyst basis, (Figure 1.9(a)), as indicated by much lower space velocity used (~0.8 NL/$g_{catalyst}$/h) for the 1%Cd-0.5%Pt promoted 15%Co/Al_2O_3 catalyst. Comparing the CH_4 and CO_2 selectivities over the Pt-Co catalyst with and without 1%Cd, it was confirmed that Cd promoter addition dramatically increased CH_4 (7 to 14%) and CO_2 (1.0 to 2.5%) selectivities. Again, it is evident that the activity was far lower than the expected decrease observed in the H_2-TPD results. Thus, we anticipate one of two scenarios may explain the data: (1) some metallic Cd may exist on the surface of metallic cobalt particles which contribute to the H_2 TPD but poison the Co sites or (2) the presence of Cd tends to promote oxidation of Co under FTS conditions, as K was observed to do in the earlier EXAFS/XANES investigation of Huffman et al. (Ref. 7).

1.1.3 Conclusions

The possibility of using selected alternative promoters (e.g., Cd, In, Sn) from the ones typically used (e.g., Re, Ru, Pt) was explored. For 25%Co/alumina catalysts, adding 1% Cd, In, or Sn was found to facilitate reduction by—at least in part—generating a heterogeneous distribution of cobalt. This consisted of larger lesser interacting cobalt clusters and smaller, more strongly interacting, cobalt species. The lesser interacting species, which tended to be larger, were identified in TPR profiles as a sharp low temperature CoO reduction peak. In XANES spectroscopy, the Cd, In, and Sn promoters were determined to be present in, at least to a significant degree, in an oxidized state. This is in contrast to commonly used promoters (e.g., Re, Ru, Pt), which were previously determined by CAER researchers to exist in a metallic state, where the promoter was in atomic coordination with cobalt with no promoter-promoter coordination being evident. Since larger cobalt clusters were suggested to be present based on chemisorption measurements, the active site densities for the promoted catalysts relative to the unpromoted 25%Co/Al_2O_3 catalyst were lower. Decreasing the cobalt loading to 15%Co significantly diminished the presence of larger non-interacting species (i.e., the sharp low temperature peak for CoO reduction was eliminated). After removing the contribution from non-interacting CoO species, the TPR peak for the reduction of strongly interacting CoO in the Cd promoted catalyst was found to occur at a measurably lower temperature than in the unpromoted catalyst. The Co clusters following activation remained slightly larger, on average, in comparison with the unpromoted 15%Co/Al_2O_3 reference catalyst. None of the promoted catalysts (i.e., with Cd, In, or Sn) exhibited surface Co^0 site densities higher than that of the unpromoted catalyst. In activity testing, the activities were even much lower than what was expected from the H_2-TPD results. Two possible explanations were proposed: (1) the promoters may be located on the surfaces of cobalt particles, blocking surface Co^0 but being able to desorb hydrogen or (2) the promoters may facilitate Co oxidation during Fischer-Tropsch synthesis, as previously observed by Huffman and coworkers when K was added to cobalt catalysts.

1.2 Exploring Ag as a Possible Replacement for Pt Promoter in Co/Al_2O_3

For economic reasons, Ag as a substitute for Pt promoter for FT Co/Al_2O_3 catalysts was advocated, due to its satisfactory ability to facilitate cobalt oxide reduction, its good catalytic performance in improving the CO conversion and selectivity and, especially, it's much lower price compared to that of Pt (i.e., $31.20/Troy oz. vs. $1683.0/Troy oz.). A comparative study between Pt and Ag promoters at several equivalent atomic loadings was performed in this work. While either Pt or Ag significantly facilitates cobalt oxide reduction supplying additional Co metal active sites compared to the unpromoted Co/Al_2O_3 catalysts, the total metal site density increased with increasing Pt loading, but become attenuated at high Ag loading. The EXAFS results indicate isolated Pt atoms interact with cobalt cluster to form Pt-Co bonds, without evidence of Pt-Pt bond formation, even at levels as high as 5 wt % Pt. In Ag promoted Co/Al_2O_3 catalyst, not only were Ag-Co bonds observed, but Ag-Ag bonds were present, even at levels as low as 0.276% Ag. The degree of Ag-Ag coordination increased as a function of Ag loading, while decreases in BET surface area and a shift to wider average pore size suggests some pore blocking by Ag at high loadings, which likely blocked access of reactant to internal cobalt sites. Therefore, although both promoters initially facilitate reduction of cobalt oxides, their local atomic structures are fundamentally different. Either Pt or Ag can significantly improve the CO conversion rate on a per gram catalyst basis of Co/Al_2O_3. Slightly adverse effects on selectivity (i.e., increased CH_4 and CO_2, at detriment to C_5+) were found with Pt, especially at higher loading, while Ag provides some benefits (i.e., slightly decreases CH_4 and CO_2, and increases C_5+) at all loadings tested in this work. Moreover, TPR and chemisorption/pulse reoxidation results show that Pt and Ag continue to be in proximity with Co following OR cycles to continue to facilitate reduction. Additional reaction tests are required to determine the impact of regeneration on performance.

1.2.1 Background

Cobalt/alumina is an effective Fischer-Tropsch synthesis (FTS) catalyst for gas-to-liquids (GTL) production from syngas with high H_2/CO ratio (~2:1). There is general agreement that reduced Co metal surface sites are active sites for FTS over this catalyst. Unlike other metals typically employed in catalysis, cobalt on alumina for FTS is often loaded in high amounts, often at or exceeding 20% by weight. Because the alumina support interacts strongly with cobalt (Refs. 11 and 12), higher loadings facilitate the reduction of cobalt oxide species during activation and make the catalyst more resistant to deactivation (e.g., by oxidation at high conversion) (Refs. 11 and 12). Despite high Co metal loadings, the support still hinders the ability of cobalt oxide to be reduced during thermal activation in H_2 at moderate temperature (e.g., 350 °C for 10 hr in H_2).

The addition of noble metal promoters (e.g., Pt, Ru, and Re) (Refs. 12 to 22) significantly enhances the reducibility of cobalt oxide interacting with the alumina support and, consequently, provides additional Co metal sites densities for the reaction in comparison with the unpromoted catalyst. A H_2 dissociation and spillover mechanism (Refs. 17, 18, and 23) is believed to be a possible way of promotion, in which the promoter metal, first reduced at lower temperature such that H_2 dissociated and spilled over from the metal promoter to form nuclei of Co^0 in the cobalt oxide, with this reduced cobalt expediting further reduction of cobalt oxide particles. Among these noble metal promoters, Pt promoter is among the most widely used in commercial FT Co/Al_2O_3 catalysts. PtO_2 has been observed after calcination (Ref. 24), while only a Pt-Co bimetallic phase was found in the $Pt\text{-}Co/Al_2O_3$ catalyst (Refs. 17, 25 and 26) after activation in H_2, as investigated by EXAFS spectroscopy. This structural coordination was suggested to be responsible for facilitating Co reduction and thereby improving the CO conversion rate on a per gram catalyst basis.

Group 11 metals (Cu, Ag, Au) were previously investigated as potential substitutes for Pt (Ref. 23), due to their ability to facilitate reduction of cobalt oxides and, in particular, due to the lower prices of Ag and Cu compared to that of noble metals like Pt. In that work (Ref. 23), we found that although all the Group 11 metals enhanced the reducibility of cobalt oxides and increased the fraction of Co reduced, there were differences in catalytic activity and selectivity: introducing Ag or Au (the latter at lower levels) improved CO conversion and slightly improved reaction selectivity relative to the unpromoted catalyst, while adding Cu, the catalytic activity and selectivity were worse than

those of the unpromoted catalyst. Because of the good performance of Ag in facilitating cobalt reduction and in performance together with its lower price compared with Au, Ag appears to be the best among Group 11 metals and to be the most promising promoter as a substitute for Pt, a promoter used commercially. Well dispersed Ag_2O was suggested to be the main Ag species in a Ag-Co/Al_2O_3 catalyst after calcination or oxidation (Refs. 23 and 27) and this species quickly reduced during activation conditions (Ref. 28). In our preliminary study of the local atomic structure of Ag-Co/Al_2O_3 catalyst Ag-Co coordination was difficult to assess due to the high loading of Ag used (Ref. 23). Notwithstanding, because of the ability of Ag to facilitate Co reduction and to slightly reduce CH_4 formation as observed in our recent work (Ref. 23), Ag-Co coordination is expected to be detected at lower Ag loadings, and this was investigated in this work using the EXAFS technique and measuring at the Ag K-edge. Adding Ag to hydrogenating catalysts can hinder the hydrogenation reaction and Ag-active metal bimetallic was proposed to be an active site (Ref. 29). This could shed light on why CH_4 selectivity is decreased in the Ag promoted Co FT catalyst.

A comparative study between Pt and Ag was conducted in this work. Although proposed in our previous report on the role of Pt (Ref. 17) and Ag (Ref. 23) promoter, one objective of this work was to determine if higher loading could further facilitate cobalt reduction, and subsequently find the point at which Pt-Pt bonds could be identified in the case of Pt promotion or the point at which Ag-Co could be found in the case of Ag, which were not disclosed before; moreover, the most appropriate Pt and Ag loading will be suggested. In so doing, different levels of atomically equivalent loadings of Pt or Ag were applied to 25%Co/Al_2O_3. Standard characterization methods (e.g., H_2 TPR, H_2 chemisorption/oxygen pulse reoxidation, X-ray diffraction, and BET) were also employed. The catalysts were thoroughly characterized at the atomic level by EXAFS spectroscopy, while electronic information was also obtained by XANES. Moreover, CSTR tests were implemented at ~50% conversion level so that FTS selectivities could be directly compared between Pt and Ag promoted cobalt catalysts. The final investigation in this work was a preliminary investigation on the potential of catalysts to be regenerated, and this was carried out using oxidation-reduction cycles. However, additional studies are needed in this area.

1.2.2 Experimental

1.2.2.1 Catalyst Preparation

The catalyst support used was Sasol Catalox-150 γ-Al_2O_3. To achieve 25%Co loading, a slurry impregnation method, which follows a Sasol patent (Ref. 11), was used. Cobalt nitrate hexahydrate ($Co(NO_3)_2 \cdot 6H_2O$) (Alfa Aesar) was employed to make the Co precursor solution. The ratio of the volume of loading solution used to the weight of alumina was 1:1, such that approximately 2.5 times the pore volume of solution was used. Two impregnation steps of cobalt nitrate were applied. Between each step the catalyst was dried under vacuum in a rotary evaporator. After the last step of cobalt addition, platinum or silver precursor solution was added to the Co/Al_2O_3 catalyst by incipient wetness impregnation. Tetra-amine platinum (II) nitrate solution and silver nitrate (Alfa Aesar) were utilized as Pt and Ag sources, respectively. A series of Pt promoted Co/Al_2O_3 catalysts was prepared with loadings of 0.5, 1, 2, 3, 4, and 5%, which are atomically equivalent to Ag loadings of 0.276, 0.553, 1.11, 1.66, 2.21, and 2.76%, respectively. Only after the final step were catalysts calcined under air flow at approximately 2 L/min at 350 °C for 4 h.

To study the potential of each catalyst to be regenerated, oxidation-reduction (OR) experiments mimicking catalyst regeneration cycles were performed for both Pt promoted and Ag promoted catalyst. First, the freshly calcined catalysts were reduced at 350 °C for 10 h under flow of 25% H_2 in helium, then cooled to room temperature under H_2 flow and purged with nitrogen and, subsequently, passivated by 1% O_2 in nitrogen flow at room temperature. After that, oxidation was performed at 350 °C for 4 h under flow of air. Two cycles of OR experiments were done with each catalyst in this study and the catalyst samples were withdrawn after each cycle for the purpose of characterization.

1.2.2.2 BET Surface Area and Porosity Measurements

The measurements of BET surface area and porosity of the calcined catalysts were conducted using a Micromeritics Tri-Star system. Before performing the test, the temperature was gradually ramped to 160 °C and the

sample was evacuated at least 12 h to approximately 50 mTorr. The BET surface area, pore volume (single point), and average pore radius (single point and BJH adsorption) were obtained for each sample.

1.2.2.3 Temperature Programmed Reduction (TPR)

Temperature programmed reduction (TPR) profiles of calcined catalysts were recorded using a Zeton-Altamira AMI-200 unit equipped with a thermal conductivity detector (TCD). Samples were pretreated by purging with argon flow at 350 °C to remove traces of water. The TPR was performed using a 10%H_2/Ar gas mixture and referenced to argon at a flow rate of 30 cm^3/min. The sample was heated from 50 to 800 °C using a heating ramp of 10 °C/min.

1.2.2.4 Hydrogen Chemisorption and Percentage Reduction by Pulse Reoxidation

Hydrogen chemisorption was conducted at using temperature programmed desorption (TPD), also measured with the Zeton-Altamira AMI-200 instrument. The sample weight was typically ~0.220 g. Catalysts were activated in a flow of 10 cm^3/min of H_2 mixed with 20 cm^3/min of argon at 350 °C for 10 h. and then cooled under flowing H_2 to 100 °C. The sample was held at 100 °C under flowing argon to remove and/or prevent adsorption of weakly bound species prior to increasing the temperature slowly to 350 °C, the reduction temperature of the catalyst. The catalyst was held under flowing argon to desorb remaining chemisorbed hydrogen until the TCD signal returned to baseline. The TPD spectrum was integrated and the number of moles of desorbed hydrogen determined by comparing its area to the areas of calibrated hydrogen pulses. The loop volume was first determined by establishing a calibration curve with syringe injections of hydrogen in helium flow. Dispersion calculations were based on the assumption of a 1:1 H:Co stoichiometric ratio and a spherical cobalt cluster morphology. After TPD of hydrogen, the sample was reoxidized at 350 °C using pulses of oxygen. The percentage of reduction was calculated by assuming that metal reoxidized to Co_3O_4. Further details of the procedure are provided elsewhere (Ref. 18).

1.2.2.5 X-Ray Diffraction (XRD)

Powder diffractograms on calcined catalysts were recorded using a Philips X'Pert diffractometer. Two different tests were performed for each sample—a short time scan over a long range and a long time scan over a short range. The objective of the short time scan was to assess the crystalline phases present using the following conditions: scan rate of 0.02°/step and scan time of 5 s/step over a 2θ range of 15° to 80°. The long time scan was conducted to quantify average Co_3O_4 domain sizes using line broadening analysis for the peak at 2θ = 37° representing (311). The latter conditions employed were a scan rate of 0.01°/step and a scan time of 30 s/step over a 2θ range of 30° to 45°.

1.2.2.6 Extended X-Ray Absorption Fine Structure (EXAFS) and X-Ray Absorption Near Edge (XANES) Spectroscopies

In situ H_2-TPR XAFS studies were performed at the Materials Research Collaborative Access Team (MR-CAT) beamline, 10BM, at Argonne National Laboratory's Advanced Photon Source. A water-cooled Si(111) monochromator selected the incident energy and was detuned to 50% of the peak intensity to reduce higher-order harmonics of the fundamental beam energy.

The experiment setup was similar to that outlined by Jacoby (Ref. 30). A stainless steel multi-sample holder (3.5 mm i.d. channels) was used to monitor the in situ reduction of 6 samples during a single TPR run. For the Pt series, approximately 10 mg of each sample was loaded as a self-supporting wafer in each channel. The charge was about 7 mg for the Ag series. The holder was placed in the center of a quartz tube, equipped with gas and thermocouple ports and Kapton windows. The amount of samples used was optimized for the Pt L_{III}-edge and Ag-K edge, considering the absorption by Al of the support. The quartz tube was placed in a clamshell furnace mounted on positioning table. Each sample cell was positioned relative to the beam by finely adjusting the position of the table to an accuracy of 20 μm (for repeat scans). Once the sample positions were fine-tuned, the reactor was purged with helium for more than 5 min at 30 ml/min then the reactant gas (H_2/He, 4%) was flowed through the samples (30 ml/min) and a temperature ramp of 0.78 °C/min (starting from ~50 °C after a more rapid startup) was initiated for the furnace.

The Pt L_{III}-edge spectra were recorded in transmission mode and a Pt metallic foil spectrum was measured simultaneously with each sample spectrum for energy calibration. X-ray absorption spectra for each sample were collected from 11632 to 12108 eV. By measuring each sample, in turn, and repeating, this allowed 33 scans to be collected for each sample over a 16.5 h period. The sample's temperature change from the absorption edge through the end of the scan was then about 4.0 °C, while each sample was measured approximately every 22.6 °C. The Ag K-edge spectra were also recorded in transmission mode and an Ag metallic foil spectrum was employed for energy calibration. X-ray absorption spectra were collected from 25266 to 26157 eV. By measuring each sample, in turn, and repeating, this allowed 33 scans to be collected for each sample over a 16.5 h period. The sample's temperature change from the absorption edge through the end of the scan was then about 3.5 °C, while each sample was measured approximately every 23.3 °C. After the sample temperature reached to 350 °C, the sample was then held at this temperature for 6 h 30 min and the scans were also done as a function of time. Then, the catalyst samples were cooled down to room temperature and the final scans were performed.

XANES spectra were processed using the WinXAS program (Ref. 31). For the case of Pt promoted catalysts, simultaneous pre and post-edge background removal was carried out using degree 2 polynomials over the ranges 11.413 to 11.498 keV and 11.662 to 12.076 keV, respectively, and normalization by division of the height of the absorption edge. For Ag promoted catalysts, XANES spectra were processed in the same manner but over the pre-edge range of 25.342 to 25.444 keV and the post-edge range of 25.615 to 25.122 keV with normalization. Once the spectra were processed, they were compared with reference compounds. For Pt-25%Co/Al_2O_3, all of the beginning spectra closely resemble the bulk PtO_2 reference compound. Therefore, the initial spectrum for each catalyst was used as the reference for PtO_2 in the sample. As the temperature trajectory was followed, it was clearly observed that a PtO_2 to PtO transition took place for all the samples, considering the white line intensities and the line shapes. Further following the temperature trajectory, the conversion from PtO to Pt^0 occurred. The catalyst spectra at 350 °C resemble the spectrum of Pt^0, so they were used as a Pt^0 reference. To specify the spectrum of PtO in the catalyst samples, which has a line shape similar to PtO_2 but with an attenuated intensity, a linear combination fitting was performed using PtO_2 and Pt^0 in samples as references. The spectrum composed of 50% PtO_2-50%Pt^0 was empirically selected as a PtO sample reference. This is in agreement with the white line intensity of PtO as compared to PtO_2 in the work of Christensen et al. (Ref. 14). Finally, a linear combination fitting was performed by using those 3 Pt reference compounds for analyzing spectra along the temperature trajectory. For Ag-25%Co/Al_2O_3 catalyst, the starting spectra of all samples did not resemble any bulk Ag compound references (i.e., AgO, Ag_2O). However, it has been previously suggested that Ag_2O was more likely to be an Ag species in calcined samples (Ref. 27). Along with the temperature trajectory, it was obvious that Ag_2O converted to Ag^0. Thus, a linear combination fitting was performed using Ag_2O and Ag^0 in the samples as references.

EXAFS spectra were also processed using WinXAS (Ref. 31). Initially, the catalysts were analyzed over the k-range 2 to 12 $Å^{-1}$. For those spectra, simultaneous pre and post-edge background removal was carried out with two polynomial degree 2 functions over the ranges 11.413 to 11.498 keV and 11.662 to 12.076 keV, respectively, for Pt promoted catalysts and over the ranges 25.342 to 25.444 keV and 25.615 to 25.122 keV, respectively, for Ag promoted catalyst. The spectra were normalized by dividing by the height of the edge jump. Spectra were then calibrated versus the Pt^0 or Ag^0 reference spectrum, and then converted to k-space. A cubic weighted degree 7 spline was used to remove the background of the $\chi(k)$ function. Finally, the data in k-space were Fourier transformed to R-space using a Bessel window (using a k^3-weighting for Pt promoted catalysts and k^1-weighting for Ag promoted catalysts). EXAFS fittings were carried out using the catalysts in their final state following TPR and cooling. All catalysts displayed high quality data over the k-range of 2 to 12 $Å^{-1}$ range. In R-space for Pt promoted catalysts, the first Pt-Co coordination shell was isolated by employing a Bessel window and then taking the back-Fourier Transform. After converting to $\chi(k)$, fitting of the spectra was carried out in k-space using FEFFIT (Ref. 32). The k-range employed was 3 to 12 $Å^{-1}$. The FEFF program (Ref. 33) was used to construct a model of Pt-Co FCC to be used in fitting, and the atomic coordinates of Pt FCC (with lattice parameters) were inputted to the FEFF program with the aid of the program Atoms (Ref. 34). In order to use coordination number as a fitting parameter, the amplitude reduction factor S_0^2 must be fixed for all scattering paths in the solid, and it was assumed to be 0.9 by the zeroth order approximation. For Ag promoted catalysts, the first Ag-Co and Ag-Ag coordination shells in R-space were identified and also isolated by using a Bessel

window and then back Fourier transformed to k-space. Fitting was performed over the k-range of 2 to 10 $Å^{-1}$. The model for Ag consisted of Ag-Co and Ag-Ag bonds generated by the FEFF and Atoms programs. The amplitude reduction factor S_0^2 of 0.9 was also applied.

1.2.2.7 Catalytic Activity Testing

FTS reaction tests were conducted using a 1 L CSTR equipped with a magnetically driven stirrer with turbine impeller, a gas-inlet line, and a vapor outlet line with a stainless steel (SS) fritted filter (7 μm) placed external to the reactor. A tube fitted with a SS fritted filter (2 μm opening) extends below the liquid level of the reactor for withdrawing reactor wax to maintain a nearly constant liquid level in the reactor. Separate mass flow controllers were used to control the flow of hydrogen and carbon monoxide at the desired flow rate. The reactant gases were premixed in a vessel before entering the reactor. Carbon monoxide was passed through a vessel containing lead oxide-alumina to remove traces of iron carbonyls. The mixed gases entered the CSTR below the stirrer operated at 750 rpm. The reactor slurry temperature was maintained constant by a temperature controller.

Prior to performing the reaction test, the catalyst (~13.0 g) was ground and sieved to 45 to 90 μm, and then loaded into a fixed-bed reactor for ex-situ reduction at 350 °C under atmospheric pressure for 15 h using a gas mixture of H_2/He (60 NL/h) with a molar ratio of 1:3. The reduced catalyst was then transferred to a 1 L continuously stirred tank reactor (CSTR) containing 315 g of melted Polywax 3000, by pneumatic transfer under the protection of a N_2 inert gas. Weighing the reactor before and after the transfer of catalyst was done to ensure that all catalyst powder was successfully transferred to the reactor. The transferred catalyst was further reduced in-situ at 230 °C at atmospheric pressure using pure hydrogen (30 NL/h) for another 10 h before starting the FTS reaction.

In this study, the FTS conditions used were 220 °C, 2.2 MPa, H_2/CO = 2.1. The reactant gas mixture was analyzed prior to sending to the reactor to ensure the composition. The reaction products were continuously removed from the vapor space of the reactor and passed through two traps, a warm trap maintained at 100 °C and a cold trap held at 0 °C. The uncondensed vapor stream was reduced to atmospheric pressure. The gas flow was measured using a wet test meter and analyzed by online GC. The accumulated reactor liquid products were removed every 24 h by passing through a 2 μm sintered metal filter located below the liquid level in the CSTR. Conversions of CO were obtained by gas-chromatography analysis (micro-GC equipped with thermal conductivity detectors) of the outlet gas product. The reaction products were collected in three traps maintained at different temperatures; a hot trap (200 °C), a warm trap (100 °C), and a cold trap (0 °C). The products were separated into different fractions (rewax, wax, oil, and aqueous) for quantification. However, the oil and wax fractions were mixed prior to GC analysis (Ref. 23). To investigate the effect of Pt and Ag on the activity and selectivity, a reference CO conversion of about 50% was used and achieved by adjusting the space velocity in all cases. Activities were compared by adjusting space velocity and measuring the space velocity used to achieve 50%CO conversion, while selectivities were directly compared at the same level of conversion.

1.2.3 Results and Discussion

1.2.3.1 BET and Porosity Measurements

The results of surface area and porosity data as measured by N_2 physisorption at 77 K are shown in Table 1.7. Sasol Catalox-150 γ-Al_2O_3 was used as a catalyst support and its specific BET surface is 150 m^2/g. Because the analysis was taken for calcined catalysts, Co_3O_4 was deemed to be a major cobalt oxide compound in this catalyst (Ref. 35). The 34%Co_3O_4 by weight was calculated by assuming 25 wt% Co metals in Co/Al_2O_3 catalyst were completely converted to Co_3O_4 after calcination. Thus, if Al_2O_3 is the only contributor to the area, then the area of 25%Co/ Al_2O_3 catalysts should be 150 × 0.66 = 99 m^2/g, which is very closed to the measured value of 98.4 m^2/g. Interestingly, Pt promoter seems to have an effect on the BET results, namely, increasing Pt loading evidently increases BET surface area and slightly decreases average pore radius. On the other hand, adding Ag promoter did not significantly alter the BET results of the catalyst, even at high Ag loadings.

TABLE 1.7.—THE RESULTS OF BET SURFACE AREA AND POROSITY MEASUREMENTS, HYDROGEN CHEMISORPTION/PULSE REOXIDATION, AND X-RAY DIFFRACTION OF CATALYSTS

Catalyst	BET SA, m^2/g	Pore volume,[a] cm^3/g	Average pore radius, nm	H_2 desorbed per $g_{catalyst}$, µmol/g	Uncorrected metal dispersion, %	Uncorrected Co dispersion,[b] %	Uncorrected Co average diameter,[b] nm	O_2 uptake per $g_{catalyst}$, µmol/g	O_2 uptake by Co per $g_{catalyst}$,[c] µmol/g	Percent reduction of Co	Corrected metal dispersion, %	Corrected Co dispersion,[b] %	Corrected Co average diameter,[b] nm	Estimate diameter Co^0 from XRD,[d] nm
25%Co/Al_2O_3	98.4	0.234	4.5	53.6	2.5	2.5	40.8	1008	1008	35.6	35.6	7.1	14.6	10.4
0.5%Pt-25%Co/Al_2O_3	98.5	0.218	4.4	132.9	6.2	6.3	16.5	1759	1733	61.3	10.1	10.3	10.0	10.4
1.0%Pt-25%Co/Al_2O_3	103.9	0.255	4.9	157.6	7.3	7.4	13.9	1856	1805	63.8	11.4	11.7	8.8	-
2.0%Pt-25%Co/Al_2O_3	108.8	0.229	4.2	151.2	7.0	7.1	14.4	1699	1596	56.4	12.1	12.8	8.1	9.7
3.0%Pt-25%Co/Al_2O_3	111.9	0.226	4.2	172.2	7.8	8.1	12.7	1799	1646	58.2	13.1	13.9	7.4	-
4.0%Pt-25%Co/Al_2O_3	113.6	0.237	4.2	163.5	7.4	7.7	13.5	1719	1514	53.5	13.2	14.3	7.2	-
5.0%Pt-25%Co/Al_2O_3	123.4	0.228	3.7	185.1	8.4	8.7	11.8	1758	1502	53.1	15.0	16.4	6.3	8.6
0.276%Ag 25%Co/Al_2O_3	95.5	0.224	4.7	113.0	5.3	5.3	19.3	1688	1688	59.7	8.5	8.9	11.5	9.2
0.553%Ag 25%Co/Al_2O_3	101.4	0.237	4.7	109.1	5.1	5.1	20.1	1784	1784	63.1	7.7	8.2	12.7	-
1.11%Ag 25%Co/Al_2O_3	102.1	0.245	4.8	108.4	5.0	5.1	20.2	1717	1717	60.7	8.2	8.4	12.3	10.0
1.66%Ag 25%Co/Al_2O_3	100.5	0.245	4.9	97.8	4.5	4.6	22.4	1700	1700	60.1	6.9	7.7	13.5	-
2.21%Ag 25%Co/Al_2O_3	97.3	0.236	4.9	90.3	4.1	4.3	24.2	1748	1748	61.8	6.5	6.9	15.0	-
2.76%Ag 25%Co/Al_2O_3	95.6	0.222	4.7	100.7	4.5	4.8	21.7	1729	1729	61.1	7.0	7.8	13.3	9.8

[a]Single point
[b]Assume H_2 desorbed from only Co metal sites.
[c]Assume oxidation of Pt^0 to PtO_2 (Ref. 24) and no oxidation of Ag^0 (Ref. 14).
[d]From analysis of 2θ peak at 37º for Co3O4 (3 1 1) and assuming a contraction of 0.75 in converting to the metal after reduction.

1.2.3.2 Temperature Programmed Reduction

As observed in previous studies, the TPR profiles in Figure 1.10 show that either Pt or Ag promoter can significantly facilitate cobalt oxide reduction. As demonstrated in previous work (Ref. 36), the TPR profile of a Co/Al_2O_3 catalyst is typically comprised of two main peaks; the first peak centered at around 320 °C representing the chemical change of Co_3O_4 to CoO and the another broader peak (about 3 times the area) near 590 °C expressing the subsequent conversion of CoO to metallic Co^0. In a typical TPR profile of both unpromoted and promoted Co/Al_2O_3 catalysts, the first peak is normally sharper than the second peak since the reduction of Co_3O_4 is facile regardless of either metal-support interaction or cluster size, while the subsequent reduction of CoO likely depends on cluster size, with the smaller more strongly interacting clusters being more difficult to reduce (Refs. 12, 18, 22, 25, 37, 38, and 39). Besides the two prominent peaks presented in unpromoted Co/Al_2O_3 catalyst (bottom), a shoulder peak on the second peak at around 700 °C was also observed. This peak was thought of as the smallest Co surface species, with the greatest interaction with the support, while some cobalt remains unreduced until even higher temperatures and is related to a small amount of cobalt that is sacrificed as cobalt aluminate (Ref. 18).

Figure 1.10(a) shows the effect of Pt and Pt loading on TPR profiles. The 0.5%Pt by weight forces the center of the first peak shift to ~175 °C (145 °C shift) and the second peak to 420 °C (170 °C shift) relative to the unpromoted Co/Al_2O_3 catalyst. Increasing Pt causes further decreases in the reduction temperatures of cobalt oxides, but with diminishing returns. Similarly, the addition of 0.276%Ag (atomically equivalent to 0.5%Pt) also shifts both peaks to lower temperatures, to ~270 °C (50 °C shift) and to ~420 °C (170 °C shift) for the first and the second peaks, respectively. Compared with Pt, although Ag addition did not shift the first peak (left) to the low temperature achieved with Pt, interestingly, the shift of the second peak (right) is nearly the same. To complete cobalt oxide reduction to metal particles, reduction temperature used depends on the extent of reduction of the second peak ($CoO \rightarrow Co^0$). Thus, it can be concluded that Ag may serve as a suitable substitute for Pt in facilitating Co reduction. Moreover, the reduction temperature of cobalt oxide appears to decrease with increasing Ag loading, but with marginal improvements. It is widely suggested that H_2 dissociation and spillover on the Pt metal surface is likely to be a catalytic mechanism for accelerating cobalt oxide reduction (Refs. 18, 23, 36, and 38), even though the precise

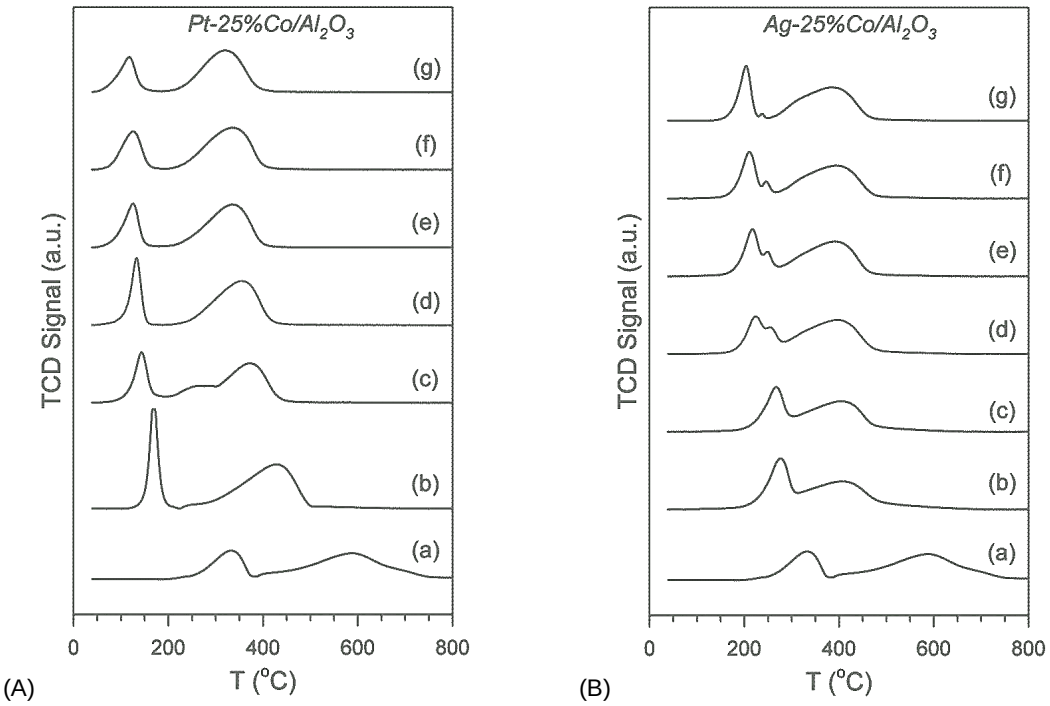

Figure 1.10.—(A) TPR profiles of (a) unpromoted and Pt promoted 25%Co/Al2O3 catalysts, including (b) 0.5%, (c) 1.0%, (d) 2.0%, (e) 3.0%, (f) 4.0%, and (g) 5.0% by weight Pt. (B) TPR profiles of (a) unpromoted and Ag promoted 25%Co/Al_2O_3 catalysts, including (b) 0.276%, (c) 0.553%, (d) 1.11%, (e) 1.66%, (f) 2.21%, and (g) 2.76% by weight Ag, atomically equivalent to those of Pt, respectively.

mechanism remains unclear. However, EXAFS results from our previous work (Ref. 17) and of (Ref. 26) have shown that Pt is in contact with Co at the atomic level, forming Pt-Co bonds, and therefore a chemical effect (i.e., alloy as an active phase) should also be considered. The promotion of Ag in Co/Al_2O_3 catalyst was also reported in our previous work (Ref. 23), and a preliminary XAS study showed that highly dispersed silver oxide particles were present and likely to be in close proximity to cobalt oxide in freshly calcined catalysts. After reduction, the Ag metal phase was detected at high Ag loading. Therefore, it is reasonable to suggest H_2 dissociation and spillover on the Ag metal surface as a possible mechanism. It is important to determine if Ag-Co bonds are detected at lower Ag loadings.

1.2.3.3 Hydrogen Chemisorption/Pulse Reoxidation and XRD

Evidence from TPR profiles illustrates that adding either Pt or Ag leads to a substantial improvement in the reduction of cobalt oxides in Co/Al_2O_3 catalysts and, moreover, the type of metal promoter (i.e., Pt or Ag) and their loadings appear to exhibit significant differences in reducing cobalt oxides. To verify whether those improvements translate into improved Co metal site densities and how well Pt or Ag facilitate Co oxide reduction as a function of loading, H_2 chemisorption and pulse reoxidation were utilized. Chemisorption of hydrogen following reduction in hydrogen at 350 °C for 10 h at atmospheric pressure was utilized to obtain the number of metal surface atoms, which is calculated by the amount of H_2 desorbed from TPD analysis (Ref. 18). It was found that with Pt the number of metal sites more than doubled compared to the unpromoted catalyst, and metal site density also increased with increasing Pt loading. For Ag promoter, metal site density also approximately doubled but appeared to decrease with further increases in Ag loading. These improvements for both Pt and Ag promoted catalysts are consistent with the temperature shifts observed in TPR in Figure 1.10 as mentioned previously. Because of the ability of Pt and Ag metal to adsorb H_2, the measurement of the actual Co^0 metal surface sites may be complicated. Thus, in this report, we represent the dispersion by 2 terms: total metal dispersion and Co^0 metal dispersion (by assuming H_2 only from Co

surface). By taking into account both Co and metal promoter, the uncorrected metal dispersion (i.e., which erroneously presumes that the Co and metal promoter are completely reduced) shown in column 6 of Table 1.7 was increased significantly after adding promoter. Adding 5.0% Pt by weight shifts % metal dispersion to 8.36% (threefold higher than unpromoted), which is also more pronounced than at lower Pt loading. This is different from the case of Ag, where increasing Ag slightly decreases % metal dispersion relative to lower Ag loadings, while just up to around a twofold higher improved % metal dispersion from the unpromoted catalyst was observed at the lowest loading of 0.276%Ag (atomically equivalent to 0.5%Pt). By ignoring H_2 chemisorption on metallic Pt and Ag, the uncorrected Co dispersion is obtained, and uncorrected Co dispersion is slightly higher than uncorrected metal dispersion but the same trend remains. Quantifying the degree of reduction of cobalt is necessary in order to obtain the corrected metal dispersion and a more accurate estimate of Co cluster size. The oxygen pulse reoxidation experiment was immediately performed after the TPD experiment. The total oxygen consumed is directly related to total metal reduced with the assumption that Co oxidized into Co_3O_4. For metal promoted Co/Al_2O_3 catalyst, the possibility of metallic metal promoter to be simultaneously oxidized with Co metal during pulse reoxidation must be considered. Pt metal should be oxidized into PtO_2 after complete reoxidation by oxygen pulses. The previous study of the oxidation of Pt(1 1 1) by gas phase oxygen atoms by Weaver et al. (Ref. 24) suggested PtO_2 as a main platinum oxide species instead of PtO after oxidation at 177 °C; moreover it can be thermally tolerated up to 427 °C (Ref. 24). The thermal decomposition of PtO_2 ($PtO_2 \rightarrow Pt + O_2$) on carbon has been reported at 500 °C (Ref. 40), so that PtO_2 is more likely to exist after oxygen pulse reoxidation in our case. Accordingly, to correct O_2 consumption by Co metal sites, O_2 consumed by Pt ($Pt + O_2 \rightarrow PtO_2$) must be deducted. In the case of Ag, the O_2 consumed by Ag metal is negligible because of the instability of any silver oxide forms at 350 °C, at which pulse reoxidation is performed (Ref. 23).

It is clear that addition of either Pt or Ag led to a considerable increase in the extent of reduction relative to the unpromoted catalyst (i.e., ~70% increase for either 0.5%Pt or 0.276%Ag promoted catalysts), which is consistent with the results of reduction temperature shifts to lower temperature as observed in the TPR profiles. Therefore, it should be stressed that the role of Pt and Ag promoter is not merely to improve the reducibility of cobalt oxide but primarily to augment the Co^0 active site densities, as previously demonstrated (Refs. 17, 18, 23, 25, 26, and 36). Considering the effect of Pt loading, it appears that increasing Pt slightly decreases %Co reduction at high loading, as estimated by O_2 titration, and this is consistent with TPR. This in turn impacts the corrected average Co cluster size, which appears to become smaller as Pt loading increases. It is suggested that higher Pt contents lead to a greater fraction of smaller cobalt oxide clusters being reduced, thereby resulting in an increase in the fraction of smaller Co clusters.

The trend of Co cluster size versus Pt loading is further supported by the size estimated by X-ray diffraction (i.e., the Co crystal size of Co_3O_4 at $2\theta = 37°$ after applying a contraction factor of 0.75). XRD results show that in all cases, the estimated Co^0 size is similar. Interestingly, while at low loadings of either Ag or Pt, the chemisorption results are close to the estimates from XRD, at higher loadings of Pt there is a deviation toward slightly smaller size, and with Ag there is a deviation toward slightly larger size. The latter may in part reflect a diffusion problem of O_2 penetrating the core of larger metal particles (Ref. 16). As we will show from reaction testing data, the deviations are likely due not to a real change in actual cluster size, but rather to promoter location. With Pt, it appears that there may be a fraction of Pt exposed on the surface and contributing to the H_2-TPD. With Ag, there is likely a fraction that essentially blocks Co surface sites, resulting in a slight attenuation of the Co site density. While an increase in BET surface area and a decrease in average pore radius after increasing Pt loading suggest that at the higher Pt loadings, a fraction of Pt resides on the support, because no Pt-Pt bonds are observed in EXAFS (to be discussed) suggests that the Pt is incorporated with Co^0 clusters during reduction. For Ag promoter, the agglomeration of Ag to form larger Ag clusters during reduction at 350 °C was proposed in our previous report (Ref. 23). Thus, the possibility of some pore blocking at high Ag loading following activation should be considered. Note that there was no significant change in BET results even at high Ag loadings after calcination, implying that the Ag is, prior to reduction, well dispersed on the surface of Co/Al_2O_3 catalyst as small Ag_2O clusters (Refs. 23 and 27). The Ag_2O clusters formed after calcination are likely located near Co_3O_4 to play a pivotal role in facilitating cobalt oxide reduction as described above. In conclusion, although Ag promoter is able to satisfactorily

promote Co reduction, it may be unable to provide similar Co site densities as observed with Pt promoter. However its promoting ability and lower cost make it alluring as a possible alternative promoter.

1.2.3.4 XANES and EXAFS Spectroscopies

The normalized XANES spectra measured at the Pt L_{III}-edge in Figure 1.11(A) consist of two spectra of the 0.5%Pt-25%Co/Al_2O_3 catalysts: the one calcined (350 °C, in air flow, 4 h) and the other reduced (350 °C, in 4%H_2/He flow, 10 h), Pt metal, and two platinum oxides: PtO and PtO_2. The Pt L_{III} absorption edge at ~11.566 keV of the calcined catalyst is close to that of PtO_2, which absorbs at 11.566 keV edge (i.e., +2 eV shift from E_0 of 11.564) (Ref. 14). By comparing the XANES region (i.e., $E_0 - 100$ eV < E < $E_0 + 40$ eV; E_0 = 11.564 keV), the XANES line shapes of calcined Pt-25%Co/Al_2O_3 and PtO_2 are also similar. Moreover, the white intensity of calcined catalyst more closely resembles that of PtO_2 rather than PtO. The white line intensity in this case for Pt is related to the d-electron density of states (Ref. 41). An increase in the white line intensity directly shows a decrease in the number of electrons in the d orbital, such that the white line of PtO (Pt^{2+}) and PtO_2 (Pt^{4+}) can be distinguished. An investigation of Pt in calcined Pt/Co catalyst has also shown that Pt is in the Pt^{4+} oxidation state (Ref. 25). On the other hand, after reduction PtO_2 is converted into Pt metal as evidenced by comparing the XANES spectrum to that of the Pt metal reference.

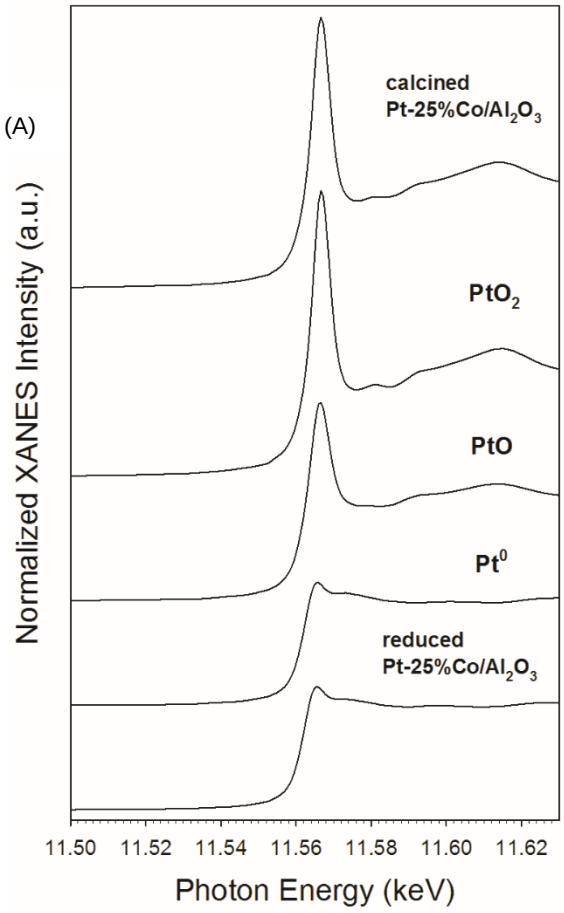

Figure 1.11.—(A) Normalized XANES spectra at the Pt L_{III}-edge of Pt-25%Co/Al_2O_3 catalysts (calcined and reduced) and Pt reference compounds; PtO, PtO_2, and Pt^0. (B) (left) TPR-XANES spectra and (right) their corresponding linear combination fittings from reference spectra in Figure 1.11(A) of, moving down, 0.5%Pt-25%Co/Al_2O_3; 2.0%Pt-25%Co/Al_2O_3; and 5.0%Pt-25%Co/Al_2O_3. (C) Normalized XANES spectra at the Pt L_{III}-edge of Pt promoted Co/Al_2O_3 catalysts with different loadings; (solid line) 0.5%Pt, (dotted line) 2.0%Pt, and (dashed line) 5.0%Pt, after TPR after cooling to ambient conditions.

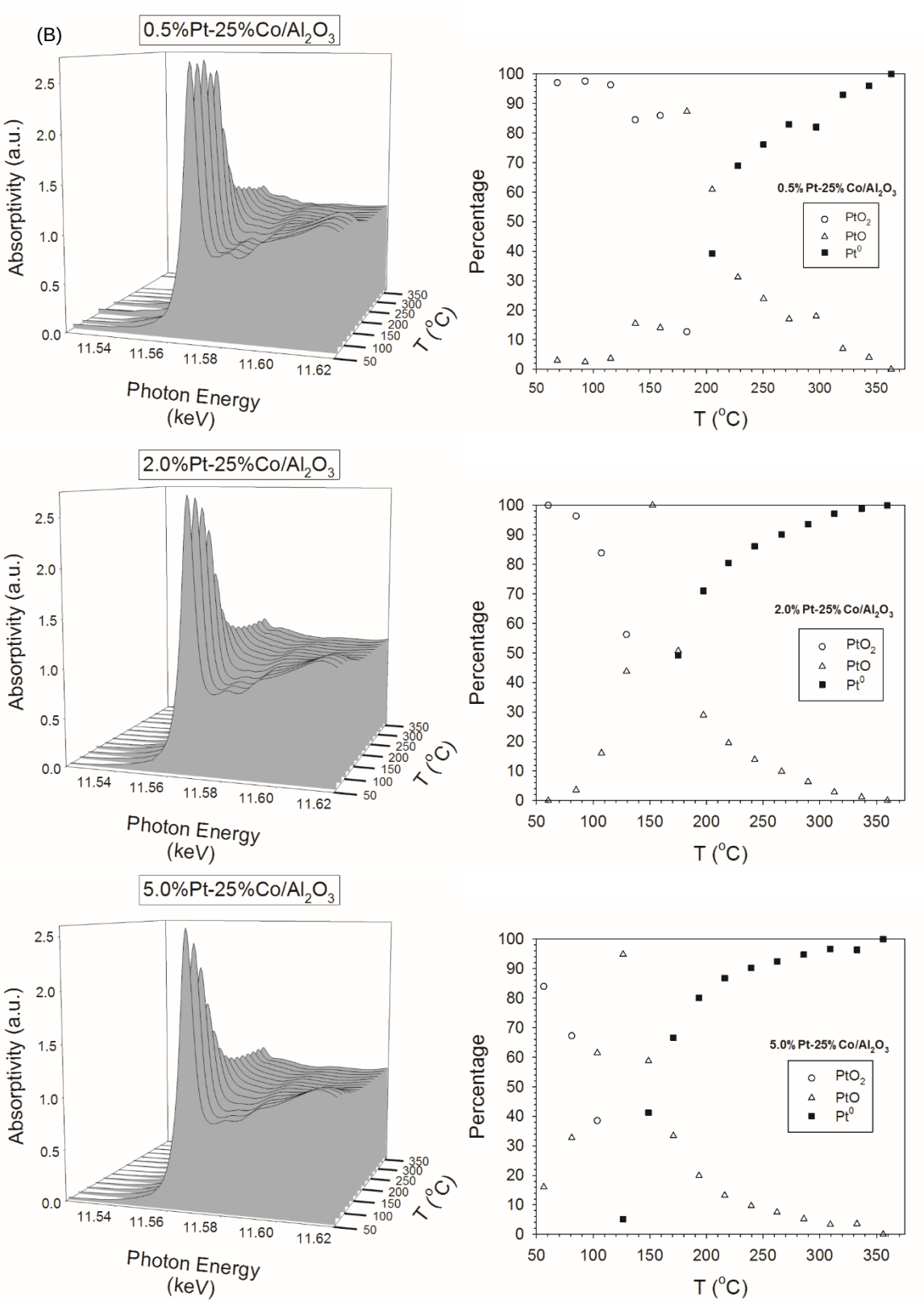

Figure 1.11.—Continued.

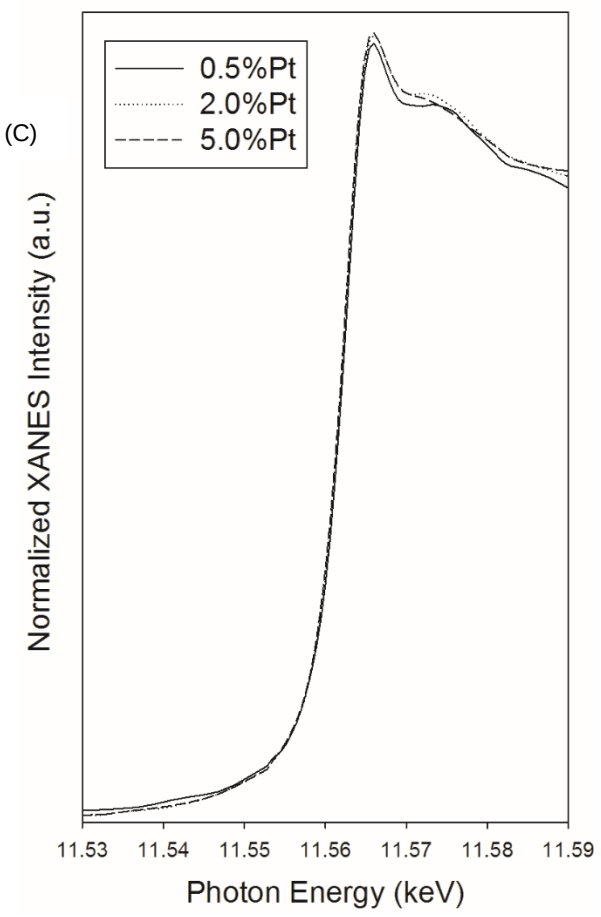

Figure 1.11.—Concluded.

To observe the temperature-dependent changes of the oxidation state of Pt during H_2 reduction, the TPR-XANES technique was applied. TPR-XANES spectra of Pt- 25%Co/Al_2O_3 catalyst with 3 different Pt loadings are depicted in Figure 1.11(B). It is clearly seen that XANES spectra of all catalysts change significantly with increasing reduction temperature as platinum oxides are converted to metallic Pt. Platinum (II) oxide (PtO) is an intermediate Pt species, which is detectable by XANES. A lower white line intensity compared to PtO_2, a higher white line intensity compared to Pt metal, and a +1 eV shift from E_0 at the Pt L_{III}–edge were evident. Thus, linear combination fittings of the XANES spectra of the catalyst samples were performed using PtO_2, PtO, and Pt metal XANES spectra and the fitting results are shown on the right side of Figure 1.11(B). It was found that Pt loading has a measurable effect on its reducibility. Increasing Pt noticeably decreases the reduction temperature of PtO_2 and PtO, respectively, thereby allowing the Pt metal to form at lower temperature. The 18%PtO was found in 5.0%Pt-25%Co/Al_2O_3 catalyst, even at the temperature of reduction as low as 50 °C. The maximum content of PtO in each catalyst sample was found at different temperatures, namely, 185, 150, and 125 °C for 0.5%Pt, 2.0%Pt, and 5.0%Pt-25%Co/Al_2O_3, respectively. The onset temperature of Pt metal formation was also found to decrease with increasing loading (210, 175, and 125 °C were observed at 0.5%Pt, 2.0%Pt, and 5.0%Pt-25%Co/Al_2O_3, respectively). However, platinum oxides in all catalysts were successfully reduced into Pt metal at 350 °C, as also shown in Figure 1.11(C). In conclusion, the rate of platinum oxide conversion to Pt metal is improved by adding more Pt. It has been suggested that a nucleation/growth model may dominate this reduction process. That is, once Pt metal nuclei have formed, they serve to facilitate other nearby metal oxides to be reduced, which is possibly by a H_2 dissociation and spillover mechanism; moreover, increasing Pt loading, while it is costly to do so, accelerates this process. Pt metal formed during the reduction process facilitates not merely

further platinum oxide reduction but cobalt oxide reduction as well, as the reduction temperatures of cobalt oxides were obviously shifted to lower temperature for Pt-25%Co/Al_2O_3 catalyst as shown in Figure 1.10(A).

To investigate the local atomic structure of Pt promoted Co/Al_2O_3 catalysts, EXAFS analysis was performed. Figure 1.12(A) provides the k^3-weighted EXAFS Fourier Transform magnitude spectra of the Pt L_{III}-edge for relevant platinum reference compounds (i.e., Pt^0 and PtO_2) for calcined and reduced catalysts. The FT magnitude spectrum of the calcined catalyst is comprised of peaks for Pt-O and Pt-Pt coordination. The spectra differed from bulk PtO_2, as the peaks representing the first shell coordination of Pt-O and Pt-Pt are both shifted to lower distance compared to the bulk PtO_2, possibly due to the contraction of those bonds for small platinum oxide particles. After reduction, the reduced catalyst showed a distinct peak at about 2.1 Å in the phase-uncorrected spectra. This peak position is not the first coordination shell of Pt metal, which is located at around 2.7 Å in the phase uncorrected spectra. The change in Pt coordination environment with the reduction temperature can be observed in TPR-EXAFS spectra in Figure 1.12(B). At low temperature Pt coordinates with both oxygen and Pt atoms as Pt is in the form of PtO_2; then, at around 175 °C Pt-O coordination decreases, while a distinct peak (~ 2.1 Å) starts to form and becomes more obvious as the reduction temperature increases. As Pt atom was the core atom, the change in the position of the FT magnitude of Pt-Pt bond (~0.6 Å shift closer to the Pt core atom) indicates that Pt-Pt bonds were not detected after reduction but, rather, Pt-Co bonds were formed (Refs. 17, 25, and 26). Though Pt-Co bond formation has been explored, the effect of Pt loading on the formation of this bimetallic bond has not been disclosed. The results of the modeling procedure using FEFFIT for the k^3-weighted EXAFS Fourier transform and filtered k^3-weighted $\chi(k)$ spectra of Pt-promoted catalyst following TPR experiment and cooling to ambient conditions are shown in Figure 1.12(C). The well-defined peak corresponds to Pt-Co bonding (Refs. 17 and 26). The solid lines in Figure 1.12(C) show the experimental data, while the circles provide the best fit. The fitting parameters are summarized in Table 1.8. Generally, the r-factor value of <0.02 indicates a good fit; all catalyst spectra fall below this value. The results suggest that the majority of Pt is in intimate contact with the cobalt cluster. The preference of Pt to form bonds with Co is supported by results measured for samples with different Pt loading, even when high amounts of Pt are applied. Moreover, increasing Pt does not appear to have a significant effect on Pt-Co coordination number among reduced catalysts with different Pt loading (see numerical results of Pt-Co coordination number in column 2 of Table 1.8). Figure 1.12(D), a graph of overlays, depicts a comparison of Pt-Co FT magnitude peak intensity of all catalysts after reduction, and although some differences in intensity are observed, they are not statistically significant, as mentioned previously. Thus, it is suggested that even at Pt loadings as high as 5%, Pt^0 still remains in good contact with Co^0. While the authors are fully aware that high costs already preclude the use of Pt at high loadings, the loading study serves as a point of reference for comparing potentially less expensive promoters, where higher promoter loadings may be deemed acceptable.

TABLE 1.8.—RESULTS OF EXAFS FITTING PARAMETERS FOR REFERENCES ACQUIRED NEAR THE Pt L_{III}-EDGE. THE FITTING RANGES WERE APPROXIMATELY Δk = 3 TO 12 $Å^{-1}$ AND ΔR = 1.6 TO 2.83 Å, S_0^2 = 0.9

Catalyst	N Pt-Co	R Pt-Co, Å	e_0, eV	σ^2, $Å^2$	r-factor
0.5%Pt-25%Co/Al_2O_3	6.6 (0.59)	2.549 (0.007)	6.00 (1.02)	0.0068 (0.00087)	0.0060
1.0%Pt-25%Co/Al_2O_3	7.0 (0.67)	2.558 (0.008)	5.99 (1.09)	0.0076 (0.00097)	0.0067
2.0%Pt-25%Co/Al_2O_3	7.6 (0.61)	2.555 (0.006)	6.18 (0.915)	0.0069 (0.00079)	0.0048
3.0%Pt-25%Co/Al_2O_3	6.7 (0.61)	2.557 (0.007)	5.64 (1.05)	0.0067 (0.00090)	0.0064
4.0%Pt-25%Co/Al_2O_3	7.2 (0.67)	2.557 (0.007)	5.83 (1.06)	0.0062 (0.00088)	0.0065
5.0%Pt-25%Co/Al_2O_3	6.6 (0.63)	2.560 (0.008)	5.54 (1.08)	0.0072 (0.00094)	0.0067

(A)

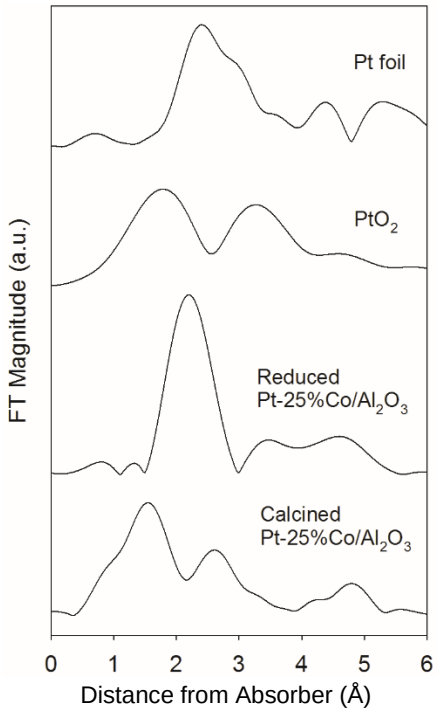

(B)

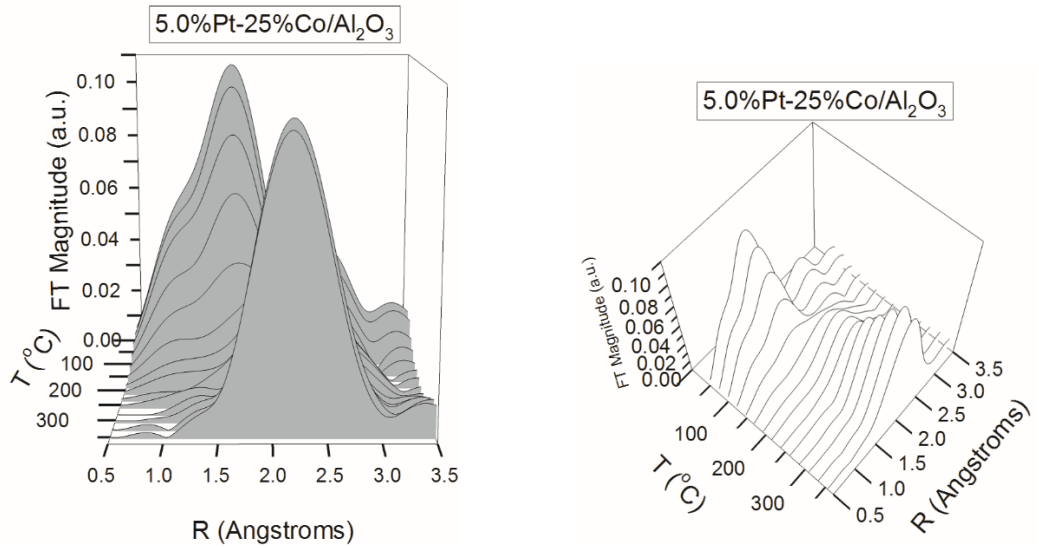

Figure 1.12.—(A) k^3-Weighted EXAFS Fourier Transform magnitude spectra of Pt promoted Co/Al_2O_3 catalysts and Pt reference compounds. (B) TPR-EXAFS k^3-Weighted Fourier Transform magnitude spectra of 5.0%Pt-25%Co/Al_2O_3, (C) k^3-weighted EXAFS Fourier Transform magnitude spectra of Pt-promoted catalysts after TPR after cooling to ambient conditions: (a) raw $k^3 \cdot \chi(k)$ vs. k data; (b) filtered $k^3 \cdot \chi(k)$ vs. k data (solid line) and resulting fitting (filled circles); (c) Fourier transform magnitude spectra (solid line), and first shell fitting (filled), moving downward, (I) 0.5%Pt-25%Co/Al_2O_3; (II)1.0%Pt-25%Co/Al_2O_3; (III) 2.0%Pt-25%Co/Al_2O_3; (IV) 3.0%Pt-25%Co/Al_2O_3; (V) 4.0%Pt-25%Co/Al_2O_3; (VI) 5.0%Pt-25%Co/Al_2O_3. (D) k^3-Weighted Fourier Transform magnitude spectra after the TPR after the catalysts were cooled to ambient conditions, (a) 0.5%Pt-25%Co/Al_2O_3; (b) 1.0%Pt-25%Co/Al_2O_3; (c) 2.0%Pt-25%Co/Al_2O_3; (d) 3.0%Pt-25%Co/Al_2O_3; (e) 4.0%Pt-25%Co/Al_2O_3; (f) 5.0%Pt-25%Co/Al_2O_3.

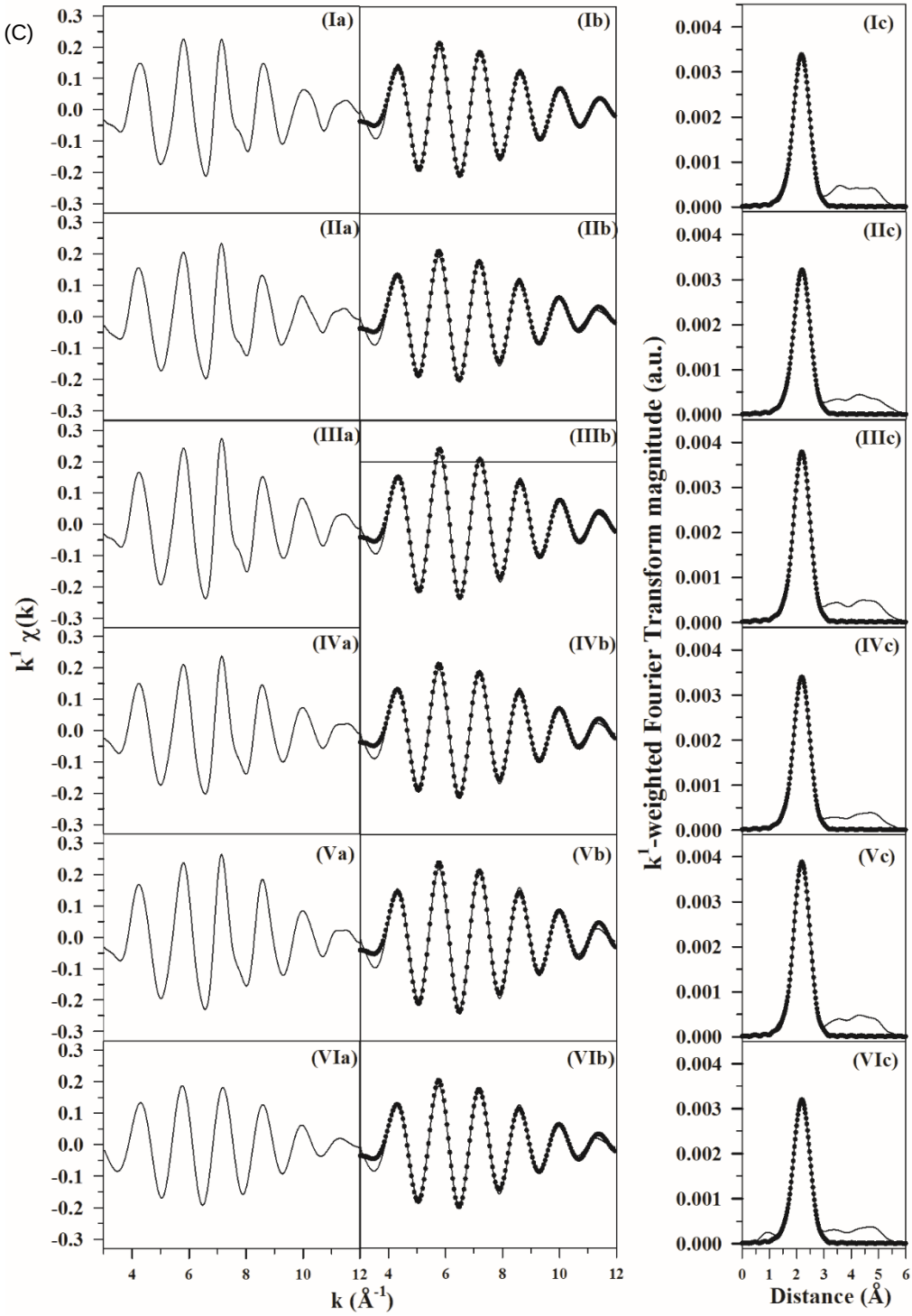

Figure 1.12.—Continued.

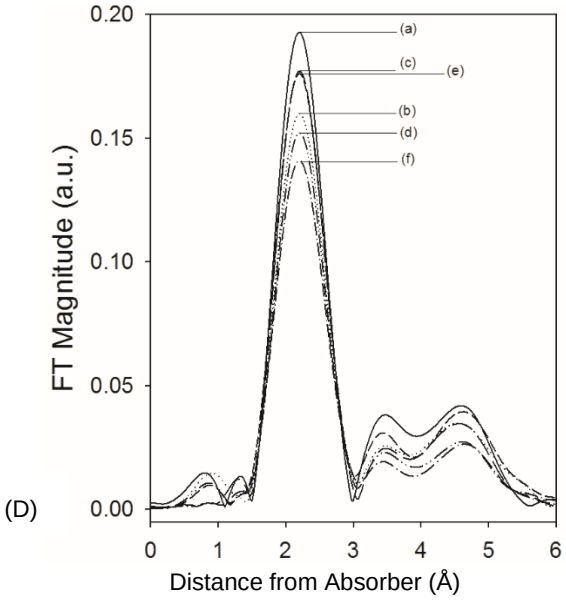

Figure 1.12.—Concluded.

Investigating silver promoter in Ag promoted Co/Al_2O_3 catalyst, XAS scanning at the Ag K-edge energy was performed for both relevant Ag reference compounds and catalysts (before and after reduction). As a result, the XANES spectra and the local atomic structure of Ag in this catalyst were revealed in this work. As shown in Figure 1.13(A), Ag in the calcined Ag-25%Co/Al_2O_3 catalyst did not resemble either bulk Ag_2O or bulk AgO references. Referring to results from previous work (Ref. 27), which investigated Ag_2O-B_2O_3 mixed oxides and with our previous report (Ref. 23), the spectrum representing the calcined catalyst is likely indicative of highly dispersed Ag_2O particles located in close proximity to cobalt oxide domains. On the other hand, the spectrum of reduced 0.276%Ag-25%Co/Al_2O_3 matches that of the Ag foil. Moreover, EXAFS fitting demonstrated that Ag-Ag coordination number in the reduced catalyst is not as large as that of the Ag foil (i.e., with FCC structure and first shell coordination number of 12). To observe electronic changes of Ag during the reduction process, a TPR-XANES experiment was conducted and the resulting spectra of catalysts with 3 different Ag loadings are depicted in Figure 1.13(B). In Figure 1.13(B) (left), the white line intensity decreased with increasing reduction temperature, indicating a gradual change from oxide to metal. A linear combination fitting of the XANES of the catalyst samples with different Ag loadings using the Ag_2O and Ag metal XANES spectra leads to the results in Figure 1.13(B) (right). As the amount of Ag increases, Ag metal tends to form at lower temperature. The nearly equal amount (50%-50%) of Ag_2O and Ag metal is observed at 165, 130, and 110 °C in 0.276%Ag, 1.11%Ag, and 2.76%Ag-25%Co/Al_2O_3 catalysts, respectively. The silver oxide present on each catalyst is completely reduced to the metallic form of Ag after H_2 activation at 350 °C, as shown in Figure 1.13(C). A comparison of normalized XANES spectra of Ag-promoted Co/Al_2O_3 catalysts was obtained by scanning the catalysts after TPR and cooling to ambient conditions. Thus, following activation in H_2, highly dispersed silver oxides in this catalyst are transformed to Ag metal, which further facilitates the reduction of Co_3O_4 and, subsequently, CoO species, perhaps via a H_2 dissociation and spillover mechanism (Refs. 18 and 36).

Figure 1.14(A) shows the k^1-weighted EXAFS Fourier Transform magnitude spectra of silver reference compounds (Ag^0, Ag_2O, and AgO) and catalysts (before and after reduction). In good agreement with the interpretation of the XANES spectra, the EXAFS spectra show that neither the Ag_2O spectrum nor the AgO spectrum is identical to that of the calcined catalyst, implying that silver oxides in the calcined catalyst interact with the Al_2O_3 support. After reduction, two prominent peaks were formed. By first qualitatively comparing peaks with the Ag^0 foil, the one located at a distance (~2.8 Å) further from the absorbing Ag atom suggests Ag-Ag coordination, while the nearer peak

(~2.6 Å) appears to indicate Ag-Co coordination. However, it should be noted that a satellite peak for the Ag foil also appears at this lower distance. Thus, more rigorous fitting is required to demonstrate the identity of atoms in the first coordination shell. The peak corresponding to those bond distances become more prominent with increasing degree of reduction, as shown in Figure 1.14(B). To verify those peaks, a fitting procedure using FEFFIT for the k^1-weighted EXAFS Fourier transform and filtered k^1-weighted $\chi(k)$ spectra was performed for the spectra recorded after reduction and cooling to close to ambient conditions. The results of the fit are displayed in Figure 1.14(C) and fitting parameters are summarized in Table 1.9. A fitting was attempted for the 0.276%Ag-25%Co/Al_2O_3 catalyst using only Ag-Ag coordination, but this resulted in a very poor fitting (Table 1.9). Thus, the peak at lower distance is not solely due to the presence of a satellite peak for Ag-Ag coordination, as observed in the Fourier transform magnitude spectrum of Ag^0 foil. The model with the best fitting was obtained when the first and the second peak in reduced catalysts were fitted with a model that included both Ag-Co and Ag-Ag coordination, respectively. The first shell of Ag-Co coordination number follows the trend 0.276%Ag-25%Co/Al_2O_3 > 0.553%Ag-25%Co/Al_2O_3 = 1.11%Ag-25%Co/Al_2O_3 = 1.66%Ag-25%Co/Al_2O_3 > 2.21%Ag-25%Co/Al_2O_3 > 2.76%Ag-25%Co/Al_2O_3. On the other hand, the trend of first shell Ag-Ag coordination number is opposite, with Ag likely forming isolated particles at higher Ag loading. This is evident when the spectra are superimposed in Figure 1.14(D). Therefore, the results expand upon our previous work for Ag-Co/Al_2O_3 catalyst, and reveal that in addition to the formation of Ag-Ag bonds due to segregation of Ag during reduction (Ref. 23), Ag-Co bonds are indeed present, such that this bimetallic species may play a role in facilitating Co reduction, as well as impacting catalytic performance during FTS.

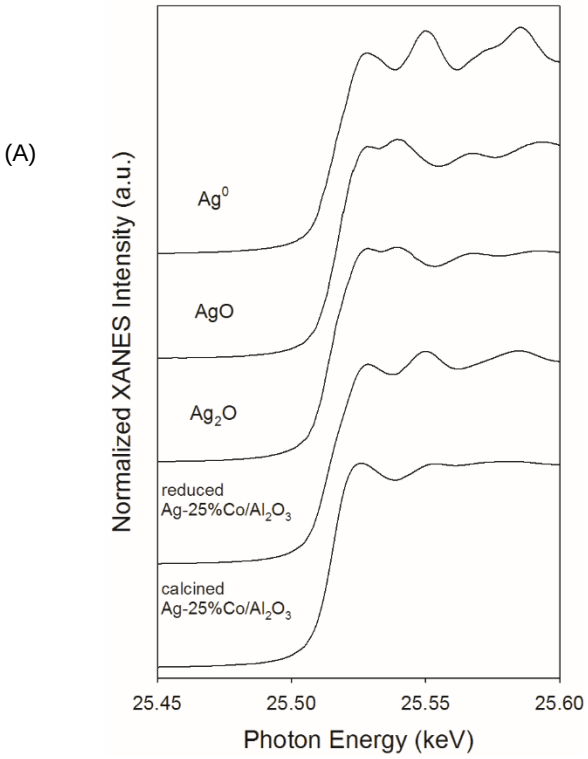

Figure 1.13.—(A) Normalized XANES spectra at the Ag K-edge of Ag-25%Co/Al_2O_3 catalysts (calcined and reduced) and Ag reference compounds; AgO, Ag_2O, and Ag^0. (B) (left) TPR-XANES spectra and (right) their corresponding linear combination fittings from reference spectra in Figure 1.13(A) of, moving down, 0.276%Ag-25%Co/Al_2O_3; 1.11%Ag-25%Co/Al_2O_3; and 2.76%Ag-25%Co/Al_2O_3. (C) Normalized XANES spectra at the Ag K-edge of Ag promoted Co/Al_2O_3 catalysts with different loadings; (solid line) 0.276%Ag, (dotted line) 1.11%Ag, and (dashed line) 2.76%Ag, after TPR after cooling to ambient conditions.

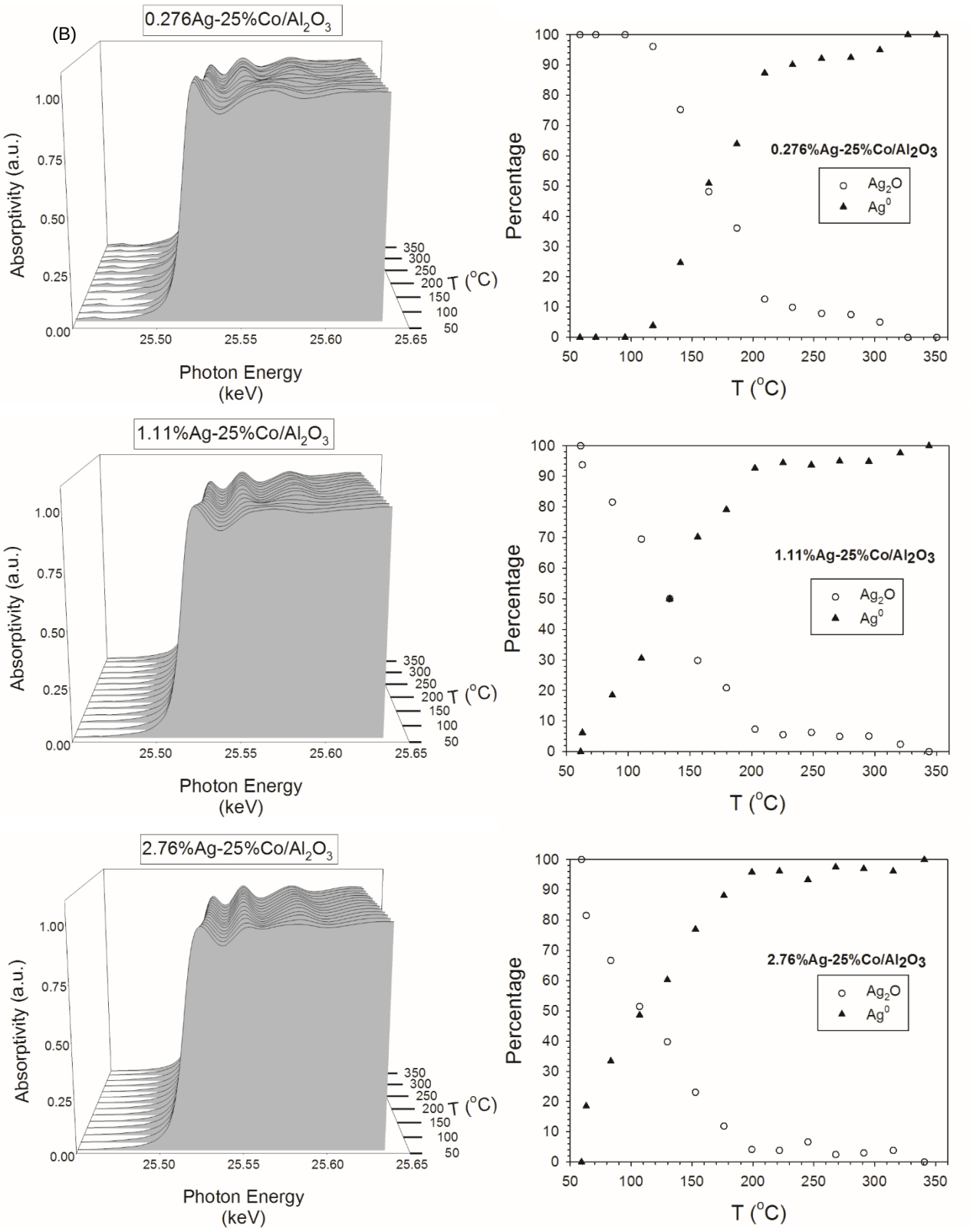

Figure 1.13.—Continued.

(C)

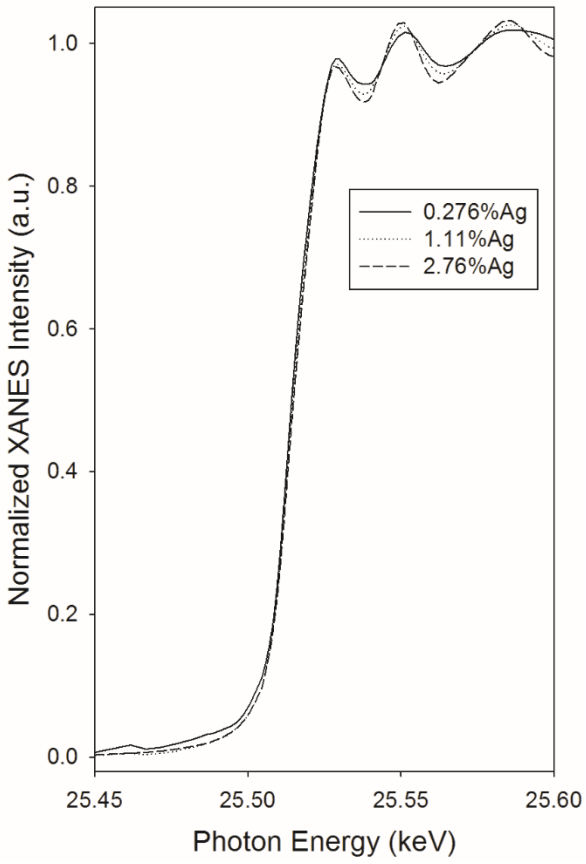

Figure 1.13.—Concluded.

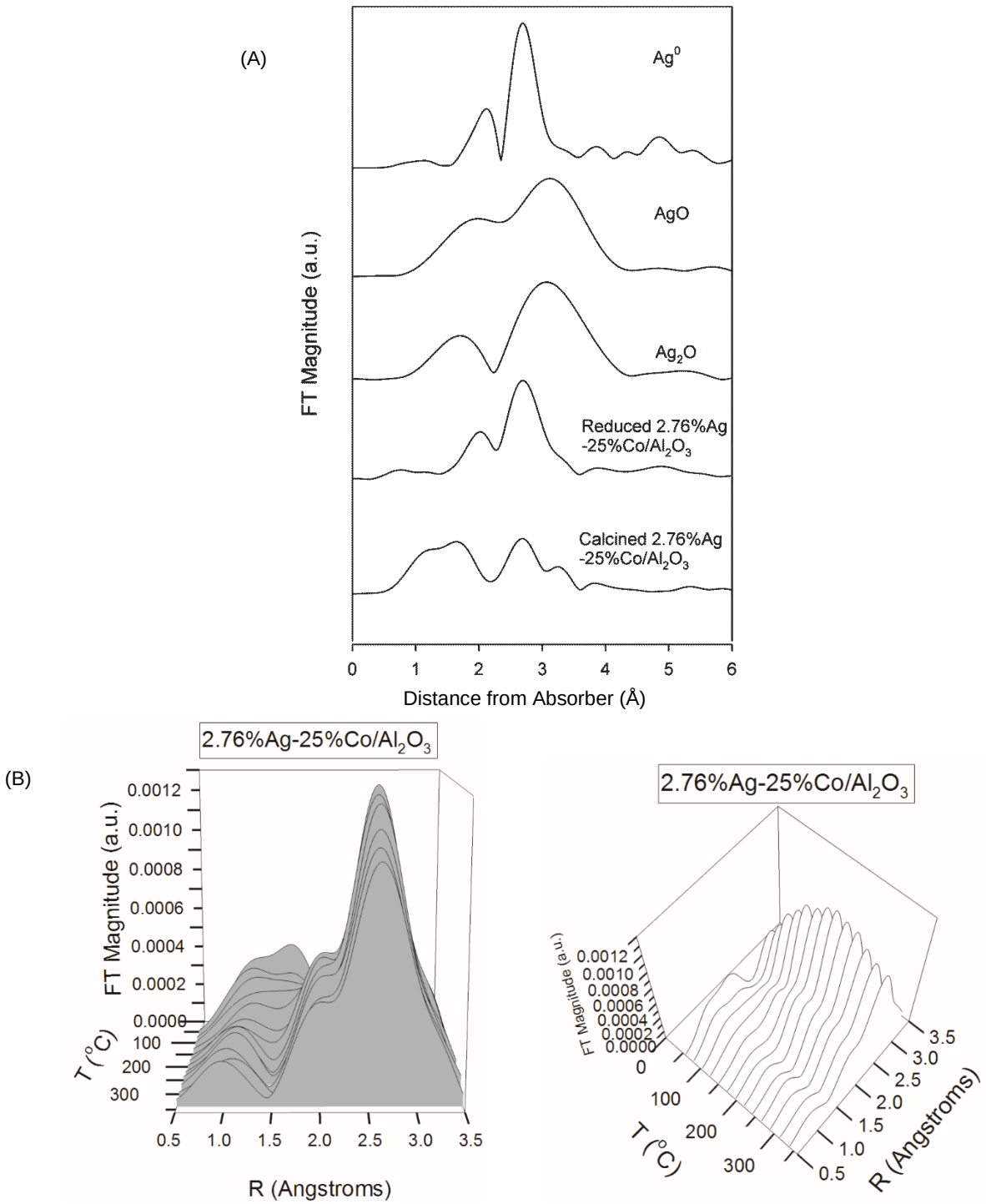

Figure 1.14.—(A) k^1-Weighted EXAFS Fourier Transform magnitude spectra of Ag promoted Co/Al_2O_3 catalysts and Ag reference compounds (not to scale), (B) TPR-EXAFS k^1-Weighted Fourier Transform magnitude spectra of 2.76%Ag-25%Co/Al_2O_3, (D) k^1-weighted EXAFS Fourier Transform magnitude spectra of Ag-promoted catalysts after TPR after cooling to ambient conditions: (a) raw $k^1 \cdot \chi(k)$ vs. k data; (b) filtered $k^1 \cdot \chi(k)$ vs. k data (solid line) and resulting fitting (filled circles); (c) Fourier transform magnitude spectra (solid line), and first shell fitting (filled), moving downward, (I) 0.276%Ag-25%Co/Al_2O_3; (II)0.553%Ag-25%Co/Al_2O_3; (III) 1.11%Ag-25%Co/Al_2O_3; (IV) 1.66%Ag-25%Co/Al_2O_3; (V) 2.21%Ag-25%Co/Al_2O_3; (VI) 2.76%Ag-25%Co/Al_2O_3. (C) k^1-Weighted Fourier Transform magnitude spectra after the TPR after the catalysts were cooled to ambient conditions, (a) 0.276%Ag-25%Co/Al_2O_3; (b) 0.553%Ag-25%Co/Al_2O_3; (c) 1.11%Ag-25%Co/Al_2O_3; (d) 1.66%Ag-25%Co/Al_2O_3; (e) 2.21%Ag-25%Co/Al_2O_3; and (f) 2.76%Ag-25%Co/Al_2O_3.

(C)

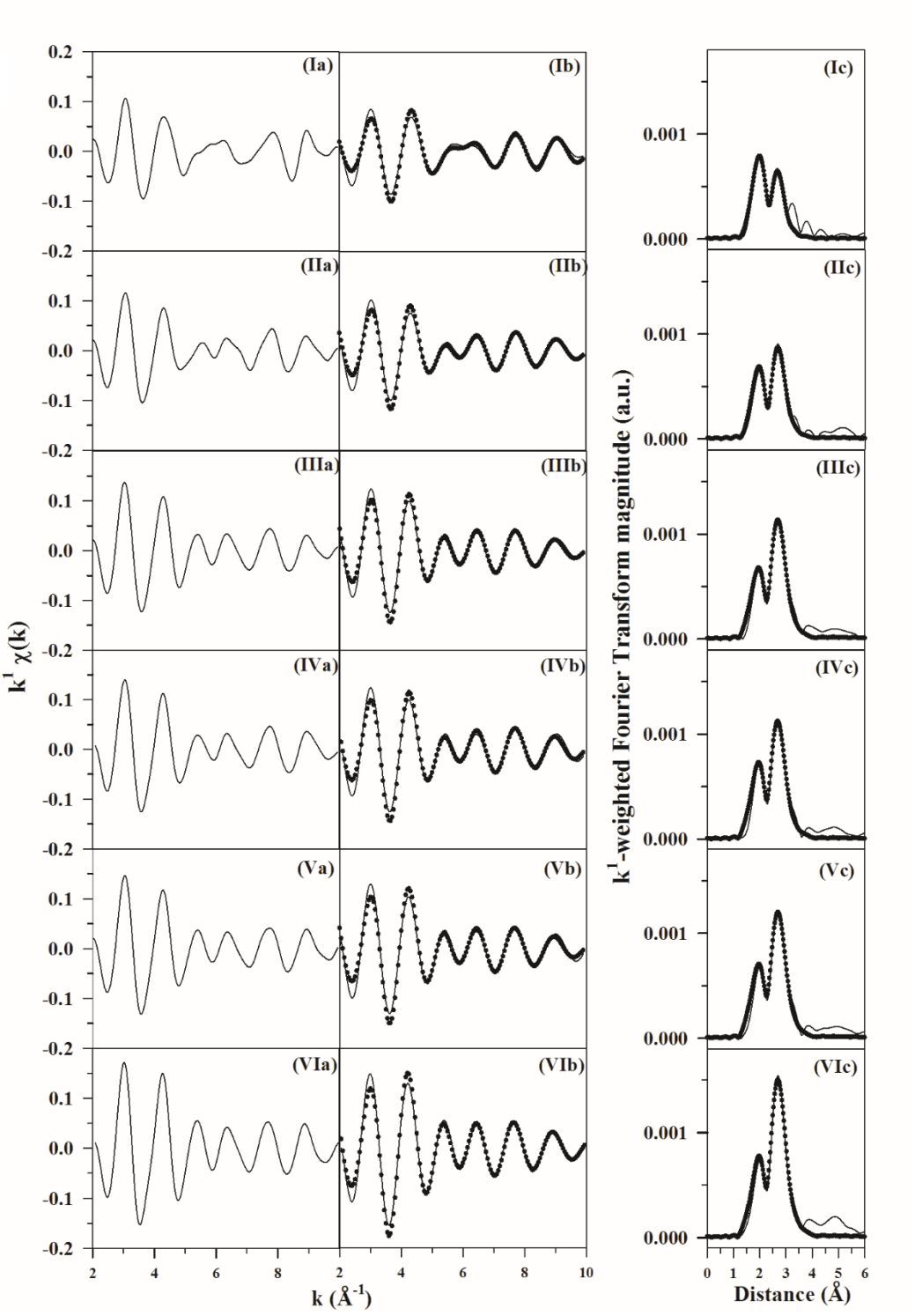

Figure 1.13.—Continued.

(D)

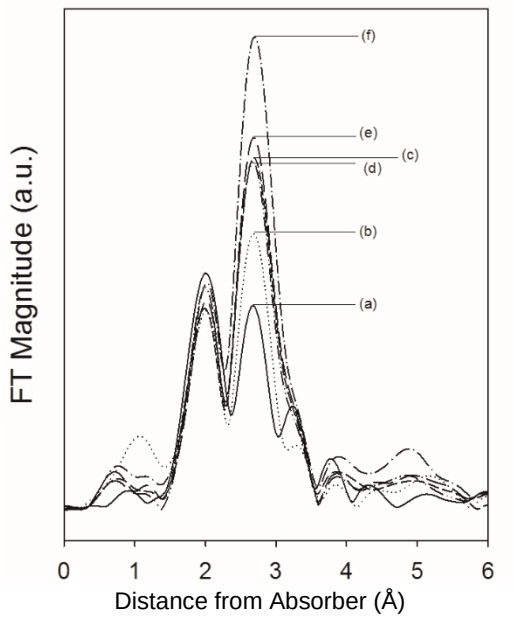

Figure 1.13.—Concluded.

TABLE 1.9.—RESULTS OF EXAFS FITTING PARAMETERS FOR REFERENCES ACQUIRED NEAR THE Ag K-EDGE. THE FITTING RANGES WERE APPROXIMATELY Δk = 2-10 $Å^{-1}$ AND ΔR = 1.5-3.1 Å, S_0^2 = 0.9

Catalyst	N Ag-Co	R Ag-Co, Å	N Ag-Ag	R Ag-Ag Å	N_{Ag-Co}/N_{Ag-Ag}	e_0, eV	σ^2, $Å^2$	r-factor
Ag foil	-	-	12	2.858	-	0.370	0.0106	0.015
				(0.0081)		(0.493)	(0.0007)	
Ag-Ag fitting only								
0.276%Ag-25%Co/Al_2O_3	-	-	6.6 (4.5)	2.764 (0.084)	-	–1.38 (3.48)	0.0277 (0.0178)	0.212
Ag-Co and Ag-Ag fitting								
0.276%Ag-25%Co/Al_2O_3	2.0 (0.46)	2.676 (0.017)	3.4 (0.59)	2.758 (0.018)	0.59	–1.92 (1.00)	0.0112 (0.0027)	0.022
0.553%Ag-25%Co/Al_2O_3	1.8 (0.46)	2.657 (0.018)	5.0 (0.64)	2.786 (0.014)	0.36	–0.879 (0.724)	0.0147 (0.0021)	0.016
1.11%Ag-25%Co/Al2O_3	1.8 (0.49)	2.649 (0.020)	7.2 (0.73)	2.810 (0.012)	0.25	–0.541 (0.582)	0.0169 (0.0019)	0.011
1.66%Ag-25%Co/Al_2O_3	1.8 (0.57)	2.663 (0.025)	6.7 (0.86)	2.804 (0.014)	0.27	–0.896 (0.751)	0.0155 (0.0023)	0.017
2.21%Ag-25%Co/Al_2O_3	1.7 (0.59)	2.660 (0.026)	7.4 (0.90)	2.817 (0.014)	0.23	–0.506 (0.691)	0.0164 (0.0022)	0.015
2.76%Ag-25%Co/Al_2O_3	1.4 (0.52)	2.667 (0.030)	8.7 (0.85)	2.829 (0.011)	0.16	–0.340 (0.570)	0.0155 (0.0017)	0.0098

The coordination of the promoter with Co is fundamentally different, as Ag offers a much lower degree of coordination to Co on a per atom basis relative to Pt at the same atomic ratio. Moreover, Ag-Ag first shell coordination was observed even at the lowest Ag loadings after complete activation in H_2, while Pt-Pt bonds were not apparent, even at levels as high as 5%Pt. However, either Pt or Ag promoted Co/Al_2O_3 catalysts can significantly facilitate the reduction of cobalt oxides as shown by the results of TPR and H_2 chemisorption/pulse reoxidation above. This

significantly different atomic structure of Ag promoter relative to Pt, a commercial promoter, could conceivably pose problems in terms of maintaining coordination following regeneration cycles.

To begin to address this point, oxidation-reduction cycles mimicking the catalyst regeneration cycles were carried out on both promoted catalysts and preliminary results will be described. First, catalytic performance during FTS using a CSTR will be discussed.

1.2.3.5 Catalytic Testing

As demonstrated in the literature, adding either Pt or Ag promoter can significantly improve CO conversion on Co/Al_2O_3 catalyst on a per gram catalyst basis (Refs. 21, 23, 25, and 38). The enhancement in conversion rate after introducing metal promoter stresses that one primary role of promoters is to provide a higher Co metal active site density for carrying out the reaction. Note that not all metals found to promote reduction led to improved X_{co}; Cu was one metal that clearly promoted Co oxide reduction, but led to negative effects on both CO conversion and product selectivity (Ref. 23). In addition to the aim of improving the reducibility of cobalt oxide and enhancing the CO conversion rate, it was also our intent to further investigate the possibility of decreasing the hydrogenating activity of Co with the aim of decreasing light products (e.g., CH_4) and CO_2 and thus increase liquid HC product selectivity (C_5+). Comparisons of product selectivity generated from Pt and Ag promoted catalysts were thus conducted at the same level of conversion. The CO conversion was set at ~50% (i.e., industrially relevant conditions) by adjusting space velocity as a basis of comparison. The influences of Pt and Ag promoter and loadings on product selectivities are summarized in Table 1.10.

TABLE 1.10.—ACTIVITY AND SELECTIVITY OF THE FISCHER-TROPSCH SYNTHESIS REACTION ON UNPROMOTED Co/Al_2O_3 CATALYST COMPARED TO Pt AND Ag PROMOTED Co/Al_2O_3 CATALYSTS [a]

Catalyst	TOS, h	CO conversion, %	Space velocity $NL/g_{catalyst}/h$	Hydrocarbon selectivity, carbon atom%		CO_2 sel., %
				CH_4	C_5+	
$25\%Co/Al_2O_3$						
	8.7 to 53	51.0	3.4 to 4.2	8.3	82.5	0.8
	53.145	51.4	2.8	8.9	80.0	0.9
$0.5\%Pt\text{-}25\%Co/Al_2O_3$						
	6.3 to 58	52.0	1.7 to 12	9.1	81.2	1.1
	58 to 121	48.2	1.1 to 1.7	10.9	78.9	1.4
$2.0\%Pt\text{-}25\%Co/Al_2O_3$						
	6.0 to 58	45.0	9.0 to 12.0	9.1	81.9	1.1
	58 to 143	50.6	6.2 to 6.9	9.2	81.2	1.8
$5.0\%Pt\text{-}25\%Co/Al_2O_3$						
	6.0 to 55.0	52.5	10 to 16.0	9.5	80.7	3.2
	71 to 175	49.5	9.1 to 10	9.9	79.0	4.0
$0.276\%Ag\text{-}25\%Co/Al_2O_3$						
	6.0 to 48	46.4	8.8 to 12	7.4	84.1	0.4
	56 to 149	49.4	4.5 to 7.0	7.9	82.3	0.5
$1.11\%Ag\text{-}25\%Co/Al_2O_3$						
	6.0 to 48	48.1	8.3 to 12	7.3	83.7	0.4
	55 to 145	50.1	5.0 to 6.2	8.4	81.4	0.6
$2.76\%Ag\text{-}25\%Co/Al_2O_3$						
	6.0 to 46	44.5	7.0 to 12	7.6	84.1	0.6
	49 to 120	48.7	3.4 to 4.8	8.3	81.2	0.8

[a]Reaction conditions: 220 °C, 300 psig, $H_2/CO = 2.1$

For Pt promoted catalyst, it is obvious that Pt slightly increases the formation of CH_4 and CO_2 and decreases C_5+ as compared to the unpromoted catalyst at ~50% CO conversion. However, Pt promoter significantly increased the catalyst initial activity on a per gram catalyst basis, as indicated by the much higher space velocities (12-16 NL/g-cat/h) used to achieve ~50% CO conversion at the beginning of FTS for the 0.5-5%Pt promoted Co catalysts relative to the unpromoted 25%Co/Al_2O_3 catalyst (4.2 NL/g-cat/h). Considering the effect of Pt loading with time on stream (TOS), once CO_2, CH_4 and C_5+ selectivities were established, their changes with time on stream were unnoticeable. CO_2 selectivity was found to increase measurably (0.8, 1.1, and 3.2% for unpromoted, 0.5%Pt-promoted, and 5%Pt promoted, respectively) with increasing Pt loading. The catalysts deactivated with time, and the space velocity was adjusted to maintain ~50%CO conversion. Another interesting perspective is the effect of Pt loading on the activity of the catalyst on per gram basis. Considering space velocity adjustments, it is clear that higher space velocities were applied in the case of higher Pt loading. This means that Pt does help to promote CO conversion per unit mass of catalyst. Nevertheless, the product selectivity does not remain the same, and Pt tends to contribute to higher CH_4 and, especially, to more CO_2. Consequently, another important conclusion to be drawn from this work is that while high levels of Pt loading are able to produce higher CO conversion, it comes at the expense of slight losses in favorable C_5+ selectivity. The remarkable increase in CO_2 selectivity with increasing Pt also suggests that the water-gas shift (WGS) reaction pathway is enhanced, as Pt metal likely serves as an active site for this reaction (Refs. 42, 43, 44, and 45), perhaps by facilitating the dehydrogenation of formate during steam-assisted forward formate decomposition (Ref. 46). With higher water gas shift reaction rates, higher CO_2 and H_2 levels are obtained and, subsequently, the additional H_2 may accelerate the hydrogenation reaction on Co sites, thus obstructing the long chain HC growth on these sites, in agreement with the lower C_5+ selectivities and higher methane selectivity as mentioned previously. Therefore, in order to apply Pt as a promoter for Co/Al_2O_3 FT catalyst, CO conversion and product selectivities must be compromised, such that low Pt loadings are warranted, aside from the cost factor.

For Ag promoted catalyst, the result in selectivity is intriguing as Ag promoter was confirmed to lower the chain termination rate of Co, as a decrease in methane selectivity was obtained, and C_5+ HC product selectivity increased. CO_2 selectivity was also diminished, indicating that Ag metal inhibits CO_2 formation. This means that Ag metal inhibits the water gas shift (WGS) reaction, in contrast to Pt metal. With increasing Ag loading, initially the catalyst still performed with higher C_5+ selectivity in line with the lower loaded Ag promoted catalyst, but CH_4 and CO_2 selectivities tended to slightly increase during ~150 h of testing. Because local atomic structure shows that Ag-Co bond formation is favorable at lower loading, it is suggested that this Ag-Co interaction may selectively inhibit some active sites for CH_4 and CO_2 formation, while at high Ag loading, silver tends to form more Ag metal clusters and thus higher Ag-Ag coordination; this tendency may result in sites for inhibiting CH_4 being lost with time on-stream for the more heavily Ag loaded catalysts. It has been previously reported that Ag-active metal alloys in catalysts for selective hydrogenation reactions of butadiene and acetylene do suppress hydrogenation reactions (Refs. 29 and 47). At longer times on stream, slight increases in CH_4 and CO_2 selectivities and slight decreases in C_5+ selectivity were observed for all loadings; however, the selectivities are still better than both the unpromoted catalyst as well as the Pt-promoted catalyst. To reiterate, the negative selectivity changes with TOS might be due to the segregation of Ag during the reaction that leads to the formation of a separate Ag metallic phase (Ref. 23), while losing Ag-Co coordination that retards CH_4 and CO_2 formation. As with Pt promoted catalyst, the CO conversion of Ag promoted catalysts also declined along with TOS, such that lower space velocities were required to retain the ~50% CO conversion level. Unlike the case of Pt promoter, increasing Ag loading decreased catalyst activity on a per gram catalyst basis, as clearly observed by the lower space velocity that was needed to make equivalent 50% CO conversion when higher loadings of Ag were applied. This suggests that Ag metal clusters dominating at high Ag loading impede access of reactants to Co active sites, either by pore blocking or covering of sites. Among different Ag loadings the best Ag loading was found to be the lowest level (0.276%Ag), providing the highest activity coupled with the highest C_5+ selectivity among all the catalysts tested.

To summarize thus far, although there was found a fundamental difference in the local atomic structure between Pt and Ag promoter in Co/Al_2O_3 catalysts, both are able to effectively catalyze the reduction of cobalt oxide and provide

higher Co^0 site densities for the reaction relative to the unpromoted catalyst; moreover, they also provide good activity for the FT reaction with satisfactory selectivities, especially in the case of Ag that can slightly lower CH_4 and CO_2 formation and improve C_5+ product selectivities.

1.2.3.6 ROR Cycles

To make further a comparison between Pt and Ag, a preliminary investigation of their ability to be regenerated (i.e., whether they can maintain good contact with Co and facilitate Co reduction or not following OR cycles) is also included. 0.5%Pt (i.e., most commercially relevant loading) and 0.276%Ag loadings (atomically equivalent) were selected for this purpose. The approach of using oxidation-reduction (OR) cycles was employed in this case to simulate catalyst regeneration. Specifically, the ability of the promoter to continue to facilitate Co oxide reduction following oxidation was evaluated by TPR as shown in Figure 1.15(A) for Pt-promoted catalysts and Figure 1.15(B) for Ag-promoted catalysts, as well as by H_2-chemisorption/pulse reoxidation as tabulated in Table 1.11. The impact on BET surface area and porosity was also examined (Table 1.11).

Figure 1.15(A) demonstrates that after the first and second RO cycles, Pt promoter continues to facilitate the reduction of cobalt oxides, as clearly shown by the low temperatures of reduction of both peaks compared to those of the unpromoted catalyst. Although the profiles of Pt promoted catalyst after the first and second RO appear to be similar, they differed from that of the freshly calcined Pt promoted catalyst (b). The main differences are that the first reduction peak of fresh catalyst is narrower than that of RO samples, suggesting some difference in structure probably due to ripening, and that the second peak is shifted to slightly lower temperature after OR cycle, implying that a significant amount of Pt likely remains in contact with Co to serve to facilitate Co_3O_4 and CoO reduction after OR cycles. The tolerance of Pt as a promoter was also stressed by H_2-chemisorption/pulse reoxidation data in Table 1.11. The results show that the metal site density still remains nearly the same after OR cycles and, moreover, the percentage of reduction, corrected dispersion, and corrected cluster size remained essentially intact. However, the BET and porosity data in Table 1.11 show a negative impact. BET surface area and pore volume tend to decrease somewhat, while average pore radius tends to increase after OR cycles, the latter suggesting some pore blocking of the narrower pores by metal oxide particles.

TABLE 1.11.—COMPARATIVE RESULTS OF BET SURFACE AREA, POROSITY MEASUREMENTS AND HYDROGEN CHEMISORPTION/PULSE REOXIDATION OF PROMOTED CATALYSTS BEFORE AND AFTER REDUCTION-OXIDATION CYCLES

Catalyst	BET SA, m^2/g	Pore volume,[a] cm^3/g	Average pore radius, nm	H_2 desorbed per $g_{catalyst}$, µmol/g	Uncorrected metal dispersion, %	Uncorrected Co dispersion,[b] %	Uncorrected Co average diameter,[b] nm	O_2 uptake per $g_{catalyst}$, µmol/g	O_2 uptake by Co per $g_{catalyst}$,[c] µmol/g	Percent reduction of Co	Corrected metal dispersion, %	Corrected Co dispersion,[b] %	Corrected Co average diameter,[b] nm
Calcined 0.5%Pt-25%Co/Al_2O_3	98.5	0.218	4.4	132.9	6.2	6.3	16.5	1759	1733	61.3	10.1	10.3	10
1st RO 0.5%Pt-25%Co/Al_2O_3	78.4	0.211	5.4	148.0	6.9	6.9	14.8	1792	1766	62.5	11.1	11.2	9.2
2nd RO 0.5%Pt-25%Co/Al_2O_3	72.9	0.205	5.6	135.3	6.3	6.4	16.2	1880	1854	65.6	9.6	9.7	10.7
Calcined 0.276%Ag 25%Co/Al_2O_3	95.5	0.224	4.7	103.7	4.9	4.9	21.1	1698	1698	60.1	8.1	8.1	12.7
1st RO 0.276%Ag 25%Co/Al_2O_3	80.7	0.218	5.4	106.0	5.0	5.0	20.6	1650	1650	58.4	8.5	8.6	12.0
2nd RO 0.276%Ag 25%Co/Al_2O_3	76.1	0.214	5.6	100.6	4.7	4.7	21.7	1673	1673	59.2	7.9	8.0	12.9

[a]Single point

[a]Assume H_2 desorbed from only Co metal sites.

[b]Assume oxidation of Pt^0 to PtO_2 (Ref. 23) and no oxidation of Ag^0 (Ref. 14).

Considering Ag-promoted catalysts, Ag promoter remains in proximity to Co and still plays a role in facilitating cobalt oxide reduction after OR cycles, as evident in the TPR profiles in Figure 1.15(B) of RO samples compared to the unpromoted catalyst. In a similar trend to that of Pt promoted catalyst, Ag allows cobalt oxide to be reduced at lower temperature after OR cycles. The TPR profile shapes of the first and second RO samples are quite similar to each other but, as in the case of Pt, differed slightly from that of the freshly calcined catalyst. Also, as in the case of Pt, results of BET and porosity in Table 1.11 for Ag-25%Co/Al_2O_3 catalyst reveal that some pore blocking of narrower channels occurred after RO cycles, as the BET surface area decreased slightly, accompanied by a slight increase in average pore radius. Nevertheless, the results of H_2-chemisorption/oxygen pulse reoxidation shows that the metal site density, percent reduction, percent corrected dispersion, and estimated corrected cluster diameter even after the second RO remains satisfactory. Therefore, it is recognized that, although the structure of Ag is likely somewhat altered after OR cycling, enough Ag promoter remains in contact with cobalt oxide to facilitate its reduction. Thus, while it can be concluded that both Pt and Ag retain the ability to promote cobalt oxide reduction, it remains to be shown that catalyst performance is regenerated. For example, one primary question is the location of promoter in relation to Co^0 and whether it impedes cobalt sites. H_2 chemisorption only measures metal site density and does not distinguish between the metal from which it is evolved. It will be important to rule out excessive surface enrichment of Ag on cobalt particles, for example.

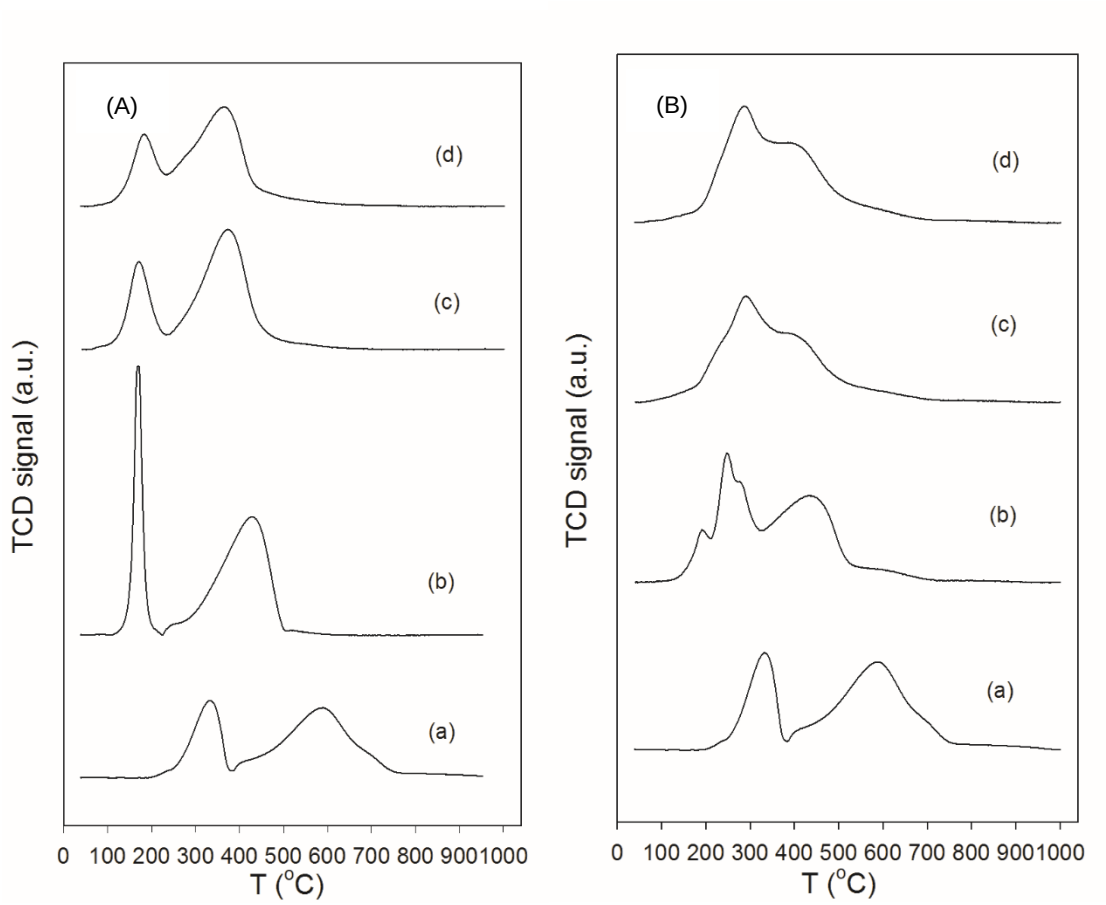

Figure 1.15.—(A) Comparative TPR spectra of (a) unpromoted 25%Co/Al_2O_3 catalyst with 0.5%Pt-25%Co/Al_2O_3, moving up, (b) calcined, (c) 1st RO, (d) 2nd RO. (B) Comparative TPR spectra of (a) unpromoted 25%Co/Al_2O_3 catalyst with 0.276%Ag-25%Co/Al_2O_3, moving up, (b) calcined, (c) 1st RO, (d) 2nd RO.

1.2.4 Conclusions

A series of Pt loaded cobalt catalysts was prepared as a reference for comparing the effectiveness of Ag as a promoter, as it is much less costly. In agreement with our previous reports, Pt and Ag promoters do facilitate the reduction of cobalt oxides and improve the number of active Co metal surface sites. Although increasing Ag enhances Co reduction, in contrast to Pt the metal site density does not increase with further increase in loading. While it is known that Pt in Co/Al_2O_3 catalyst is in intimate contact at the atomic level with cobalt clusters, with Pt-Co bonds being readily observed, this work demonstrates that this holds true even at very high promoter loadings. Ag promoter can also interact with Co to form Ag-Co bond in Ag promoted Co/Al_2O_3 catalysts. However, unlike Pt promoter, Ag promoter also displays coordination to other Ag atoms and a peak for Ag-Ag first shell coordination after complete activation in H_2 is evident. Moreover, the fraction of Ag in coordination with Co decreases as a function of Ag promoter loading, revealing that the interaction of Ag with Co is not as high as in the case of Pt. While either Pt-Co bonds or Ag-Co bonds formed in Co/Al_2O_3 can significantly facilitate the reduction of cobalt oxides, the fundamentally different atomic structure of the Ag promoter relative to Pt plays a different role in product selectivity of the Fischer-Tropsch synthesis reaction. Pt promoter increases CH_4 and CO_2, at the expense of C_5+. The greater the amount of Pt, the higher the CH_4 and CO_2 selectivities. Water gas shift (WGS) activity of Pt is at least in part responsible for the adverse effect. Interestingly, compared to both Pt promoted and unpromoted catalysts, Ag promoter at all loadings decreases CH_4 and CO_2 and benefits C_5+ selectivity. However, increasing Ag does not improve selectivity but rather worsens it relative to lower loadings, which may be attributed losses in Ag-Co bonding that inhibits excessive hydrogenation and/or WGS. The ability of Pt and Ag promoted catalysts to retain the capability of facilitating cobalt oxide reduction after oxidation-reduction cycles suggests that sufficient contact of Pt with Co in $0.5\%Pt\text{-}25\%Co/Al_2O_3$ and Ag with Co in $0.276\%Ag\text{-}25\%Co/Al_2O_3$ catalyst was maintained after OR cycles. Actual regeneration of cobalt surface must be examined by carrying out reaction tests after regeneration in order to rule out excessive surface enrichment of Co^0 by Ag^0. Despite a somewhat lower performance for promoting Co metal site density relative to Pt, the satisfactory activity and higher selectivity obtained with Ag promoter and, in particular, its much lower price relative to Pt, makes Ag an important candidate as a possible substitute.

1.3 Exploring Zr as a Support Modifier in Narrow/Wide Pore Co/Al_2O_3

In the first year reporting period, two series of 25%Co/alumina catalysts containing Zr with 1, 5, 10, and 15% loadings were prepared using the incipient wetness impregnation (IWI) method to first add the Zr using zirconyl nitrate as the precursor. Following calcination, cobalt was added by either IWI or by a slurry phase impregnation (SPI), where the pores were overfilled with loading solution according to a Sasol recipe (Ref. 48). The IWI catalysts were labeled NASA117, 118, 119, and 120 for the 1, 5, 10, and 15% Zr loadings using the IWI method, while the SPI catalysts were labeled NASA121, 122, 123, and 124 for the same Zr loadings. The γ-Al_2O_3 support was 150 m^2/g.

During the second year reporting period, it was decided that NASA researchers would prepare a 1%Zr loaded 25%Co/Al_2O_3 catalyst (labeled ABD002) using a wider pore support, Puralox HP14/150, and that the investigation would center on comparing the wide pore catalyst (ABD002) with the narrow pore catalyst (NASA121). For the purpose of comparison by characterization, two additional batches of catalyst were prepared: an unpromoted narrow pore 25%Co/Al_2O_3 catalyst labeled NASA125 and an unpromoted wide pore 25%Co/Al_2O_3 catalyst labeled JSK004 (NASA researchers).

1.3.1 Background

The impact of Zr on Co/Al_2O_3 catalysts through support modification is not well defined. CAER researchers previously showed (Ref. 49) that Zr modification to a SiO_2-supported 20%Co catalyst decreases reducibility somewhat (from 73 to 51%) due to the greater interaction of cobalt oxides with the Zr-modifier (also observed in TPR profiles, as shown in Figure 1.16). However, at the same time, the average Co cluster size decreased due to the stabilization of smaller clusters (from 48.4 to 18.8 nm). The net result was an increase in the cobalt site density as measured by H-TPD (from 13.2 to 47.6 μmol of H_2 desorbed per gram of catalyst). These impacts are due to the fact that Zr modifier changes the support interaction from a weak one (SiO_2 alone) to a moderate one. Chemisorption results from this previous work (Ref. 49) are summarized in Table 1.12.

TABLE 1.12.—(TOP) IMPACT OF PREPARATION METHOD AND CO LOADING ON THE EXTENT OF REDUCTION AND SIZE OF COBALT CLUSTERS FOLLOWING STANDARD REDUCTION IN HYDROGEN AT 350 °C FOR 10 h. (BOTTOM) IMPACT OF Zr ADDITION ON THE REDUCIBILITY, COBALT SIZE, AND SITE DENSITY OF SiO_2 AND Al_2O_3 SUPPORTED Co CATALYSTS

Catalyst	Support BET SA, m^2/g	Prep	μmol H_2 desorbed per $g_{catalyst}$	Uncorrected percent dispersion	O_2 uptake μmol per $g_{catalyst}$	Percent reduction	Corrected percent dispersion	Corrected diameter, nm
Impact of preparation, surface area, and Co loading on reducibility and cobalt size								
15%Co/Al_2O_3	200	IWI	71	5.5	495	29	19	5.4
15%Co/Al_2O_3	150	IWI	79	6.2	823	49	14	7.4
15%Co/Al_2O_3	150	Slurry	57	4.5	823	49	9.3	11.1
25%Co/Al_2O_3	150	IWI	103	4.8	1814	64	7.6	13.7
25%Co/Al_2O_3	150	Slurry	78	3.7	1174	42	8.7	11.8
Impact of Zr on SiO_2 and Al_2O_3 supported cobalt catalysts prepared by sequential IWI								
20%Co/SiO_2	295	IWI	13	1.6	1652	73	2.1	48.4
20%$Co/10\%ZrO_2$-SiO_2	295	IWI	48	2.8	1149	51	5.5	18.8
15%Co/Al_2O_3	200	IWI	67	5.3	509	30	18	5.9
15%$Co/10\%ZrO_2$-Al_2O_3	200	IWI	46	3.6	195	11	32	3.2

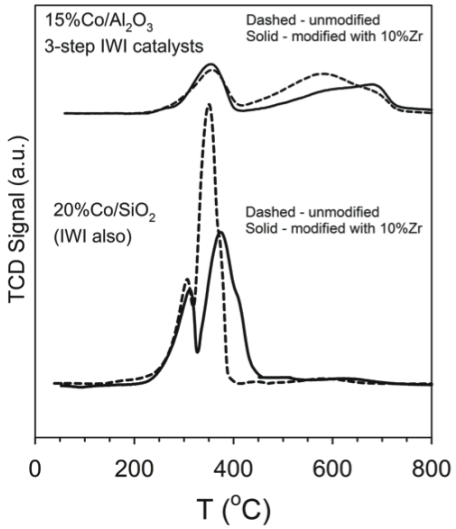

Figure 1.16.—Zr-addition by IWI and calcination to produce a modified support, followed by sequential IWI of cobalt nitrate and calcination, produces smaller cobalt species inside the support pores, and that interact more strongly with the support—whether the support be (bottom) silica or (top) alumina.

Alumina is a strongly interacting support. Previous work (Ref. 49) showed that addition of Zr by IWI and calcination to produce a modified support, followed by sequential IWI of cobalt nitrate and calcination (to make 10%Zr-15%Co/Al_2O_3), generated smaller cobalt species (~3.2 nm) inside the support pores relative to unpromoted 15%Co/Al_2O_3. These smaller species interacted more strongly with the support, shifting the TPR profile to higher temperature (Figure 1.16, from previous work (Ref. 49)). In the case of 10%Zr-15%Co/Al_2O_3, the extent of reduction was just 11% relative to 30% for the unpromoted catalyst. Thus, the majority of cobalt oxides were in a reducibility regime that could not be accessed by standard reduction at 350 °C, and this adversely impacted the site density as measured by chemisorption (45.5 μmol per g of catalyst relative to 66.9 μmol per g of catalyst for the unpromoted). Chemisorption results from this previous work (Ref. 49) are summarized in Table 1.12.

Jongsomjit et al. (Ref. 50) also observed in TPR profiles that Zr addition led to a significant peak at higher temperature relative to the unpromoted catalyst. The support utilized was Condea Vista B (209 m^2/g) and the levels of Zr were 2.2, 5.4, and 10.8%. Zr was added by incipient wetness impregnation of zirconium n-propoxide in n-propanol, followed by air calcination at 350 °C, prior to standard aqueous IWI of cobalt nitrate, and re-calcination at 300 °C in air. At all Zr levels, they also observed a less significant peak that was located at lower temperatures relative to the unpromoted catalyst, and CAER researchers believe that this may be due to a fraction of cobalt that was forced either to the pore mouth area or outside of the pores. The explanation is by no means simple.

CAER researchers have previously observed (Ref. 49) significant differences in how the preparation method and loading of Co affect the location and size of cobalt clusters. At low loadings of 15%Co, the sequential IWI method is very effective in depositing cobalt within the pores of the alumina, and the cobalt oxides exhibit a strong interaction with alumina. At a higher loading of 25%Co (i.e., close to commercial loading), a fraction of cobalt oxide is forced outside of the pores, is less interacting, presumably larger in size, and reduces at lower temperatures (Figure 1.17, previous work (Ref. 49)). The slurry method tends to produce a similar cobalt size regardless of loading (i.e., 15 or 25%). We have found that the slurry method produces cobalt sizes higher on average than that produced by the IWI method at low loading (all cobalt within pores) and smaller on average than that produced by the IWI method at higher loading (i.e., with the bimodal cobalt distribution). Table 1.12 summarizes the impact of loading and preparation method on cobalt size and percentage of reduction.

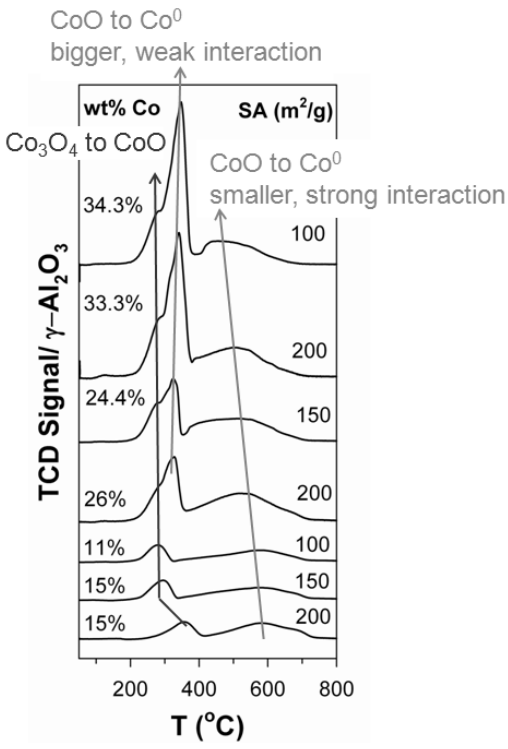

Figure 1.17.—Impact of loading and support surface area of Co/alumina catalysts prepared by sequential IWI on the location of cobalt oxides, and reducibility.

Thus, zirconia may impact different fractions of cobalt differently. If zirconia (or even a fraction of cobalt) blocks pores, a fraction of cobalt may be forced to the pore mouth or onto the external surface of the catalyst and be agglomerated (i.e., larger in size). If, however, zirconia acts to narrow the pores, the cobalt deposited within the pores may be smaller and in greater interaction with the support, hindering cobalt oxide reduction.

1.3.2 Experimental

1.3.2.1 Catalyst Preparation

In the first year reporting period, two series of 25%Co/alumina catalysts containing Zr with 1, 5, 10, and 15% loadings were prepared using the IWI method to first add the Zr using zirconyl nitrate as the precursor. Following calcination, cobalt was added by either IWI or SPI. The IWI catalysts were labeled NASA117, 118, 119, and 120 for the 1, 5, 10, and 15% Zr loadings using the IWI method, while the SPI catalysts were labeled NASA121, 122, 123, and 124 for the same Zr loadings. The γ-Al_2O_3 used was Catalox 150 (150 m^2/g).

In the second year reporting period, the decision was made to change the focus of the investigation somewhat. CAER utilized the unpromoted 25%Co/Al_2O_3 catalyst (NASA125) and the 1%Zr-25%Co/Al_2O_3 catalyst (NASA121), which were prepared using Catalox 150 narrow pore support. These were compared with the unpromoted 25%Co/Al_2O_3 (JSK004) and the 1%Zr-25%Co/Al_2O_3 catalyst (ABD002), which were prepared by NASA researchers using Puralox HP14/150 wide pore support.

1.3.2.2 BET Surface Area and Porosity Measurements

The measurements of BET surface area and porosity of the calcined catalysts were conducted using a Micromeritics Tri-Star system. Before performing the test, the temperature was gradually ramped to 160 °C and the sample was evacuated at least 12 h to approximately 50 mTorr. The BET surface area, pore volume (single point), and average pore radius (single point and BJH adsorption) were obtained for each sample.

1.3.2.3 Temperature Programmed Reduction (TPR)

Temperature programmed reduction (TPR) profiles of calcined catalysts were recorded using a Zeton-Altamira AMI-200 unit equipped with a thermal conductivity detector (TCD). Samples were pretreated by purging with argon flow at 350 °C (heating ramp rate of 10 °C/min) to remove traces of water and then cooled to 50 °C. The TPR was performed using a 10%H_2/Ar gas mixture at 30 cm^3/min and referenced to pure argon at a flow rate of 30 cm^3/min. The sample was heated from 50 to 800 °C using a heating ramp of 10 °C/min.

1.3.2.4 Hydrogen Chemisorption and Percentage Reduction by Pulse Reoxidation

Hydrogen chemisorption was conducted using temperature programmed desorption (TPD), also measured with the Zeton-Altamira AMI-200 instrument. A sample weight of typically ~0.220 g was used for all hydrogen chemisorption experiments. Catalysts were activated in a flow of 10 cm^3/min of H_2 mixed with 20 cm^3/min of argon at 350 °C for 10 h. and then cooled under flowing H_2 to 100 °C. The sample was held at 100 °C under flowing argon to remove and/or prevent adsorption of weakly bound species prior to increasing the temperature slowly to 350 °C, the reduction temperature of the catalyst. The catalyst was held under flowing argon to desorb remaining chemisorbed hydrogen until the TCD signal returned to baseline. The TPD spectrum was integrated and the number of moles of desorbed hydrogen determined by comparing its area to the areas of calibrated hydrogen pulses. The loop volume was first determined by establishing a calibration curve with syringe injections of hydrogen in helium flow. Dispersion calculations were based on the assumption of a 1:1 H:Co stoichiometric ratio and a spherical cobalt cluster morphology. After TPD of hydrogen, the sample was reoxidized at 350 °C using pulses of oxygen. The percentage of reduction was calculated by assuming that metal reoxidized to Co_3O_4. Further details of the procedure are provided elsewhere (Ref. 48).

1.3.2.5 X-Ray Diffraction (XRD)

Powder diffractograms on calcined catalysts were recorded using a Philips X'Pert diffractometer. Two different tests were performed for each sample—a short time scan over a long range and a long time scan over a short range. The objective of the short time scan was to assess the crystalline phases present using the following conditions: scan rate of 0.02°/step and scan time of 5 s/step over a 2θ range of 15° to 80°. The long time scan was conducted to quantify average Co_3O_4 domain sizes using line broadening analysis for the peak at 2θ = 37° representing (311). The latter conditions employed were a scan rate of 0.01°/step and a scan time of 30 s/step over a 2θ range of 30° to 45°.

1.3.2.6 X-ray Absorption Spectroscopy (EXAFS/XANES) Measurements

X-ray absorption spectroscopy (XAS) on reference (Co foil) and freshly activated unpromoted and Zr-promoted cobalt catalyst samples was conducted at Brookhaven National Laboratory (Beamline X-18b). The beamline was equipped with a Si(111) channel cut monochromator. A crystal detuning procedure was used to remove harmonic content from the beam and make the relative response of the incident and transmission detectors more linear. The X-ray flux for the beamline was *ca.* 1×10^{10} photons per second at 100 mA and 2.8 GeV; the usable energy range was from 5.8 to 40 keV. EXAFS/XANES spectra were recorded in transmission mode near the Co K edge. Sample thickness was determined by calculating the amount in grams per square centimeter of sample (w_D) by utilizing the following thickness equation

$$w_D = \ln(I_o/I_t)/\sum\{(m/r)_j w_j\} \quad (4)$$

where m/r is the total cross section (absorption coefficient/density) of element "j" in the sample at the absorption edge of the EXAFS element under consideration (units, $cm^2\ g^{-1}$), w_j is the weight fraction of element j in the sample and $\ln(I_o/I_t)$ was taken over a typical range of 1 to 2.5. Wax was utilized to fix the sample in the activated state (i.e., after H_2 reduction for 10 h at 350 °C), and such that a pellet could be formed. In addition, the pellet was sealed from ambient air. Smooth self-supporting pellets, free of pinholes, were loaded into the XAS cell. EXAFS data reduction

and fitting were carried out using the WinXAS (Refs. 51, 52 (Atoms), 53 (FEFF), and 54 (FEFFIT)) programs. The *k*- and *r*-ranges for fittings were chosen to be 3 to13 $Å^{-1}$ and 1.5 to 3 Å, respectively. The CoO reference was obtained from the TPR trajectory of a 15%Co/Al_2O_3 catalyst, at the point of maximum CoO content (Ref. 55).

1.3.2.7 Catalytic Activity Testing

FTS reaction tests were conducted using a 1 L CSTR equipped with a magnetically driven stirrer with turbine impeller, a gas-inlet line, and a vapor outlet line with a stainless steel (SS) fritted filter (7 µm) placed external to the reactor. A tube fitted with a SS fritted filter (2 µm opening) extends below the liquid level of the reactor for withdrawing reactor wax to maintain a nearly constant liquid level in the reactor. Separate mass flow controllers were used to control the flow of hydrogen and carbon monoxide at the desired flow rate. The reactant gases were premixed in a vessel before entering the reactor. Carbon monoxide was passed through a vessel containing lead oxide-alumina to remove traces of iron carbonyls. The mixed gases entered the CSTR below the stirrer operated at 750 rpm. The reactor slurry temperature was maintained constant by a temperature controller.

Prior to performing the reaction test, the catalyst (~13.0 g) was ground and sieved to 45 to 90 µm, and then loaded into a fixed-bed reactor for ex-situ reduction at 350 °C under atmospheric pressure for 15 h using a gas mixture of H_2/He (60 NL/h) with a molar ratio of 1:3. The reduced catalyst was then transferred to a 1 L continuously stirred tank reactor (CSTR) containing 315 g of melted Polywax 3000, by pneumatic transfer under the protection of a N_2 inert gas. Weighing the reactor before and after the transfer of catalyst was done to ensure that all catalyst powder was successfully transferred to the reactor. The transferred catalyst was further reduced in-situ at 230 °C at atmospheric pressure using pure hydrogen (30 NL/h) for another 10 h before starting the FTS reaction.

In this study, the FTS conditions used were 220 °C, 2.2 MPa, H_2/CO = 2.1. The reactant gas mixture was analyzed prior to sending to the reactor to ensure the composition. The reaction products were continuously removed from the vapor space of the reactor and passed through two traps, a warm trap maintained at 100 °C and a cold trap held at 0 °C. The uncondensed vapor stream was reduced to atmospheric pressure. The gas flow was measured using a wet test meter and analyzed by online GC. The accumulated reactor liquid products were removed every 24 h by passing through a 2 µm sintered metal filter located below the liquid level in the CSTR. Conversions of CO were obtained by gas-chromatography analysis (micro-GC equipped with thermal conductivity detectors) of the outlet gas product. The reaction products were collected in three traps maintained at different temperatures; a hot trap (200 °C), a warm trap (100 °C), and a cold trap (0 °C). The products were separated into different fractions (rewax, wax, oil, and aqueous) for quantification. However, the oil and wax fractions were mixed prior to GC analysis. To investigate the effect of Zr and pore size on the activity and selectivity, a reference CO conversion of about 50% was used and achieved by adjusting the space velocity in all cases. The catalyst activity was compared using the adjusted space velocity required to achieve 50%CO conversion, and selectivities were directly compared at the same level of conversion.

1.3.3 Results and Discussion

1.3.3.1 BET and Porosity Measurements

BET results are provided in Table 1.13 and Figure 1.18 shows the pore size distributions of (bottom) supports, (middle) unpromoted 25%Co/Al_2O_3 catalysts, and (top) 1%Zr-promoted 25%Co/Al_2O_3 catalysts prepared on (left) wide pore Puralox HP14/150 and (right) narrow pore Catalox 150 γ-Al_2O_3. With the narrow pore catalyst, neither the addition of cobalt nor the inclusion of Zr significantly impacted the main pore size, though a decrease in pore volume was noted with the addition of Co. On the other hand, addition of cobalt to the wide pore support not only decreased the pore volume, but also altered the pore size distribution by shifting the maximum to smaller size. Addition of Zr did not affect the pore volume significantly relative to the unpromoted catalyst.

TABLE 1.13.—BET AND POROSITY MEASUREMENTS OF SUPPORTS, UNPROMOTED, AND Zr-DOPED Co/ALUMINA

Description	BET SA, m^2/g	Pore volume,[a] cm^3/g	Average pore radius,[a] nm	Pore volume,[b] cm^3/g	Pore volume,[c] cm^3/g	Average pore radius,[b] nm	Average pore radius,[c] nm
Supports							
Catalox150 narrow pore γ-Al_2O_3	149.3	0.493	5.39	0.500	0.499	5.39	4.75
Puralox HP14/150 wide pore γ-Al_2O_3	152.6	0.919	12.55	0.924	0.924	10.33	9.02
Unpromoted catalysts							
25%Co/Al_2O_3 (narrow pore)	98.4	0.224	4.54	0.221	0.225	4.82	4.43
25%Co/Al_2O_3 (wide pore)	109.2	0.383	7.01	0.394	0.393	6.71	6.19
Zr-promoted catalysts							
1%Zr-25%Co/Al_2O_3 (narrow pore)	97.0	0.224	4.61	0.221	0.225	4.95	4.57
5%Zr-25%Co/Al_2O_3 (narrow pore)	95.8	0.200	4.17	0.195	0.199	4.60	4.21
1%Zr-25%Co/Al_2O_3 (wide pore)	103.2	0.392	7.60	0.411	0.410	4.55	4.11

[a] Single point
[b] BJH adsorp
[c] BJH desorp

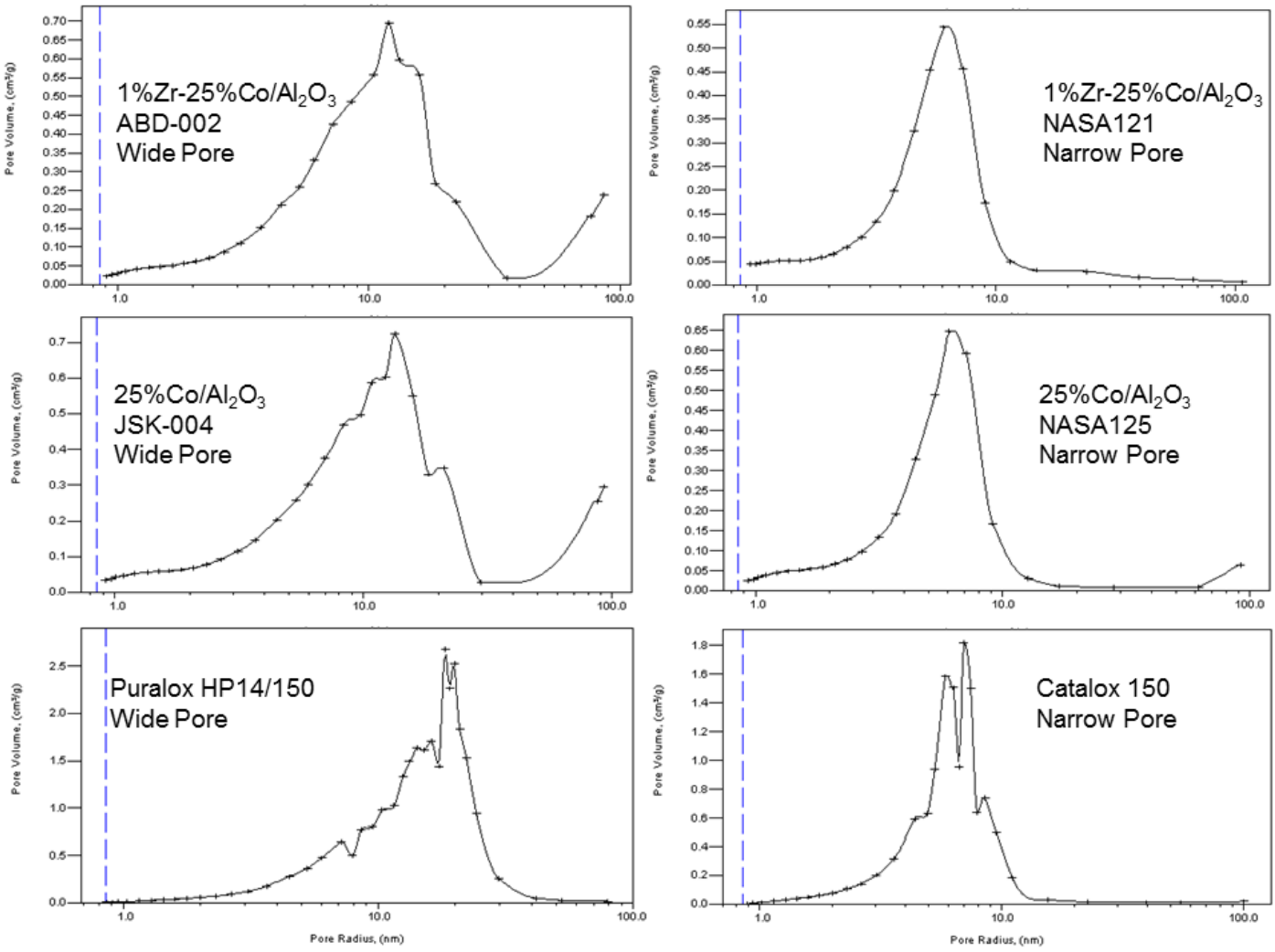

Figure 1.18.—Pore size distributions of (bottom) supports, (middle) unpromoted 25%Co/Al_2O_3 catalysts, and (top) 1%Zr-promoted 25%Co/Al_2O_3 catalysts prepared on (left) wide pore Puralox HP14/150 and (right) narrow pore Catalox 150 γ-Al_2O_3.

1.3.3.2 X-Ray Diffraction, TPR, and Hydrogen Chemisorption / Pulse Reoxidation

X-ray powder diffractograms are presented in Figure 1.19. In accordance with the Scherrer equation, the sharper lines of the narrow pore catalysts indicates a larger average Co_3O_4 cluster size after calcination relative to the wider pore catalysts. The results suggest that a fraction of cobalt was forced external to the mouth of pores or external to the pores in the narrow pore catalysts. The presence of Zr on the wider pore catalyst decreased the size of Co_3O_4 clusters in the 1%Zr doped wide pore catalyst, perhaps due to a slight narrowing of the average pore size upon addition of Zr.

TPR profiles are presented in Figure 1.20 and Figure 1.21. Figure 1.20 reveals that Zr addition did not have a significant impact with the narrow pore catalyst, and a slight shift to lower temperature was observed, possibly due to a particle size effect. While the XRD results indicate that the Co_3O_4 particles are slightly smaller with the Zr-doped narrow pore catalyst, the H-chemisorption results (Table 1.14) suggest a slightly larger particle size once reduction has taken place. TPR profiles are in agreement with a larger size forming during reduction, which weakens the interaction with the support and shifts the profile to slightly lower temperatures. Extent of reduction was observed to be about 10% higher from O_2 titration measurements. Higher extent of reduction was also observed in XANES spectroscopy, as apparent in the decrease in the white line intensity (Figure 1.22) and the increase in Co-Co metal coordination in EXAFS coupled with decreasing Co-O coordination (Figure 1.23 and Table 1.15). This result was somewhat unexpected, as we originally anticipated that the smaller pore size of the narrow pore catalyst would lead to a smaller average size.

The wide pore catalyst very obviously exhibited a smaller average cluster size, as determined by both XRD (Figure 1.23, Table 1.14) and chemisorption (Table 1.14). Moreover, the impact of Zr was as expected from our previous study using the IWI method (Ref. 49), where the Co was suggested to reside with the pores. The addition of Zr narrowed the pore size slightly (as measured by BJH adsorption). The smaller resulting Co clusters were in stronger interaction with the support, as a characteristic increase in reduction temperature for CoO to Co^0 reduction was observed in TPR for the Zr doped catalyst, which is in line with our previous study.

In terms of site densities, moving from the narrow pore catalyst to wide pore increased the site density by ~25 to 55%. Adding Zr to the wide pore catalyst increased the site density by an additional ~18%. In Figure 1.21, dashed lines represent TPR following standard reduction in H_2 and demonstrate that residual cobalt oxides remain on the catalyst due to incomplete reduction. Thus, the site densities could likely be improved further by adding a reduction promoter (e.g., Ru, Ag, Re, Ir, Pt, or Au).

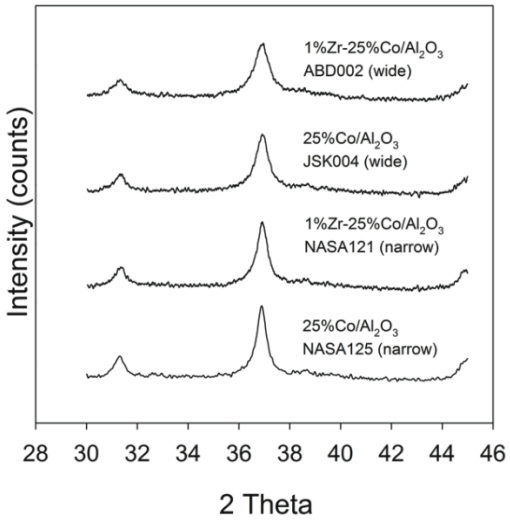

Figure 1.19.—XRD patterns of unpromoted and Zr-promoted narrow and wide pore 25%Co/Al_2O_3 catalysts.

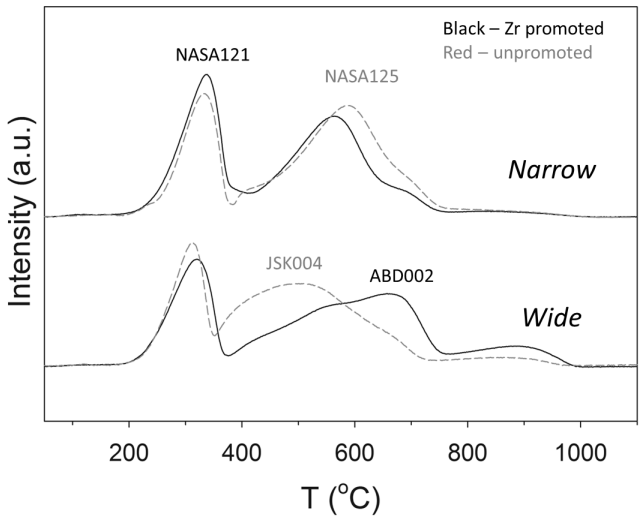

Figure 1.20.—Impact of support pore size and Zr-doping on the manner in which cobalt oxides reduce over 25%Co/Al_2O_3 catalysts with or without 1%Zr. The gray dashed lines represent the unpromoted catalysts while the solid lines are 1%Zr-doped catalysts.

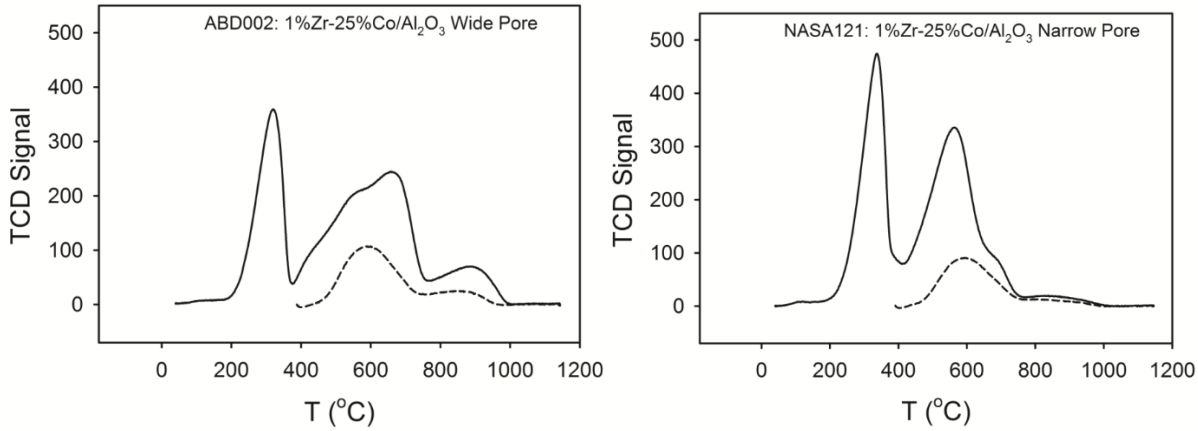

Figure 1.21.—The dashed lines are for TPR following standard reduction in H_2 and demonstrate that residual cobalt oxides remain on the catalyst due to incomplete reduction.

TABLE 1.14.—RESULTS OF HYDROGEN CHEMISORPTION / PULSE REOXIDATION AND X-RAY DIFFRACTION LINE BROADENING ANALYSIS OF UNPROMOTED AND Zr-DOPED Co/ALUMINA CATALYSTS

	Support/catalyst	Pore	H_2 desorbed per $g_{catalyst}$, µmol/$g_{catalyst}$	Uncorrected percent dispersion	Uncorrected diameter, nm	O_2 consumed, µmol/g	Percent reduction of Co	Corrected percent dispersion	Corrected diameter, nm	Co_3O_4 diameter from XRD
NASA125	25%Co/Al_2O_3	Narrow	53.6	2.53	40.8	1008	35.6	7.1	14.6	14.2
NASA121	1%Zr 25%Co/Al_2O_3	Narrow	67.9	3.2	32.3	1323	46.8	6.8	15.1	13.9
NASA121 repeat	1%Zr 25%Co/Al_2O_3	Narrow	65.7	3.1	33.3	1282	45.3	6.8	15.1	
JSK-004	25%Co/Al_2O_3	Wide	83.4	3.93	26.2	1373.5	48.6	8.0	12.8	11.9
ABD002	1%Zr 25%Co/Al_2O_3	Wide	94.8	4.47	23.1	1398	49.4	9.0	11.4	9.4
ABD002 repeat	1%Zr 25%Co/Al_2O_3	Wide	103.2	4.86	21.2	1316	46.5	10.5	9.9	

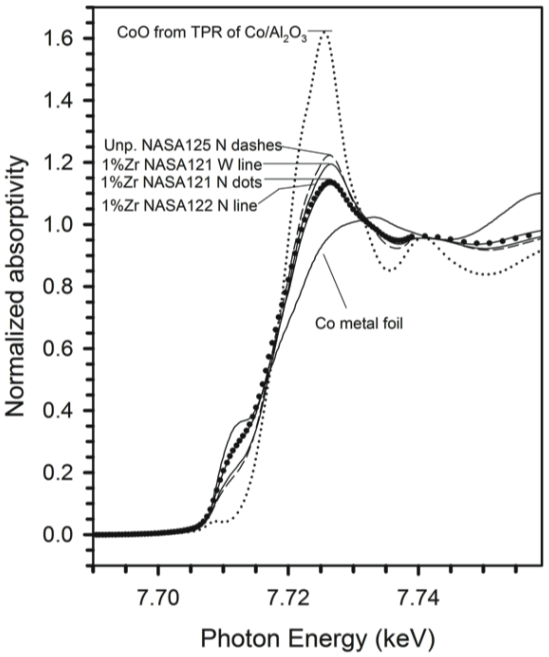

Figure 1.22.—Normalized XANES spectra of the activated Zr-promoted catalysts.

TABLE 1.15.—RESULTS OF EXAFS FITTING PARAMETERS FOR REFERENCES ACQUIRED NEAR THE Co K EDGE. THE FITTING RANGES WERE Δk = 3 TO 13 $Å^{-1}$ AND ΔR = 1.5 TO 3.1 Å. S_0^2 WAS SET TO 0.9

Sample Description	N Co-O in CoO	R Co-O in CoO, Å	N Co-Co in Co^0	R Co-Co in Co^0, Å	N Co-Co in CoO	R Co-Co in CoO, Å	e_0, eV	σ^2, $Å^2$	r-factor
Co metal	---	------	12 (set)	2.491 (0.0042)	---	------	7.97 (0.837)	0.00334 (0.00021)	0.0087
CoO powder reference	2.6 (0.5)	2.103 (0.019)	---	------	6.5 (1.0)	3.014 (0.010)	1.48 (1.40)	0.00686 (0.00130)	0.024
25%Co/Al_2O_3 (narrow pore, NASA125)	1.9 (0.3)	2.080 (0.019)	1.8 (0.4)	2.520 (0.014)	3.8 (0.6)	3.021 (0.014)	1.32 (1.64)	0.00786 (0.00153)	0.017
1%Zr-25%Co/Al_2O_3 (narrow pore, NASA121)	1.0 (0.2)	2.075 (0.025)	2.2 (0.4)	2.509 (0.011)	2.0 (0.3)	3.022 (0.016)	0.926 (1.62)	0.00632 (0.00126)	0.017
5%Zr-25%Co/Al_2O_3 (narrow pore, NASA122)	0.9 (0.2)	2.061 (0.031)	3.2 (0.4)	2.506 (0.0086)	1.8 (0.3)	3.013 (0.016)	–0.698 (1.42)	0.00582 (0.000993)	0.011
1%Zr-25%Co/Al_2O_3 (wide pore, ABD002)	1.4 (0.2)	2.062 (0.021)	2.5 (0.4)	2.522 (0.012)	2.8 (0.4)	3.025 (0.015)	2.02 (1.65)	0.00750 (0.00138)	0.014

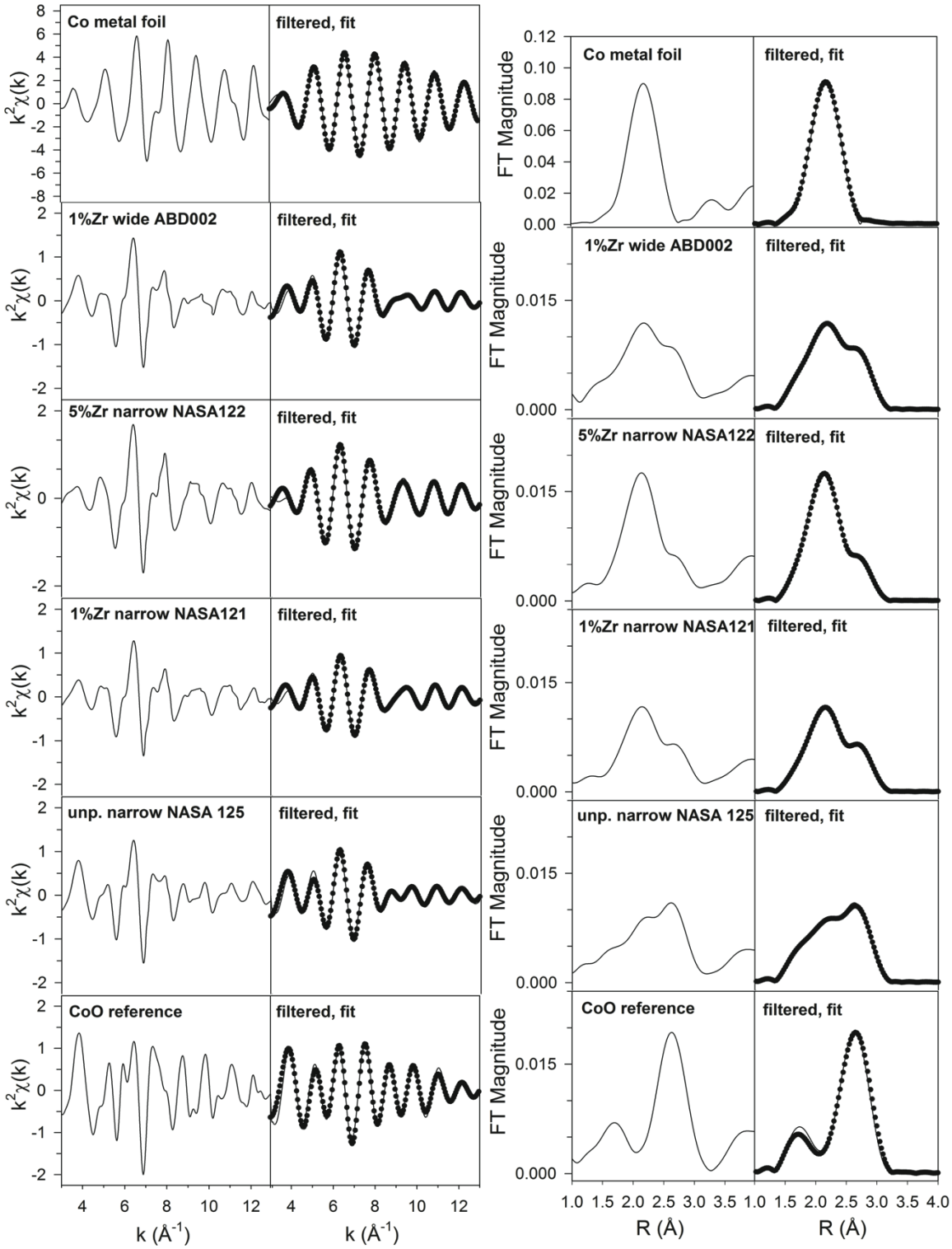

Figure 1.23.—EXAFS results at the Co K-edge for (top) Co metal foil and freshly activated (2nd from top) 1%Zr-25%Co/Al_2O_3 wide pore ABD002; (3rd) 5%Zr-25%Co/Al_2O_3 narrow pore NASA122; (4th) 1%Zr-25%Co/Al_2O_3 narrow pore NASA121 (5th) unpromoted 25%Co/Al_2O_3 narrow pore NASA125, and (bottom) CoO, including the raw k^2 weighted χ(k) versus k, (middle) the filtered χ(k) versus k and (dotted) the fitting; and (right) the raw Fourier transform magnitude spectrum and the filtered spectrum and (dotted) result of the fitting.

1.3.3.3 Catalytic Testing-Effect of Zr Promoter and Support Type on Fischer-Tropsch Synthesis

Figure 1.24 shows the CO rate as a function of time on stream (up to 150 h) over 0 to 5% Zr promoted 25%Co catalysts supported on the narrow pore and wide pore Al_2O_3 supports. The rates were obtained at about 50% CO conversion by adjusting space velocity, so that the reactant and byproduct H_2O partial pressures could be maintained relatively constant, and the differences in activity and selectivities among the catalysts, if present, will be reflected. At the beginning of the FTS reaction, the Co catalysts containing 1 and 5% Zr displayed 25 to 70% higher activity than the unpromoted 25%Co/Al_2O_3 for both the narrow and wide pore supported catalysts, and the CO rates of the narrow pore catalysts increased with increasing Zr loading from 1 to 5% (narrow pore: 0.004 and 0.055 vs. 0.032 mol/$g_{catalyst}$/h; wide pore: 0.063 vs. 0.05 mol/$g_{catalyst}$/h). However, after about 50 h, the activities of the narrow pore Zr-Co catalysts decreased and were close to that of the unpromoted Co/Al_2O_3 catalyst. Note that deactivation for the all catalysts continued after 50 h, but were much slower relative to those at the initial period. More interesting results are that the wide pore unpromoted and Zr promoted Co catalysts displayed much higher activity than the narrow pore catalysts, and the wide pore unpromoted 25%Co/HP-14/150 catalysts were quite stable during 150 h of testing at 50% CO conversion. These results clearly suggest that Zr promoter increased activity of the Co catalyst on a per g catalyst basis, and that the wide pore Al_2O_3 support benefited the Co catalyst activity. This should be attributed to increases in cobalt surface site densities, either due to increased Co reduction and/or Co dispersion by Zr promoter or larger pore as discussed previously.

Table 1.16 lists average values of CO rates and hydrocarbon selectivities and CO_2 selectivities of all five Co/Al_2O_3 catalysts in the periods of 8 to 50 h and 50 to 120 h. The results of mean CO rates are consistent with the results shown in Figure 1.24. The mean CO rates shown in Table 1.16 indicate that Zr promoter accelerated catalyst deactivation, and wide pore support shows lower deactivation rate. The order of deactivation rate ($100\times (r_{CO,\ initial}-r_{CO,end})/r_{CO,initial}$) during about 120 to 140 h of testing is as follows: wide pore unpromoted 25%Co/Al_2O_3 (5.2%) < wide pore 1%Zr-25%Co/Al_2O_3 (22.8%) < narrow pore unpromoted 25%Co/Al_2O_3 (27.6%) < narrow pore 1%Zr-25%Co/Al_2O_3 (33.3%) < narrow pore 5%Zr-25%Co/Al_2O_3 (41.1%).

TABLE 1.16.—ACTIVITY, SELECTIVITIES TO CH_4, C_2-C_4, C_5 AND CO_2 OVER UNPROMOTED AND ZR PROMOTED 25%Co/Al_2O_3[a]

TOS, h	$X_{CO,}$ %	$r_{CO,}$ mol/$g_{catalyst}$/h	Usage ratio	Selectivity, C_{atom} %			CO_2 selectivity, %
				CH_4	C_2-C_4	C_{5+}	
Unpromoted 25%Co/Al_2O_3 (narrow pore)							
8 to 53	51.04	0.0286	2.14	8.31	9.23	82.46	0.75
53 to 145	51.44	0.0207	2.16	8.90	11.08	80.02	0.85
1%Zr-25%Co/Al_2O_3 (narrow pore)							
8 to 50	51.90	0.0315	2.10	7.28	7.19	85.54	0.80
50 to 121	49.42	0.0210	2.11	8.21	9.32	82.47	0.75
5%Zr-25%Co/Al_2O_3 (narrow pore)							
8 to 49	50.97	0.0358	2.13	7.05	7.75	85.20	0.49
49 to 121	47.36	0.0211	2.18	8.00	10.19	81.81	0.63
Unpromoted 25%Co/Al_2O_3 (wide pore)							
8 to 50	53.69	0.0479	2.19	5.85	4.98	89.18	0.62
50 to 147	50.85	0.0454	2.21	6.31	5.71	87.99	0.51
1%Zr-25%Co/Al_2O_3 (wide pore)							
9 to 48	50.67	0.0523	2.19	6.35	5.56	88.09	0.37
48 to 122	48.91	0.0404	2.23	6.75	6.41	86.84	0.48

[a]Reaction conditions: 220 °C, 2.17 MPa, and $H_2/CO = 2.1$.

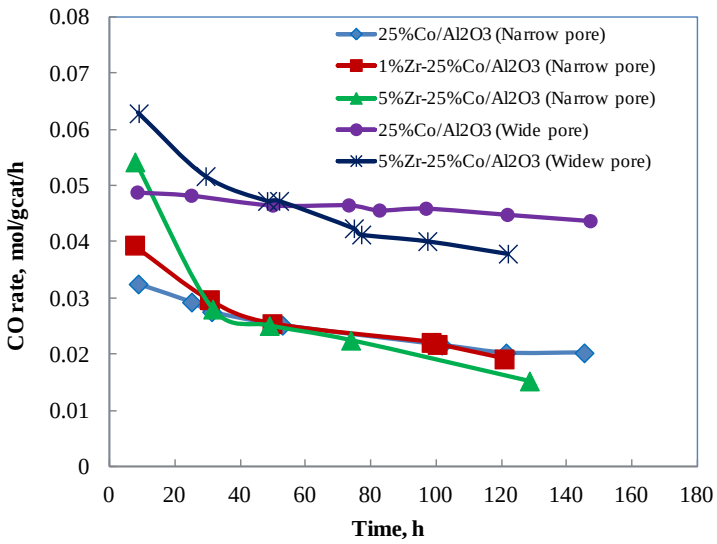

Figure 1.24.—Effect Zr loading and pore size on CO rate. Reaction conditions: 220 °C, 2.17 MPa, H_2/CO = 2.1, X_{CO} = 49-51%.

Figure 1.25(a) and (b) demonstrate the changes in CH_4 and C_{5+} selectivities, respectively, with time over the narrow and wide pore Co/Al_2O_3 catalysts obtained at about 50% CO conversion. During the entire testing periods, the wide pore Co/Al_2O_3 catalysts clearly yielded lower CH_4 selectivity (5.8 to 6.8 vs. 7 to 9.0%) and higher C_{5+} selectivity (87 to 90% vs. 88 to 80%) compared to the narrow pore Co/Al_2O_3 catalysts, and the selectivities in all cases are relatively stable after 50 h. Addition of Zr onto the narrow Al_2O_3 support decreased CH_4 selectivity and increased C_{5+} selectivity of the Co/Al_2O_3 catalyst, and increasing Zr content from 1 to 5% led to a greater change in selectivities for the narrow pore Co/Al_2O_3 catalysts. However, addition of Zr to the wide pore Al_2O_3 catalyst support resulted in slightly increasing CH_4 selectivity and decreasing C_{5+} selectivity. The conclusion from the mean values of the selectivities shown in Table 1.16 are consistent with those from Figure 1.25(a) and (b). The different selectivity trends observed for the narrow and wide pore Co/Al_2O_3 catalysts might be associated with pore size and Co distribution on the catalyst surface. The change in CO_2 selectivity with time is shown in Figure 1.26 and Table 1.16 The wide pore support offered slightly lower CO_2 selectivity (< 0.5%) than the narrow pore support (> 0.5%) after 20 h. The addition of Zr promoter slightly decreased CO_2 for both of the supports, suggesting Zr promoter slightly suppressed the water-gas shift (WGS) reaction.

The effects of alumina pore size and Zr promoter, including its loading, on the C_2-C_4 olefin to paraffin (O-T-P) ratios and their mean contents are shown in Figure 1.27 and Table 1.17. Higher O-T-P ratios and higher olefin contents for the C_2-C_4 gaseous products of the unpromoted wide pore Co/Al_2O_3 catalyst were clearly observed relative to the unpromoted narrow pore Co/Al_2O_3 catalyst. However, the presence of Zr increased the C_2-C_4 O-T-P ratios and the olefin contents for the narrow pore Al_2O_3 support but decreased the ratios and the olefin contents for the wide pore support. The results suggest that the hydrogenation rate was enhanced for the narrow pore Al_2O_3 support, and the presence of Zr promoter lowered the hydrogenation rate for the case of the narrow pore. The increase in O-T-P ratios with the presence of Zr in the narrow pore is in agreement with the study of Xiong et al. (Ref. 56) with Zr modified Co/Al_2O_3.

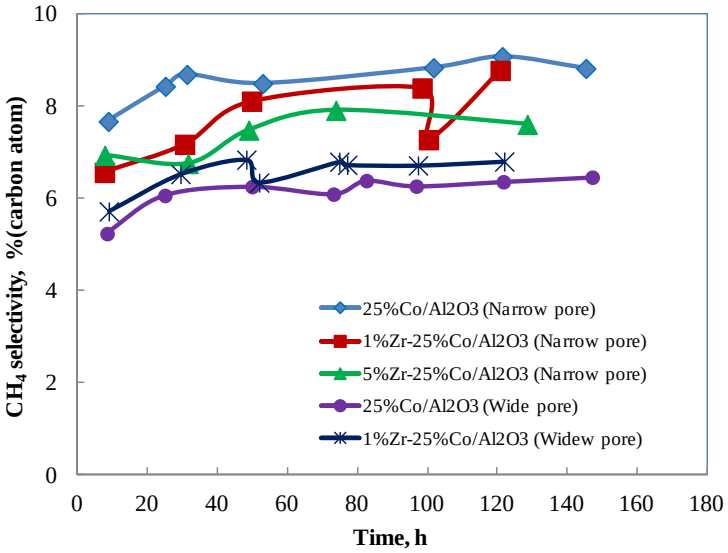

(a)

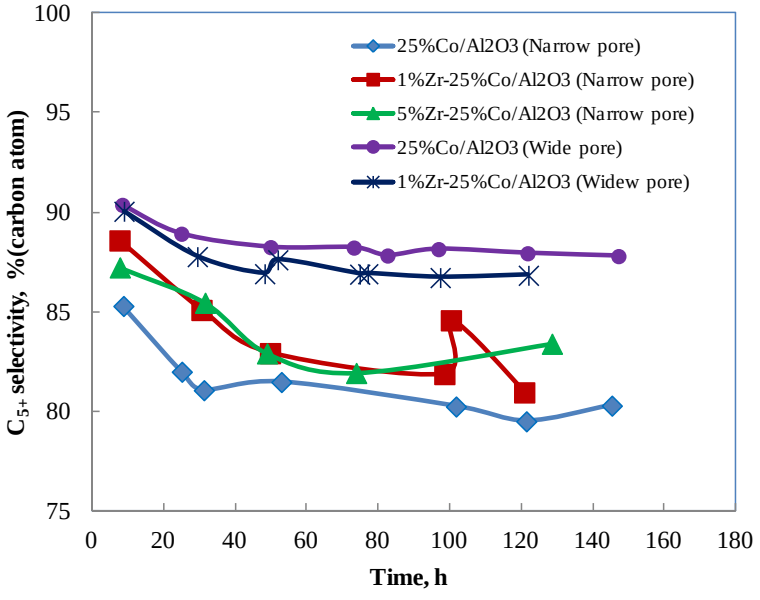

(b)

Figure 1.25.—Effect Zr loading and pore size on (a) CH_4 selectivity, (b) C_{5+} selectivity. Reaction conditions: 220 °C, 2.17 MPa, H_2/CO = 2.1, X_{CO} = 49-51%.

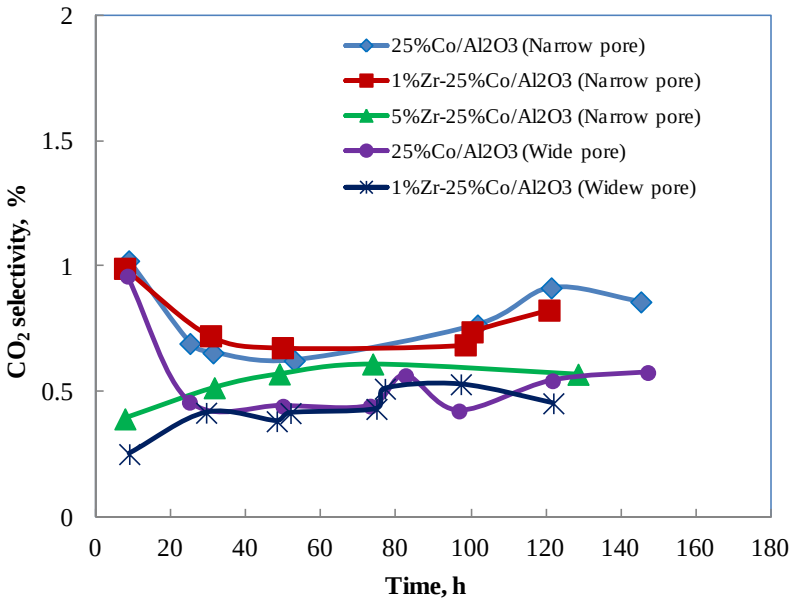

Figure 1.26.—Effect Zr loading and pore size on CO_2 selectivity. Reaction conditions: 220 °C, 2.17 MPa, H_2/CO = 2.1, X_{CO} = 49-51%.

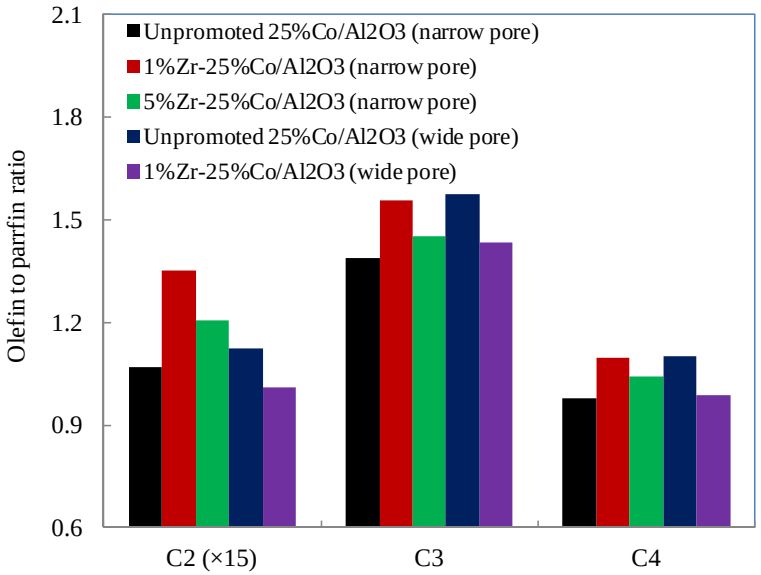

Figure 1.27.—Effect Zr loading and pore size on average olefin/paraffin ratio. Reaction conditions: 220 °C, 2.17 MPa, H_2/CO = 2.1, X_{CO} = 49-51% and 8-145 h.

TABLE 1.17.—C_2-C_4 OLEFINS AND PARAFFINS SELECTIVITIES OVER UNPROMOTED AND Zr PROMOTED 25%Co/Al_2O_3[a,b,c,d]

TOS, h	X_{CO}, %	Selectivity, %							
		C_2		C_3		C_4		C_4	
		Olefin	Paraffin	Olefin	Paraffin	Olefin	Paraffin	1-olefin	2-olefin
Unpromoted 25%Co/Al_2O_3 (narrow pore)									
8 to 53	51.04	6.62	93.38	58.76	41.24	50.20	49.80	45.76	4.44
53 to 145	51.44	6.70	93.30	57.18	42.82	48.23	51.77	44.05	4.17
1%Zr-25%Co/Al_2O_3 (narrow pore)									
8 to 50	51.90	8.56	91.44	61.58	38.42	52.62	47.38	49.13	3.49
50 to 121	49.42	7.94	92.06	60.11	39.89	51.87	48.13	48.09	3.78
5%Zr-25%Co/Al_2O_3 (narrow pore)									
8 to 49	50.97	7.20	92.80	59.67	40.33	51.22	48.78	47.52	3.70
49 to 121	47.36	7.81	92.19	58.52	41.48	50.58	49.42	46.87	3.72
Unpromoted 25%Co/Al_2O_3 (wide pore)									
8 to 50	53.69	6.30	93.70	59.87	40.13	51.58	48.42	45.92	5.66
50 to 147	50.85	7.38	92.62	61.88	38.12	52.90	47.10	48.85	4.05
1%Zr-25%Co/Al_2O_3 (wide pore)									
9 to 48	50.67	5.85	94.15	57.52	42.48	48.37	51.63	43.72	4.65
48 to 122	48.91	6.73	93.27	60.18	39.82	50.91	49.09	47.25	3.66

[a]Reaction conditions: 220 °C, 2.17 MPa, and $H_2/CO = 2.1$.

[b]C_i olefin selectivity, % = 100 × rates of C_i olefins/rates of C_i paraffins + rates of C_i olefins)

[c]1-C_4 olefin selectivity, % = 100 × rate of 1-C_4 olefin/rates of all C_4 hydrocarbons

[d]2-C_4 olefin selectivity, % = 100 × rate of 2-C_4 olefin/rates of all C_4 hydrocarbons

The selectivity of 1-C_4 of the five catalysts shown in Figure 1.28 offers the same conclusion. However, Figure 1.28 also shows that 2-C_4 olefin selectivity was higher in the case of the unpromoted wide pore Co/Al_2O_3 catalyst compared with that of the narrow pore unpromoted Co/Al_2O_3 catalyst, indicating that the wide pore support led to a higher isomerization rate. Regardless of alumina pore size, the Zr promoted Co/Al_2O_3 catalysts showed lower 2-C_4 olefin selectivity, suggesting that the isomerization of 1-olefins was inhibited with the presence of Zr promoter.

The wide pore Al_2O_3 support and addition of Zr promoter significantly increased Co/Al_2O_3 activity on a per g catalyst basis. Calculation of the initial Co turnover numbers of the five Co catalysts based on initial FTS rate and H_2-chemisorption results indicated that the values are nearly constant, $0.084 \pm 0.002\ s^{-1}$, suggesting that the increased activity was mainly due to the larger pore size or Zr promoter increasing Co site density (increased Co dispersion and/or Co reduction), rather than by increasing Co intrinsic activity. The wide pore Co/Al_2O_3 catalyst displayed lower CH_4 selectivity and higher C_{5+} selectivity. Smaller Co clusters present on the wide pore Co/Al_2O_3 catalyst as determined by hydrogen chemisorption (Table 1.14) and XRD (Figure 1.19) and lower H_2/CO ratio generally occurred in the case of the wide pore catalyst due to less mass transport limitations may be primarily responsible for the selectivity results. This assumption is apparently evident by the higher C_2-C_4 olefin selectivity and higher 1-C_4 olefin selectivity (lower hydrogenation) obtained for the wide pore unpromoted Co/Al_2O_3 catalyst relative to the narrow pore catalyst. It is interesting that Zr promoter led to different CH_4 and C_{5+} selectivity trends with the narrow and wide pore Co/Al_2O_3 catalysts, namely decreases and increases in CH_4 selectivity on the narrow pore and wide pore Al_2O_3 supports, respectively. The decreases in CH_4 selectivity with the narrow pore Al_2O_3 support can be attributed to the increased Co reduction degree by Zr; therefore, less cobalt oxides remained during FTS reaction, and/or a smaller Co cluster size resulted by adding the Zr promoter. On the other hand, for the wide pore Al_2O_3 support, although addition of 1% Zr also increased Co dispersion and reduced Co cluster size, the Co reduction degree was changed to a lesser degree. However, adding 1%Zr onto the wide pore support narrowed pore size (Figure 1.18 and Table 1.14), which can lead to a higher H_2/CO ratio in the pore due to possible increases in mass transfer resistance. Therefore, the synergistic

effects of Zr decreasing Co cluster size and pore size might impact CH_4 formation, resulting in slightly higher CH_4 selectivity in the case of the Zr promoted wide pore Co/Al_2O_3 catalyst.

The higher CO_2 selectivity observed with the narrow pore Co catalysts could be related to lower Co reduction. Since the WGS reaction tends to increase with the presence of higher amounts of Co oxides (Refs. 57, 58, and 59), the presence of Zr decreasing CO_2 selectivity could be related to increased Co reduction and increased FTS on smaller Co clusters (i.e., having higher site Co surface site densities).

The unpromoted wide pore Co/Al_2O_3 catalyst showed slightly higher O-T-P ratios in the carbon range of C_2 to C_4 and 1-C_4 olefin than the unpromoted narrow pore one. However, it should be kept in mind that, in all cases, the O-T-P ratio or olefin content of C_2 was about 9 to 15 times less than those of C_3 and C_4, which is due to the greater activity of ethene relative to C_3 and C_4 olefins (Ref. 60). C_3 olefin in total C_3 hydrocarbons was about 58.5 to 60% in this study, which is significantly lower than that, i.e., 85 to 86%, of the study of Feller et al. with $Zr\text{-}Co/SiO_2$ catalysts (Ref. 61). This should be mainly due to the higher temperature and much higher conversion level used in this study (220 vs. 190 °C, X_{CO}: 50% vs. 6 to 16%). Possibly, a lower hydrogen surface concentration in the case of the wide pore support compared to the narrow pore support implied by the lower CH_4 selectivity of the wide pore Co catalyst, may be responsible for the low extent of hydrogenation and slightly higher olefin selectivity in the case of the wide pore catalyst. Similarly, the increased C_2-C_4 olefin selectivity and decreased C_2-C_4 olefin selectivity in narrow or wide pore Co/Al_2O_3 catalysts, respectively, with the presence of Zr (Figure 1.27 and Figure 1.28) could be also mainly due to the adjustments of surface hydrogen concentration by the presence of Zr. For the narrow pore Co/Al_2O_3 catalyst, the presence of Zr (1-5%) resulted in lower CH_4 selectivity, suggesting a lower H_2/CO ratio in the catalyst surface. This decreased hydrogenation and increased olefin content. Furthermore, addition of Zr slightly decreased the WGS reaction rate resulting in a lower partial pressure of hydrogen; this could be another reason for the observed higher O-T-P ratios. However, in the case of the wide pore Co/Al_2O_3 catalyst, addition of Zr led to slight increases in CH_4, indicating an increased surface H concentration, consequently leading to slightly enhanced hydrogenation and a lower olefin/paraffin ratio.

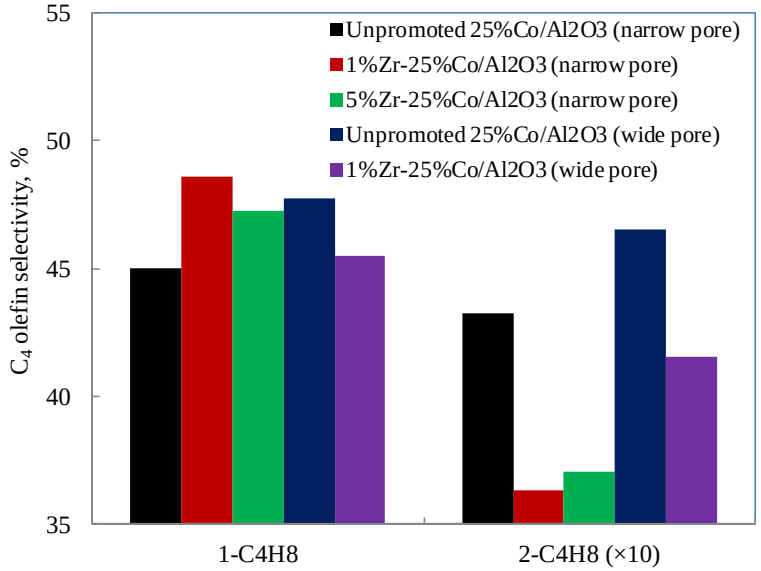

Figure 1.28.—Effect Zr loading and pore size on average selectivities to 1-butene and 2-butene. Reaction conditions: 220 °C, 2.17 MPa, H_2/CO = 2.1, X_{CO} = 49-51% and 8-145 h.

The 2-butene selectivity is more than 10 times less than 1-butene selectivity (Figure 1.28). This has been presumed to be due to a limited number of H atoms in the β-position (Ref. 61) that are required for isomerization. The presence of Zr in the Co/Al_2O_3 catalysts, regardless of support type, reduced the extent of isomerization. It has been reported that isomerization of the double bond reaction is facile on acid sites. Since the presence of Zr weakens the Co-Al interaction and increases Co reduction, the Co oxides or the interface of Co oxides with the support, reported to serve as active sites for isomerization of butene and olefins (Refs. 62 and 63), would decrease. Feller et al (Ref. 61) reported increased isomerization with increasing Zr loading when they studied the Zr effect on Co/SiO_2 catalyst behavior. They presumed that Zr catalyzed the isomerization reaction. However, this is not observed in this study. The slightly higher 2-C_4 olefin selectivity in the case of the wide pore catalyst could be due to smaller Co or CoO cluster size modified by the Zr promoter, which could increase the surface concentration of acid sites for the isomerization reaction; and/or the wide pore itself contributes less spatial resistance for isomerization.

1.3.4 Conclusions

Zr-doping is a complex subject. The method of preparation, cobalt loading, support type, and support porosity all play key factors in determining whether or not Zr doping improves Co site densities resulting in enhanced catalyst performance. When added to a weakly interacting support like SiO_2, Zr-doping can enhance the support interaction to stabilize a smaller cobalt cluster size. If Zr is added within narrow pore alumina, a strongly interacting support, as we previously observed utilizing the IWI method and lower cobalt loadings, very small strongly interacting cobalt oxides are formed which are difficult to reduce, resulting in lower cobalt site density relative to the unpromoted catalyst.

When the slurry method is used on a narrow pore support, larger cobalt clusters are formed, and the size suggests these are located at the mouth of pores and possibly external to pores. Zr-doping exacerbates this effect. The slightly larger species formed are marginally more reducible, and slight increase in site density results.

However, with wide pore alumina, the effect is very different. The cobalt is situated within pores, and Zr addition slightly narrows the pore to generate smaller, somewhat more interacting cobalt species. Because a significant fraction remains reducible, there is an important increase in the cobalt site density.

FTS over the wide and narrow pore Co/Al_2O_3 catalysts was carried out at 220 °C, 2.2 MPa, H_2/CO =2.1 and about 50% CO conversion using a 1-L CSTR for a long period time (about 150 h). Space velocity was adjusted if needed during testing. The wide pore alumina greatly improved stability of the unpromoted 25%Co/Al_2O_3 catalyst compared to the narrow pore one. During 150 h testing, the CO rate of the wide pore catalyst only lost 5.2%. Zr modified alumina supports significantly improved Co catalyst activity, but at the same time increased the catalyst deactivation rate. Calculation of Co turnover number based on FTS data and H_2 chemisorption results indicated that the pore size (wide or narrow) and Zr promoter (1 to 5%) did not change Co turn over number (intrinsic activity), suggesting the activity improvement by the larger sized pore and Zr promoter is due to increases in Co site density.

Both pore size and Zr promoter modified the catalyst selectivities. The wide pore Co/Al_2O_3 catalyst displayed lower CH_4 and higher C_{5+} selectivity, higher C_2-C_4 olefin and 2-C_4 olefin selectivities, which are possibly attributed to smaller Co cluster size, and lower hydrogenation rate or less spatial resistance in the wide pore catalyst. It was found that the effect of Zr on catalyst selectivity depends on alumina pore size. Addition of Zr to narrow pore alumina decreased CH_4, increased C_{5+} selectivity and C_2-C_4 olefin selectivity, but the opposite selectivity trends were found with the wide pore alumina catalyst. A number of possibilities were considered to explain selectivity trends - Zr adjusted Co reduction, Co size and alumina pore size and surface H_2/CO concentration by slightly adjusting WGS reaction or changes in mass transfer resistances. Zr was also found to suppress isomerization of C_4 olefin regardless of alumina pore size. This is probably due to Zr increasing acid sites by decreasing Co or CoO cluster size and/or Zr narrowing pore size and changing the spatial resistance for the reaction.

CO_2 selectivity was slightly lower for the wide pore Co/Al_2O_3 catalyst compared with the narrow pore one. The presence of Zr promoter further decreased CO_2 selectivity. Higher Co reduction (i.e., less Co oxide) for the wide pore and Zr promoted Co/Al_2O_3 catalysts might be responsible for the lower CO_2 selectivity observed.

2.0 Fischer-Tropsch Stability Issues

2.1 Effect of Cobalt Particle (Sieve) Size of a Pt Promoted Co/Al_2O_3 Catalyst

2.1.1 Introduction

The Fischer–Tropsch synthesis (FTS) is at the core of the gas-to-liquids (GTLs) processes which have recently received a renewed interest as a versatile catalytic route for producing high quality ultra-clean fuels from synthesis gas or syngas ($CO + H_2$) (Ref. 64). This interest is mainly driven by the increasingly stringent environmental legislation on transportation fuels and the possibility to monetize abundant and remote natural gas reserves as well as renewable biomass sources with independence from the petroleum supply (Ref. 65). Of particular interest is the Fischer–Tropsch derived (or synthetic) diesel fuel, which displays substantially higher cetane number (typically above 70) than that obtained in conventional refineries from crude oil while being virtually free of environmentally harmful sulfur.

Fischer–Tropsch Synthesis is catalyzed by transition metals, especially Co, Fe and Ru. Among them, cobalt-based catalysts are preferentially applied in FTS processes aimed at producing precursors of the synthetic diesel owing to their high selectivity towards long chain n-paraffins, their remarkable stability and their lower activity for the competing water gas shift reaction (WGS) as compared to alternative catalysts based on iron (Ref. 66). Optimal design of a Co FT catalyst is essential for its utilization; this goal could be achieved by decreasing the Co particle size to increase the exposed surface area per unit mass of the Co metal. However, some investigators have reported that Co particles smaller than 10 nm show a sharp drop in activity (Refs. 67, 68, 69, and 70). The pioneering study of this particle size effect was conducted by Bartholomew's group (Ref. 67) who claimed that the specific activity and molecular weight of hydrocarbon products decreased significantly with an increase of Co dispersion, consistent with a particle size effect. The catalytic performance of Co can vary with different supports, dispersions, metal loadings and preparation methods, which are indications of structure sensitivity. Interestingly, in a later work (Ref. 71), Bartholomew and co-workers pointed out that FTS under certain reaction condition can be structure insensitive. The activity and selectivity appeared to be more closely related to the chemical nature of the support rather than to Co dispersion. Subsequently similar results have been reported by several other research groups (Refs. 72, 73, 74, and 75). The consensus of these studies is that there is no intrinsic particle size effect in FTS. Recently Barbier (Ref. 68) and Bezemer and co-workers (Ref. 69) observed that the activity and selectivity are sensitive to Co particle size with particles smaller than 10 nm. More recently Borg et al. (Ref. 70) emphasized the effect of particle size on selectivity, while no relationship was found between activity and Co size. Therefore, the particle size effect of Co FT catalysts with size below 10 nm is still controversial and more work is required to clarify this fundamental issue.

In order to examine differences in the stability cobalt/alumina catalysts as a function of catalyst particle size (i.e., not Co cluster size), to find an appropriate catalyst particle size, in one of the catalysts FTS was run with different catalyst particle sizes (20 to 63 μm, 63 to 106 μm, 106 to 180 μm, and 180 to 355 μm). To conclude, it is reasonable to say that because of the complex nature of the FTS, any study of the catalytic performance of similar catalysts requires strict control of reaction conditions. For this reason, all catalysts were subjected to the same reactor setup and gaseous environment during synthesis.

2.1.2 Experimental

2.1.2.1 Catalyst Preparation

In order to examine differences in the stability cobalt/alumina catalysts as a function of catalyst particle size (i.e., not Co cluster size), two 2 kg batches of catalyst were prepared—unpromoted $25\%Co/Al_2O_3$ (NASA125) and $0.5\%Pt\text{-}25\%Co/Al_2O_3$ (NASA126). Sasol Catalox (high purity γ-alumina, 150 m^2/g) was used as the support for the cobalt catalyst. The catalyst was prepared by a slurry impregnation method, and cobalt nitrate was used as the precursor. In this method, which follows a Sasol patent (Ref. 76), the ratio of the volume of solution used to the weight of alumina was 1:1, such that the volume of solution was approximately 2.5 times the pore volume of the catalyst. Two impregnation steps were used, each to load 12.5% of Co by weight. Between each step the catalyst was dried under

vacuum in a rotary evaporator at 80 °C and the temperature was slowly increased to 100 °C. After the second impregnation/drying step, the catalyst was calcined under air flow at 350 °C. The promoter was added by incipient wetness impregnation, and the precursor utilized for noble metal addition was tetra ammine platinum (II) nitrate. After Pt addition, the sample was dried and calcined again at the same conditions as used previously. NASA126 was selected for the aging investigation. It was separated into four sieve ranges, 20 to 63 μm, 63 to 106 μm, 106 to 180 μm, and 180 to 355 μm.

2.1.2.2 BET Surface Area and Porosity Measurements

The measurements of BET surface area and porosity of the calcined catalysts were conducted using a Micromeritics Tri-Star system. Before performing the test, the temperature was gradually ramped to 160 °C and the sample was evacuated at least 12 h to approximately 50 mTorr. The BET surface area, pore volume (single point), and average pore radius (single point and BJH adsorption) were obtained for each sample.

2.1.2.3 H_2 Chemisorption and Percentage Reduction by Pulse Reoxidation

Hydrogen chemisorption was conducted at using temperature programmed desorption (TPD), also measured with the Zeton-Altamira AMI-200 instrument. The sample weight was typically ~0.220 g. Catalysts were activated in a flow of 10 cm^3/min of H_2 mixed with 20 cm^3/min of argon at 350 °C for 10 h. and then cooled under flowing H_2 to 100 °C. The sample was held at 100 °C under flowing argon to remove and/or prevent adsorption of weakly bound species prior to increasing the temperature slowly to 350 °C, the reduction temperature of the catalyst. The catalyst was held under flowing argon to desorb remaining chemisorbed hydrogen until the TCD signal returned to baseline. The TPD spectrum was integrated and the number of moles of desorbed hydrogen determined by comparing its area to the areas of calibrated hydrogen pulses. The loop volume was first determined by establishing a calibration curve with syringe injections of hydrogen in helium flow. Dispersion calculations were based on the assumption of a 1:1 H:Co stoichiometric ratio and a spherical cobalt cluster morphology. After TPD of hydrogen, the sample was reoxidized at 350 °C using pulses of oxygen. The percentage of reduction was calculated by assuming that metal reoxidized to Co_3O_4. Further details of the procedure are provided elsewhere (Ref. 77).

2.1.2.4 Catalytic Activity Testing

The FTS experiments were conducted using a 1 L CSTR equipped with a magnetically driven stirrer with turbine impeller, a gas-inlet line, and a vapor outlet line with a stainless steel (SS) fritted filter (2 μm) placed external to the reactor. A tube fitted with a SS fritted filter (0.5 μm opening) extending below the liquid level of the reactor was used to withdraw reactor wax (i.e., rewax, which is solid at room temperature), thereby maintaining a relatively constant liquid level in the reactor. Separate mass flow controllers were used to control the flow rates of hydrogen and carbon monoxide. Carbon monoxide was passed through a vessel containing lead oxide on alumina to remove traces of iron carbonyl. The gases were premixed in an equalization vessel and fed to the CSTR below the stirrer, which was operated at 750 rpm. The reactor temperature was maintained constant (± 1 °C) using a temperature controller.

Prior to performing the reaction test, the catalyst (~12.0 g) was ground and sieved to (20 to 63 μm, 63 to 106 μm, 106 to 180 μm, and 180 to 355 μm), and then loaded into a fixed-bed reactor for ex-situ reduction at 350 °C under atmospheric pressure for 15 h using a gas mixture of H_2/He (60 NL/h) with a molar ratio of 1:3. The reduced catalyst was then transferred to a 1 L continuously stirred tank reactor (CSTR) containing 315 g of melted Polywax 3000, by pneumatic transfer under the protection of a N_2 inert gas. Weighing the reactor before and after the transfer of catalyst was done to ensure that all catalyst powder was successfully transferred to the reactor. The transferred catalyst was further reduced in-situ at 230 °C and at atmospheric pressure using pure hydrogen (30 NL/h) for another 10 h before starting the FTS reaction.

In this study, the FTS conditions used were 220 °C, 2.1 MPa, H_2/CO = 2.0. The reactant gas mixture was analyzed prior to sending to the reactor to ensure the composition. The reaction products were continuously removed from the vapor space of the reactor and passed through two traps, a warm trap maintained at 100 °C and a cold trap held at 0 °C.

The uncondensed vapor stream was reduced to atmospheric pressure. The gas flow was measured using a wet test meter and analyzed by online GC. The accumulated reactor liquid products were removed every 24 h by passing through a 2 μm sintered metal filter located below the liquid level in the CSTR. Conversions of CO were obtained by gas-chromatography analysis (micro-GC equipped with thermal conductivity detectors) of the outlet gas product. The reaction products were collected in three traps maintained at different temperatures; a hot trap (200 °C), a warm trap (100 °C), and a cold trap (0 °C). The products were separated into different fractions (rewax, wax, oil, and aqueous) for quantification. However, the oil and wax fractions were mixed prior to GC analysis.

2.1.3 Results and Discussion

The results of surface area and porosity data as measured by N_2 physisorption at 77 K are shown in Table 2.1. Sasol Catalox-150 γ-Al_2O_3 was used as a catalyst support and its specific BET surface is 150 m^2/g. Because the analysis was taken for calcined catalysts, Co_3O_4 was deemed to be a major cobalt oxide compound in this catalyst (Ref. 78). A 34% Co_3O_4 by weight was calculated by assuming 25 wt% Co metals in Co/Al_2O_3 catalyst were completely converted to Co_3O_4 after calcination. Thus, if Al_2O_3 is the only contributor to the area, then the area of 25%Co/ Al_2O_3 catalysts should be 150×0.66 = 99 m^2/g. With 0.5% Pt promotion, it may drop 3 to 4%, which is ~96 m^2/g. BET surface area values are similar for different sieve size range catalysts. Catalysts were thus far characterized by hydrogen chemisorption / pulse reoxidation (Table 2.2), and no significant differences in site density, reducibility, or Co cluster size were noted among the different sieving ranges. Physical properties of all these catalysts are similar.

The effect of cobalt particle (sieve) size on the performance of a traditional cobalt catalyst (platinum promoted cobalt/alumina) was investigated during FTS using a continuously stirred tank reactor (CSTR). In this study, cobalt catalyst was sieved to four different ranges: 20 to 63 μm, 63 to 106 μm, 106 to 180 μm and 180 to 355 μm. To maintain experimental control, similar activation and reaction conditions were maintained while the cobalt particle (sieve) size was varied. The effect of cobalt particle size on the CO conversion for platinum promoted cobalt/alumina catalyst is shown in Figure 2.1. Initial CO conversion is same for all the catalysts; but the CO conversion varied by varying the sieve size ranges and with time under reaction conditions. For the 20 to 63 μm range catalyst, although

TABLE 2.1.—EFFECT OF COBALT PARTICLE (SIEVE) SIZE ON BET SURFACE AREA AND POROSITY MEASUREMENTS

Catalyst, μm	BET surface area, m^2/g	Single point pore volume, cm^3/g	Average pore radius, nm
20 to 63	96.2	0.229	4.76
63 to 106	98.3	0.234	4.75
106 to 180	98.7	0.236	4.78
180 to 355	95.3	0.223	4.67

TABLE 2.2.—EFFECT OF COBALT PARTICLE (SIEVE) SIZE ON HYDROGEN CHEMISORPTION/PULSE REOXIDATION MEASUREMENTS

Catalyst, μm	H_2 desorbed, $\mu mol/g_{catalyst}$	O_2 pulsed, $\mu mol/g_{catalyst}$	Reduction, %	Corrected dispersion, %	Corrected average diameter, nm
20 to 63	141.6	1801	63.7	10.5	9.8
63 to 106	128.9	1784	63.1	9.6	10.7
106 to 180	140.0	1870	66.1	10.0	10.3
180 to 355	-----	-----	-----	-----	-----

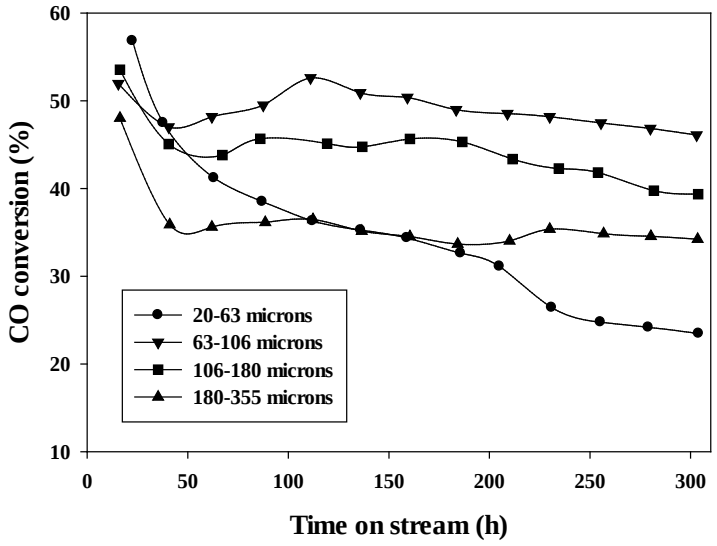

Figure 2.1.—Effect of cobalt particle (Sieve) size on CO conversion. Reaction conditions: T = 220 °C, P = 275 psig, SV-3 slph/$g_{catalyst}$, H_2/CO = 2, and startup solvent Polywax 3000.

high initial conversion was observed, it decreased in 200 h and then reached a steady-state level. For the 180 to 355 μm range catalyst, slightly higher conversion was obtained relative to the 20 to 63 μm range catalyst. Higher CO conversion and lower deactivation rate were observed with the 63 to 106 μm range catalyst. CO conversion was observed to increase according to the following trend in the particle (sieve) size: 20 to 63 μm < 180 to 355 μm < 106 to 180 μm < 63 to 106 μm. That is, conversion increases as the catalyst particle size decreases in the range tested except for the 20 to 63 μm range catalyst. At steady state CO conversion (except in the case of the 20 to 63 μm range catalyst), CO conversion decreased with increasing cobalt catalyst sieve size. CO conversion for all these catalysts slightly decreased with time. Physical properties of all these (four) catalysts were similar, such as pore size and chemisorption results (Table 2.1 and Table 2.2). These results are consistent with the view that, for the larger sieve size range, lower CO conversion or deactivation may be explained by filling with heavy wax in the interior of the catalyst particle, thereby blocking off available catalytically active sites. The high activity of the smaller sieve size range catalyst might be due to the interior pore volume being low, and thus the catalyst is more resistant to filling by heavy wax. The availability of Co surface sites thus appears to remain high. The explanation for the activity of the 20 to 63 μm range catalyst remains unknown, because its CO conversion is lower than other three catalysts, and based on our assumption it would be expected to exhibit higher activity than the other catalysts.

The effect of cobalt particle (sieve) size on product selectivity is shown in Figure 2.2 and Figure 2.3 for methane and higher hydrocarbon (C_5+), respectively. The methane selectivity slightly increased with time for all the catalysts and the corresponding C_5+ selectivity slightly decreased with time. Methane and C_5+ selectivities followed similar trends with CO conversion. With increasing the CO conversion, methane selectivity will decrease and the corresponding C_5+ selectivity will increase. The adverse selectivities are directly the result of significant deactivation, since in FTS; selectivity is a function of CO conversion. At steady state CO conversions, product selectivities were compared and are provided in Figure 2.4. At steady state CO conversion (with the exception of the 20 to 63 μm range catalyst), methane selectivity increased and the corresponding C_5+ selectivity decreased with increasing cobalt catalyst sieve size. At similar CO conversion level for all these catalysts, the product selectivities (methane and C_5+) were almost the same (Table 2.3). For the 20 to 63 μm range catalyst, methane selectivity was slightly lower and the corresponding higher hydrocarbon (C_5+) selectivity was slightly higher compared to the other catalysts.

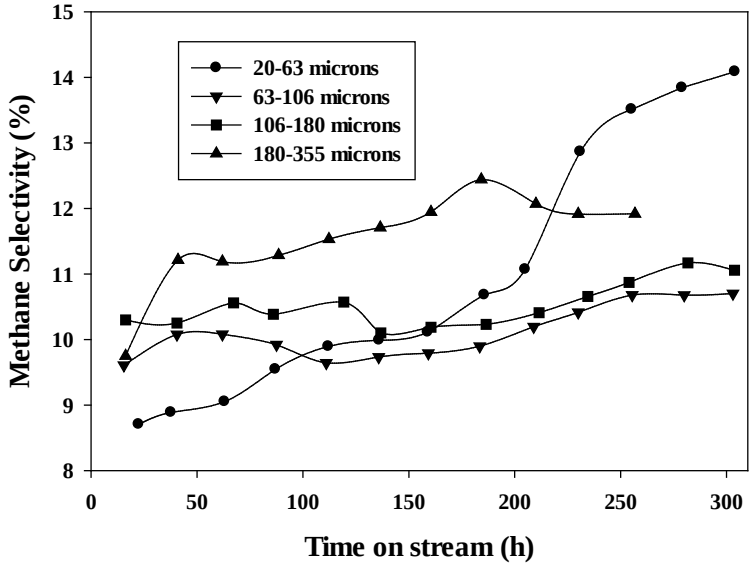

Figure 2.2.—Effect of cobalt particle (Sieve) size on methane selectivity. Reaction conditions: T = 220 °C, P = 275 psig, SV-3 slph/$g_{catalyst}$, H_2/CO = 2, and startup solvent Polywax 3000.

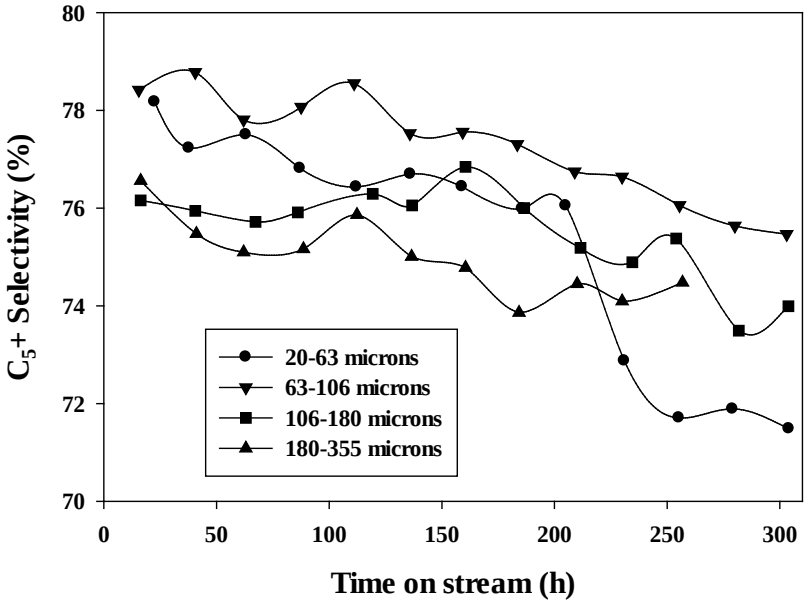

Figure 2.3.—Effect of cobalt particle (Sieve) size on C_5+ selectivity. Reaction conditions: T = 220 °C, P = 275 psig, SV-3 slph/$g_{catalyst}$, H_2/CO = 2, and startup solvent Polywax 3000.

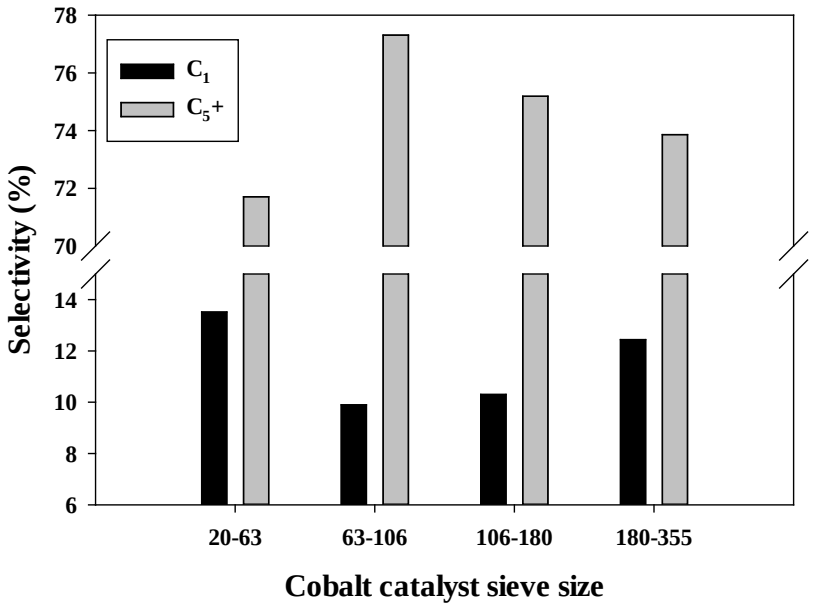

Figure 2.4.—Effect of cobalt particle (Sieve) size on selectivity at steady state CO conversion. Reaction conditions: T = 220 °C, P = 275 psig, SV-3 slph/$g_{catalyst}$, H_2/CO = 2, and startup solvent Polywax 3000.

TABLE 2.3—EFFECT OF COBALT PARTICLE (SIEVE) SIZE ON PRODUCT SELECTIVITY AT SIMILAR CO CONVERSIONS

Catalyst, μm	CO conversion, %	Selectivity, %	
		C_1	C_5+
20 to 63	34.38	10.11	76.44
63 to 106	34.48	11.66	74.22
106 to 180	39.37	11.06	74.00
180 to 355	34.04	12.07	74.45

2.1.4 Conclusions

The effect of cobalt particle (sieve) size on the performance of a platinum promoted cobalt/alumina was investigated during FTS. At steady state CO conversions (with the exception of the 20 to 63 μm range catalyst), CO conversion decreased with increasing the cobalt catalyst particle (sieve) size. These results are consistent with the view that, for the larger sieve size range, deactivation may occur by filling with heavy wax in the interior of the catalyst particle, thereby blocking off available catalytically active sites. The adverse selectivities are directly the result of significant deactivation, since selectivity is a function of conversion. For the smaller sieve size range, the interior pore volume is low, and thus the catalyst is more resistant to filling by heavy wax. The availability of Co surface sites thus appears to remain high.

2.2 Fischer-Tropsch Synthesis: Oxidation of a Fraction of Cobalt Crystallites in Research Catalysts at the Onset of FT at Partial Pressures Mimicking 50% CO Conversion

CoO formed at the onset of FTS by oxidation of tiny Co crystallites was proposed as one possible culprit in catalyst deactivation. CoO formation is undesirable because it can contribute to a complex reduction/sintering mechanism as a function of time on-stream, or form difficult-to-reduce cobalt aluminate species by reaction with Al_2O_3. In this work, freshly H_2-reduced catalyst samples and Fischer-Tropsch synthesis (FTS) catalyst samples (i.e., freshly reduced and immediately exposed to the onset of FTS conditions mimicking 50% CO conversion) were prepared for the purpose of comparison. Each sample was coated in-situ using molten polywax and then solidified within the same system, so that an air-protected sample was obtained, which was further transferred and stored in inert gas. XAS was utilized as an effective tool for investigating the oxidation state of cobalt. A fraction of cobalt crystallites in the freshly reduced research catalysts having lower-than-commercial loading and smaller crystallites undergoes a degree of oxidation to CoO at the onset of FTS conditions simulating 50% CO conversion. Therefore, it is suggested that in attempts to decrease Co content by increasing the dispersion of cobalt with the aim of improving Co efficiency, very small Co crystallites are obtained, and their reoxidation at the onset of FTS should not be disregarded. Thus, catalysts should be designed to have an optimum narrow cluster size range—small enough to increase Co surface site densities, but large enough to avoid reoxidation, and the stability problems that arise from having unreduced Co in the working catalyst.

2.2.1 Introduction

The aim of decreasing deactivation rates of Co/Al_2O_3 catalysts for FTS is one of the important challenges facing the commercial development of these catalysts for the conversion of coal, biomass, and natural gas to liquid fuels as alternative resources to crude oil (Ref. 79). Therefore, we and other research groups have been rigorously investigating this issue, and plausible deactivation mechanisms have been proposed. However, there is a debate in the literature regarding whether tiny cobalt nanoparticles oxidize under realistic synthesis conditions (Ref. 80). Part of the confusion stems from the fact that while some groups are examining commercial catalysts that use heavy cobalt loadings to stabilize them against reoxidation, other groups are using research catalysts aimed at reducing the amount of expensive cobalt metal and improving Co efficiency. The other major source of confusion has to do with the time period under which catalysts are examined. While some groups examine the decay period prior to leveling off for realistic commercial catalysts under relevant FTS conditions, others are focused on the susceptibility of tiny cobalt crystallites at the onset of FTS to reoxidation at high conversions of interest. That is, the freshly activated catalyst is directly exposed to FTS conditions or conditions that mimic realistic conversions.

Typically, a slurry impregnation method is employed to prepare Co catalysts having higher loadings, while incipient wetness impregnation (IWI) is often used to prepare Co catalysts with lower loadings. The slurry impregnation method tends to produce a larger Co cluster (~8 to 15 nm by hydrogen chemisorption / pulse reoxidation (Ref. 81)) at 15 to 25% Co loadings on γ-Al_2O_3 relative to the average cluster size obtained by IWI (~5 nm by hydrogen chemisorption / pulse reoxidation (Ref. 81). However, even with an average cluster size of ~5 nm, one should consider the existence of a fraction of particles < (2 to 4.1 nm) that could undergo reoxidation as determined by recent thermodynamics studies (Ref. 82). TPR profiles for Co/Al_2O_3 catalysts show very broadened peaks for the CoO reduction step suggesting a distribution of size. Thus, reoxidation of a fraction of Co^0 crystallites to CoO is one possibility. Another possibility is loss of tiny Co^0 crystallites to the support (Refs. 83 and 84), which likely first involves CoO formation as an intermediate.

In light of recent findings, however, one must also consider that cobalt support compounds may form from the reaction of CoO left over from incomplete reduction, due to strong interaction of CoO with the Al_2O_3 support. Moodley et al. (Ref. 85) examined used catalyst samples from a CSTR reactor, and by adjusting CO conversion and total pressure to achieve $P(H_2O)$ = 10 bar, about 10% cobalt aluminate was found to form in their working catalyst (Ref. 85). The authors attributed this cobalt aluminate formation to the conversion of CoO that was present in the

catalyst due to incomplete reduction. In reexamining this issue and considering catalyst samples obtained by our group (Refs. 79 and 86), there is the possibility that a fraction of the $CoAl_2O_4$ formed in used catalyst samples came from CoO that was already present due to incomplete reduction. In support of this viewpoint, a used unpromoted $15\%Co/Al_2O_3$ catalyst (with about half the extent of reduction relative to promoted catalysts) had 2 to 3 times the amount of cobalt aluminate as compared to the used Pt and Ru promoted $15\%Co/Al_2O_3$ catalyst (Ref. 79). A transformation from CoO to $CoAl_2O_4$ retains the Co^{2+} oxidation state, but $CoAl_2O_4$ is very difficult to reduce compared to CoO. Investigating used $0.2\%Re\text{-}15\%Co/Al_2O_3$ catalyst samples periodically withdrawn from a CSTR reactor as a function of time, XAFS analysis (Ref. 86 and 87) demonstrated that considerable CoO was present initially, as peaks were present for Co-O and Co-Co in the oxide in EXAFS spectra (Ref. 86). Moreover, as the catalyst underwent initial deactivation and leveling off, the extent of Co reduction increased slowly with time on stream (Ref. 87), Co-Co coordination increased to suggest possible net sintering (Ref. 86), and a small amount of cobalt aluminate formed (Ref. 86). During the run, there was a slow decrease in the white line intensity (increasing extent of Co reduction) (Ref. 87) and a significant growth in the Co-Co coordination metal shell (Ref. 86). It is fathomable that the CoO may coalesce to form larger domains that then undergo reduction during an FT run. Cobalt metal particles present may also agglomerate or ripen, a process that could exacerbated by any additional Co^0 formed from net slow reduction of sintered CoO during the course of a run. The main point is that net oxidation *during the initial decay period* as a function of time on-stream was not observed by us.

However, it is also important to examine one other region of deactivation, and that is the onset of FTS when a freshly activated catalyst is directly exposed to high conversion FTS conditions. By a linear extrapolation to time zero, it is intriguing that only 35% cobalt reduction was obtained for our $0.2\%Re\text{-}15\%Co/Al_2O_3$ catalyst (Ref. 87) at the onset of FTS while it should have been 55% (Ref. 86) as measured for the freshly activated catalyst by O_2 pulse reoxidation. Thus, the results suggest that some reoxidation of tiny crystallites may have occurred at the *onset* of FTS at realistic conversions. The average cluster (i.e., cluster of smaller crystallites) size by hydrogen chemisorption / pulse reoxidation was ~5 nm.

The sensitivity of Co catalysts to H_2O has been explored by many research groups (Refs. 88 to 92), as water is often cited as exacerbating deactivation. At low amounts of added H_2O, a positive impact on the CO conversion rate was observed with Co/SiO_2 catalysts, but at higher levels, the catalyst underwent rapid deactivation (Ref. 91). For a $0.5\%Pt\text{-}15\%Co/Al_2O_3$ catalyst having an average Co cluster size of ~ 5.6 nm, increasing the H_2O to 28% by volume by replacing inert balancing gas led to catastrophic and irreversible deactivation (Ref. 92). Moreover, the formation of cobalt support compounds (e.g., cobalt aluminate) was identified in XANES derivative spectra (Ref. 83). Interestingly, an unpromoted catalyst containing a higher Co loading (25%Co with cobalt cluster size ~ 11.8 nm) was found to be much more robust (i.e., switching off H_2O co-feeding at 30 vol.% H_2O, the catalyst largely recovered its activity) (Ref. 88). In a repeat run where samples were retrieved from the reactor and analyzed, the catalyst displayed metallic character prior to $25\%H_2O$ addition, but during $25\%H_2O$ addition some CoO formation was observed in the XANES spectra (Ref. 88). However, after H_2O was switched off, the catalyst was found to re-reduce. This oxidation-reduction cycle led to some growth in the Co-Co metal peak for the point after the H_2O was switched off compared to the point measured prior to $25\%H_2O$ water addition. Thus, an average cobalt cluster size of ~10 nm as measured by hydrogen chemisorption/pulse reoxidation was deemed beneficial for stabilizing the catalyst against irreversible deactivation.

In a recent authoritative study, the susceptibility of Co in a Pt promoted Co/Al_2O_3 catalyst to oxidation in a commercial catalyst run in a 100 barrel/day slurry bubble column reactor was explored by Saib et al. (Refs. 93 and 94). Samples were retrieved from the reactor as a function of time on stream. The authors observed a decreasing white line intensity using XANES spectroscopy as a function of time on stream and concluded that the deactivation was not due to reoxidation of Co particles. The average crystallite (emphasis—crystallites, not cluster of crystallites) size was 6 nm, well above the 4.4 nm threshold, below which van Steen et al. (Ref. 82) have indicated oxidation may occur. The group of Claeys has obtained results using a magnetometer and XRD to show that smaller Co crystallites oxidize more readily than larger ones during FTS at useful conversions (Refs. 95 and 96). The authors observed a drop in magnetization with increasing water partial pressure which was most evident at >60% simulated conversions, which

the authors ascribed to the re-oxidation of small crystallites within the overall size distribution (Refs. 95 and 96). Moreover, in an investigation using both in-situ synchrotron XRD and XANES to follow both activation and catalyst stability during FTS at pressure of a 1%Re-20%Co/γ-Al_2O_3 catalyst with an average Co crystallite size of 10.7 nm (as measured by XRD), the catalyst was found to maintain its oxidation state and particle size during 6 h of reaction at 210 °C and 18 bar at approximately 30 to 50% CO conversion (H_2/CO ratio of 2:1). However, at higher temperature and lower pressure methanation conditions, the catalyst continued to reduce, and sintering occurred (Ref. 97). Moreover, Claeys et al. (Ref. 98) have also recently confirmed sintering of Co with time on stream during the initial decay period using a magnetometer.

There is thus reasonable evidence to suggest that CoO continues to agglomerate, reduce, and, consequently, ripen into larger Co^0 metal particles during initial catalyst deactivation prior to the longer term leveling off period (Ref. 93 to 98). However, the sources of CoO remain unclear. That is, does CoO form from the oxidation of tiny Co crystallites in research catalysts with high dispersion upon exposure to FTS conditions at useful conversions, or is the presence of CoO in the working catalyst solely from incomplete activation? We and others (Refs. 83, 85, and 86) have also observed by XANES that a fraction of cobalt in used samples is due to a cobalt support compound not present at such concentrations in the freshly activated catalyst. The question remains as to the original source of this species—is it solely due to unreduced CoO following activation that reacts with the support, or can tiny Co^0 crystallites oxidize at the onset of reaction to CoO, and in turn react with the support? Therefore, we intend to shed light on these points. The catalysts used in this study were prepared with low Co loading with the aim of deliberately preparing a small Co cluster size. The deactivation study was performed by exposing freshly reduced catalyst samples to the onset of FT conditions simulating 50% CO conversion. XANES/EXAFS were used to assess whether any change in the oxidation state of Co occurred between freshly reduced and FTS catalyst samples. Moreover, the effects of Co loading, Pt promoter, and support on the reoxidation of cobalt at the onset of FTS conditions were explored.

2.2.2 Experimental

2.2.2.1 Catalyst Preparation and Sample Preparation

Alumina (Catalox 200 γ-Al_2O_3) and granular activated carbon (Calgon) were utilized as catalyst support materials in this work. They were first calcined to remove physisorbed water before use. Alumina was calcined at 400 °C in a muffle furnace, while Calgon carbon was calcined under flow of nitrogen at 350 °C in order to avoid the oxidation of carbon during calcination. The catalysts were prepared using incipient wetness impregnation (IWI) with cobalt nitrate as the cobalt precursor. Deionized water was used to prepare a cobalt nitrate solution for Co/Al_2O_3, while acetone was instead utilized to prepare a cobalt nitrate solution for the Co/Calgon carbon catalyst. For Co/Al_2O_3, cobalt loadings of 2, 5, and 10% were prepared. To obtain 10%Co on Al_2O_3, two impregnation steps were required with drying at 95 °C under vacuum in a rotary evaporator after each impregnation. For Co/Calgon carbon catalyst, only 2%Co on Calgon carbon was prepared and multiple impregnation steps were necessary due to the solubility limit of cobalt nitrate in acetone. After each impregnation step, the catalyst was dried under vacuum using a rotary evaporator. To prepare the 0.5% by weight platinum-promoted catalyst, either tetra-amine platinum (II) nitrate solution or platinum (II) acetylacetonate powder was utilized. Platinum was added by incipient wetness impregnation (IWI), after the last cobalt impregnation step. In the case of the Pt promoted Co/Al_2O_3 catalyst, tetra-amine platinum (II) nitrate solution was used as the platinum source. For Pt promoted Co/Calgon carbon, platinum (II) acetylacetonate was used. Multiple impregnation steps were also required in the case of Co/Calgon carbon catalyst, as platinum (II) acetylacetonate only slightly dissolves in acetone. Finally, all catalysts were calcined under different conditions depending on the nature of each catalyst support—i.e., Co/Al_2O_3 and Pt-Co/Al_2O_3 catalysts were calcined under flow of air at 350 °C for 4 h, while Pt-Co/Calgon carbon catalyst was calcined under flowing nitrogen at 350 °C for 4 h.

To prepare a reduced sample, each catalyst was pressed into a flat pellet inside a 1-in. I.D. reactor with boron nitride. An 80 sccm flow of H_2 was started. The reactor was slowly (100 °C/h) brought up to an activation temperature of 400 °C for Pt-Co/Al_2O_3, 550 °C for Co/Al_2O_3, or 500 °C for Co/Calgon carbon, and held for 12 h. A separate steel tube was filled with Polywax 725 at 1 atm and brought up to 200 °C under N_2 flow (20 sccm). The reactor was cooled

to 220 °C and held. Next, the reactor was closed and H_2 flow was stopped, flow to the reactor containing the polywax was reversed and the polywax was pushed into the reactor containing the cobalt catalyst to immediately encapsulate the pellet in polywax, and preventing any oxidation from occurring.

The same initial reduction conditions were repeated for each of the Co catalysts in preparation of the FTS samples. Once the reactor was cooled to 220 °C, the reactor was slowly pressurized to 300 psig using 100 sccm of N_2. The reactor was then bypassed, and a flow of 100 sccm CO, sccm H_2 and, 100 sccm H_2O (g) was set to mimic partial pressures at 50% conversion. After a 90 min period, the water, CO and H_2 gases were shut off, and N_2 at 20 sccm allowed to enter. The inlet line was immediately bypassed to prevent any excess water from passing through the reactor. The reactor was slowly depressurized for polywax encapsulation, and the sample was stored in inert gas for EXAFS/XANES analysis.

2.2.2.2 BET Surface Area and Porosity Measurement

BET (Brunauer, Emmett, and Teller (Ref. 99)) and BJH (Barrett, Joyner, and Halenda (Ref. 100)) measurements for both supports and calcined catalysts were carried out using a Micromeritrics Tri-Star system. Prior to adsorption measurements, samples were gradually ramped to 160 °C and evacuated to approximately 50 mTorr for 12 h.

2.2.2.3 Temperature Programmed Reduction

Temperature programmed reduction (TPR) profiles of calcined catalysts were recorded using a Zeton-Altamira AMI-200 unit equipped with a thermal conductivity detector (TCD). Samples were pretreated by purging with argon flow at 350 °C to remove traces of water. The TPR was performed using a 10%H_2/Ar gas mixture (referenced to argon) at a flow rate of 30 cm^3/min. The catalyst samples were heated from 50 to 1100 °C. In the case of Co/Calgon carbon, an upper temperature limit of 800 °C was set due to the degradation of Calgon carbon at higher temperature.

2.2.2.4 Hydrogen Chemisorption and Oxygen Pulse Reoxidation

Hydrogen chemisorption was conducted using temperature programmed desorption (TPD), also measured with a Zeton-Altamira AMI-200 instrument. The sample weight was typically ~0.220 g. Catalysts were activated in a flow of 10 cm^3/min of H_2 mixed with 20 cm^3/min of argon at different reduction temperatures (i.e., 400 °C for Pt-Co/Al_2O_3, 550 °C for Co/Al_2O_3, and 500 °C for Co/Calgon carbon) for 10 h and, then, cooled to 100 °C under flowing H_2. The catalyst sample was held at 100 °C and purged with argon to remove and/or prevent adsorption of weakly bound hydrogen species prior to increasing the temperature slowly to the activation temperature of each catalyst (e.g., 400, 500, or 550 °C, respectively). At that temperature, the sample was held under flowing argon to desorb any remaining chemisorbed hydrogen until the TCD signal returned to the baseline. The TPD spectrum was integrated and the number of moles of hydrogen desorbed was determined by comparing its area against the area of calibrated hydrogen pulses. The loop volume was first determined by establishing a calibration curve with syringe injections of hydrogen in helium flow. Uncorrected dispersion and uncorrected Co cluster size were calculated by ignoring the percentage of Co reduction, with the assumption of a 1:1 H:Co stoichiometric ratio and a spherical cobalt cluster morphology, respectively. After TPD of hydrogen, the sample was reoxidized at the activation temperature using pulses of oxygen in helium. After oxidation of the cobalt metal clusters, the number of moles of oxygen consumed was determined, and the percentage of reduction was calculated by assuming that the Co^0 reoxidized to Co_3O_4. By including the percentage of Co reduced in the calculation, the corrected dispersion and corrected Co cluster size were obtained. Further details of the procedure are provided elsewhere (Ref. 81). There is, however, an exception in the case of the Co/Calgon carbon catalyst. The oxygen pulse reoxidation experiment was not possible because Calgon carbon material oxidized under oxygen pulses at high temperature. For that case, only uncorrected Co dispersion and uncorrected Co cluster size are reported.

2.2.2.5 XANES/EXAFS

XAS measurements on catalysts as well as references were conducted at the National Synchrotron Light Source (NSLS) at Brookhaven National Laboratory (beamline X-18b), Upton, New York. Some preliminary measurements were also conducted at Argonne National Laboratory's Advanced Photon Source. The beamline at NSLS was equipped with a Si(111) channel-cut monochromator. A crystal detuning procedure was employed to prevent glitches arising from harmonics. The second crystal of the channel-cut monochromator is weakly linked to the crystal and slightly spring loaded. The other side is a picomotor, a very fine high-pitch screw that turns by piezo, which allows for slight detuning of the crystal. The x-ray ring at the NSLS has a flux of 1×10^{10} photons s^{-1} at 100 mA and 2.5 GeV, and the energy-range capability at X18b is 5.8 to 40 keV. All catalyst samples were prepared at CAER in the form of catalyst particles embedded in polywax (i.e., with storage in inert gas) as previously described. XANES/EXAFS spectra were recorded at the cobalt K-edge (7.709 keV) in transmission mode and a Co metallic foil spectrum was measured simultaneously with each sample spectrum for the purpose of energy calibration.

XANES spectra were processed using the WinXAS program. A simultaneous pre- and post-edge background removal step was carried out using 2 polynomials (degree 2) over the range 7.63 to 7.67 keV and 7.79 to 8.68 keV, respectively, and the resulting spectra were normalized by dividing by the height of the absorption edge. Normalized XANES spectra were compared with those of references. In addition to a bulk CoO reference compound spectrum, a catalyst spectrum representing CoO in 15%Co/Al_2O_3 catalyst (i.e., from a TPR-XANES run previously conducted at Argonne (Ref. 101)) was also used as reference spectrum, as it is a more relevant reference spectrum for investigating CoO formation in the working Co/Al_2O_3 catalyst. XANES spectra of both reduced and FTS samples of each catalyst were directly compared in order to determine whether the freshly reduced Co^0 undergoes any oxidation at the onset of FTS.

Data reduction of EXAFS spectra was also performed using WinXAS. Following the normalization procedure previously described, spectra were converted to k-space and a k weighting of 1 was used. An advanced cubic weighted spline over 3 sections of the 2 to 14 $Å^{-1}$ range was used to remove the background of the $\chi(k)$ function. Finally, the k^1-weighted results were Fourier transformed to R-space using a Bessel window. To quantify the changes in Co-O and Co-Co coordination number, fitting of the spectra in *k* space was carried out using FEFFIT. The *k*-range used was from 2 to 14 $Å^{-1}$. Theoretical EXAFS were generated using FEFF for model cobalt metal and CoO crystal parameters generated by ATOMS. In order to use coordination number as a fitting parameter, S_0^2 was assumed to be 0.9 by the zeroth order approximation. The other fitting parameters utilized by FEFFIT included the overall E_0 shift e_0 applied to each path, an isotropic expansion coefficient α which is multiplied by the nominal length of each path, and the Debye-Waller factor, σ^2.

2.2.3 Results and Discussion

2.2.3.1 BET Surface Area and Porosity

The results of surface area and porosity data measured by N_2 adsorption-desorption at 77 K are shown in Table 2.4. The γ-alumina support is a mesoporous material (2 nm < ϕ < 50 nm) and activated Calgon carbon is a microporous material (ϕ < 2 nm), and the results of BET measurements confirm these characteristics. In comparison, the BET surface area of Calgon carbon is fivefold higher than that of alumina, while the average pore diameter is one-fifth that of alumina. Considering the Co/Al_2O_3 catalysts, at low cobalt loading (2, 5%) the effect of cobalt oxide on surface area of alumina support is not significant, as expected, but a decrease was observed at the higher loading of 10%Co. However, although a drop in surface area was obtained, it is still higher than the expected calculated value; that is, a 10%Co/Al_2O_3 catalyst corresponds to 13.62% by weight of Co_3O_4; assuming that Al_2O_3 is the only contributor to the surface area, then the area of 10%Co/Al_2O_3 catalyst should be $0.8638 \times 197.03 = 170.19$ m^2/g. The measured value is 181.90 m^2/g, so pore blocking is not deemed to be a significant issue. Adding 0.5%Pt promoter to Co/Al_2O_3 did not measurably change the BET surface area and porosity properties of the Co/Al_2O_3 catalysts. For 0.5%Pt-2%Co/Calgon

carbon, no significant changes in BET surface area and porosity properties were observed compared to those of the Calgon carbon support.

2.2.3.2 Temperature Programmed Reduction and Chemisorption

Figure 2.1 shows the TPR profiles of all catalysts. Considering unpromoted 5% and 10%Co/Al_2O_3 catalysts, their TPR profiles contain 4 major peaks; the first peak (~270 °C) and the second broad peak (~500 °C) are typically due to $Co_3O_4 \rightarrow CoO$ and $CoO \rightarrow Co^0$, respectively (Ref. 101), the third peak (~ 670 °C) appearing as a shoulder of the second peak is likely a very small CoO species interacting with the support. The fourth peak at high temperature (960 °C for 5%Co and 920 °C for 10%Co) is attributed to the decomposition of $CoAl_2O_4$ (Ref. 102). In 2%Co/Al_2O_3, only two peaks are present at 260 and 990 °C. The first one represents the transformation of Co_3O_4 to CoO and the one at high temperature indicates the presence of $CoAl_2O_4$, perhaps suggesting that a fraction of the CoO formed reacted with Al_2O_3. Interestingly, at 2%Co loading, H_2 reduction does not successfully produce an adequate fraction of Co metal due to the strong interaction between Co and the alumina support. However, at higher loadings of 5% and 10%Co, Co content is high enough to weaken the support interaction, thus allowing for a useful fraction of Co metal to be formed. Pt promoter improved the reducibility of cobalt oxides (Refs. 79, 81, 103, and 104). Although Pt enhances the reduction of Co_3O_4 to CoO in 2%Co/Al_2O_3, the second peak of $CoAl_2O_4$ still remained and appears at nearly the same temperature as that of the unpromoted catalyst (990 °C). Nevertheless, for this very low Co loading catalyst, chemisorption results indicate that a small fraction of CoO does reduce and form highly dispersed Co^0, while it also appears that a fraction of CoO reacts with the support, contributing to the $CoAl_2O_4$ peak in TPR. For Pt promoted 2%Co/Calgon, its TPR profile also shows the progression of Co_3O_4 and CoO reduction with increasing reduction temperature. Overlapping of both peaks is good evidence of a weak interaction between cobalt and carbon support, in which CoO generated from the first step of reduction promptly continues to be reduced to Co metal without significant inhibition due to the support interaction. Note that the profile for this catalyst does not proceed beyond 800 °C due to reaction of the Calgon carbon support material; however, it is not necessary to proceed to higher temperatures since the peaks of interest fell within the desired range of the TPR temperatures selected.

Hydrogen chemisorption and oxygen pulse reoxidation results are tabulated in Table 2.4. The reduction temperature applied to each catalyst was based on the TPR results in Figure 2.5 (e.g., 400 °C for Pt promoted Co/Al_2O_4, 500 °C for Pt promoted Co/Calgon, and 550 °C for unpromoted Co/Al_2O_3). As expected, the percent reduction of cobalt oxide and Co dispersion were improved in Co/Al_2O_3 catalysts after adding the Pt promoter. The Co cluster size decreased slightly in Pt promoted 5% and 10%Co/Al_2O_3 compared with those of unpromoted catalysts at the same Co contents. This is likely due to the fact that Pt assists in reducing more strongly interacting species, which tend to be smaller. At a low Co loading of 2%, there is no significant change in Co cluster size (0.5 vs. 0.4 nm) after adding Pt promoter in spite of an increase in percent reduction. Moving to Pt promoted Co/Calgon carbon catalyst, although percentage cobalt oxide reduction, corrected dispersion, and corrected Co cluster size cannot be estimated, the uncorrected values provide an upper limit to Co diameter size and a lower limit to percent dispersion. With the aim of this work being to investigate the susceptibility of tiny cobalt crystallites to reoxidation during the onset of FT reaction at 50% CO conversion, these activation temperatures are deemed appropriate.

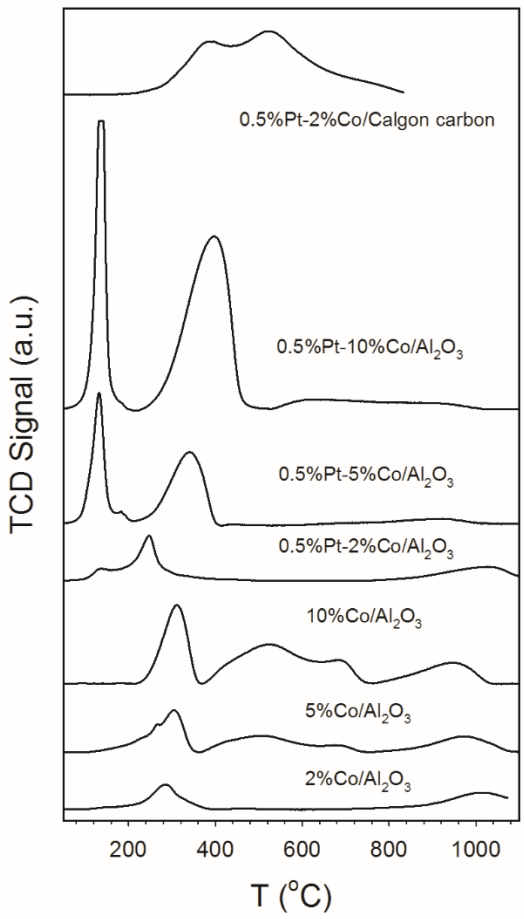

Figure 2.5.—Comparative TPR spectra of unpromoted Co/Al_2O_3 catalysts, Pt promoted Co/Al_2O_3 catalysts, and Pt promoted Co/Calgon carbon catalyst.

TABLE 2.4.—THE RESULTS OF BET SURFACE AREA AND POROSITY MEASUREMENTS AND H_2 CHEMISORPTION/O_2 PULSE REOXIDATION RESULTS OF SUPPORTS AND CATALYSTS

Catalyst	BET SA, m^2/g	Pore volume,[a] cm^3/g	Average pore radius, nm	Reduced T, °C	H_2 desorbed per $g_{catalyst}$, µmol/g	Uncorrected Co dispersion, %	Uncorrected Co average diameter, nm	O_2 uptake per $g_{catalyst}$, µmol/g	Percent reduction of Co	Corrected Co dispersion, %	Corrected Co average diameter, nm
Catalox 200 γ-Al_2O_3	197.0	0.473	5.0	----	----	----	----	----	----	----	----
Calgon carbon	1101.9	0.583	1.1	----	----	----	----	----	----	----	----
0.5%Pt -2%Co/Al_2O_3	207.5	0.438	4.2	400	77.5	45.7	2.3	35.4	16.3	280.0	0.4
0.5%Pt- 5%Co/Al_2O_3	199.6	0.425	4.4	400	79.1	18.6	5.5	342.4	60.5	30.8	3.4
0.5%Pt-10%Co/Al_2O_3	180.0	0.369	4.3	400	115.1	13.6	7.6	792.4	70.1	19.4	5.3
2%Co/Al_2O_3	207.7	0.444	4.3	550	32.2	19.0	5.4	20.0	8.9	215.0	0.5
5%Co/Al_2O_3	198.5	0.414	4.2	550	42.8	10.1	10.2	277.5	49.1	20.1	5.0
10%Co/Al_2O_3	181.9	0.374	4.1	550	79.8	9.4	11.0	655.8	58.0	16.2	6.4
0.5%Pt-2%Co/Calgon carbon[b]	1004.7	0.534	1.1	500	42.8	25.2	4.1	----	----	----	----

[a]Single point

[b]O_2 pulse reoxidation cannot be applied for Co/Calgon carbon catalyst due to oxidation of Calgon carbon support.

2.2.3.3 XANES and EXAFS

Figure 2.6 shows normalized XANES spectra of reference compounds (e.g., Co_3O_4, CoO, $CoAl_2O_4$, and Co^0 foil). A major characteristic of Co^0 is the edge peak at 7709 eV. In the oxide references, pre-edge features are associated with symmetry effects in the environment of cobalt and are due to 1s → 3d transitions (Ref. 101). The oxidic reference compounds (Co_3O_4, CoO, and $CoAl_2O_4$) display a stronger absorption white line with unique spectral features because cobalt atoms are in different Co-O environments and oxidation states. The pre-edge intensity of tetrahedral cobalt environments is stronger than that of octahedral cobalt environments (Refs. 105 and 106). A pre-edge feature is observed in all oxide compounds. Co_3O_4 is a spinel structure, with one-third of the Co^{2+} occupying tetrahedral sites and two-thirds occupying octahedral sites ($2Co^{3+}$), such that the pre-edge feature represents a combination of the more intense tetrahedral peak and the weaker octahedral peak (Ref. 101), CoO consists of Co^{2+} octahedrally coordinated with oxygen (Refs. 93 and 101), whereas $CoAl_2O_4$ is a normal spinel with Co^{2+} ions in tetrahedral sites (Refs. 93 and 105). Therefore, the intensity of pre-edge features follows the order: $CoAl_2O_4 > Co_3O_4 > CoO$. XANES spectra of supported CoO display a weak pre-edge feature. Moreover, the white line intensity and XANES shape are directly indicative of each cobalt oxide species. It is readily observed that the white line intensity in XANES spectra of supported CoO is higher than that of the CoO reference compound. This may be attributed to electron deficiencies due to a support effect (Ref. 101). Hence, the white line in the catalyst spectrum will provide a good indication as to whether oxidation occurs in Co/Al_2O_3 at the onset of the FTS run mimicking 50% Co conversion.

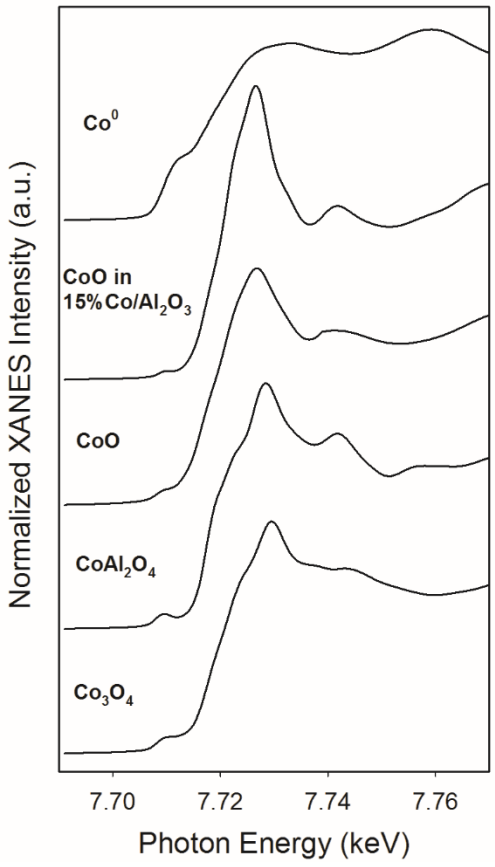

Figure 2.6.—Normalized XANES spectra of reference compounds.

XANES measurements were performed for reduced and FTS samples of each catalyst to study whether nanosized cobalt crystallites oxidize at the onset of FTS conditions. Figure 2.7 shows normalized XANES spectra of reduced and FTS samples of each catalyst, in which solid lines represent reduced catalysts while dashed lines show the results of FTS samples. The white line intensity of 0.5%Pt-2%Co/Al_2O_3 after exposure to FTS conditions is slightly higher than that of the reduced sample. It appears that there is little reduction during activation, while most of the cobalt oxides remain unreduced. This is consistent with the O_2 pulse reoxidation result that shows that only ~16% Co reduction is achieved with this catalyst. Moreover, a low peak intensity for Co^0 and an intense white line indicate low extent of reduction. Nevertheless, there is a small fraction of reduced Co that becomes oxidized as a slightly higher white line intensity is obtained during FTS. Moving to higher Co loading catalysts, 0.5%Pt-5%Co/Al_2O_3 and 0.5%Pt-10%Co/Al_2O_3, normalized XANES spectra reveal that cobalt in the reduced samples is mostly in metallic form. 10%Co does provide more Co metal than 5%Co, as a stronger edge peak for the metal is observed, along with a lower white line intensity. Following FTS conditions, a significant fraction of Co metal in these catalysts is oxidized and an increase in white line intensity with a decrease in the edge peak intensity for metallic cobalt is clearly observed. This reoxidation of Co metal into CoO at the onset of FTS run is because the $H_2O/(H_2+CO)$ ratio is high enough to oxidize the tiniest of the Co^0 crystallites (Refs. 79, 80, 82, 83, 86, 88, 89, 90, 94, 107, and 108) in the size distribution.

Comparing the activated Pt promoted and unpromoted 10%Co/Al_2O_3 catalysts, the white line is significantly lower for the Pt promoted catalyst. Reoxidation of Co metal in the unpromoted catalyst also occurred, but the difference is greater in the case of the Pt promoted catalyst. Since Pt facilitates the reduction of more strongly interacting CoO species, which tend to be smaller, it is not surprising that this higher density of smaller species would be more susceptible to reoxidation.

It is clear that Co metal dominates in the reduced sample of 0.5%Pt-2%Co/Calgon carbon; a comparison with the 0.5%Pt-2%Co/Al_2O_3 catalyst provides a testimony to the weaker support interaction of the cobalt/carbon catalyst. 0.5%Pt-2%Co/Calgon carbon catalyst also exhibited reoxidation of a fraction of Co^0 after switching to FTS conditions. A higher white line intensity in normalized XANES spectra and lower edge peak intensity for metallic Co^0 resulted after switching to FTS. Thus, catalysts having weakly interacting supports are not immune to the effect of reoxidation of the smallest Co^0 crystallites.

EXAFS results in Figure 2.8 are in agreement with the XANES results previously discussed. Qualitatively, in reduced samples (solid line), it is suggested that the peak of Co-O coordination appears as a minor shoulder to the Co-Co metal coordination peak in all catalysts, except 0.5%Pt-2%Co/Al_2O_3. The presence of Co-O bonding indicates that the reduced catalysts still contain a minor oxidized cobalt component (e.g., CoO). The dashed lines of Figure 2.8 represent the resulting EXAFS spectra after exposure to FTS conditions. Decreases in the peak associated with Co-Co coordination in the metal and increases in Co-O coordination are suggested. Moreover, Figure 2.9 also shows the results of the fitting using FEFFIT for the k^1-weighted EXAFS Fourier transform magnitude spectra and filtered k^1-weighted $\chi(k)$ spectra of Co supported catalysts. The solid lines in Figure 2.9 are the experimental data, while the circles provide the best fit. The results of fitting parameters are summarized in Table 2.5. Generally, the r-factor value of <0.02 indicates a good fit, and all catalyst spectra fall at or below this value. Qualitatively, the well-defined peak in the fitting corresponds to Co-Co bonding, while the shoulder peak is likely due primarily to Co-O bonding.

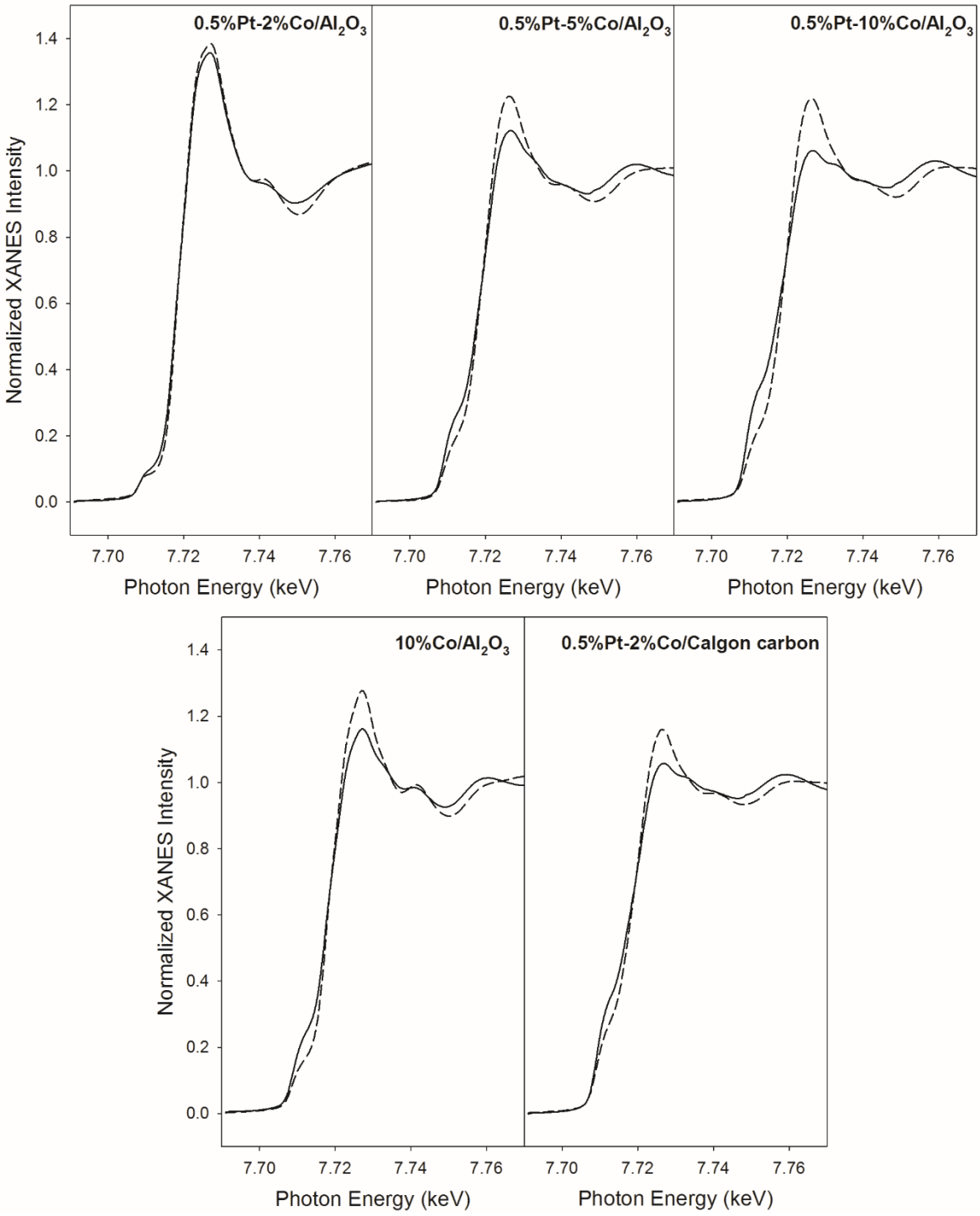

Figure 2.7.—Comparative normalized XANES spectra (Top) and their corresponding derivative spectra (Bottom) of (solid line) reduced sample and (dashed line) FTS sample of Pt-Co/Al_2O_3, Co/Al_2O_3, and Pt-Co/Calgon carbon catalysts.

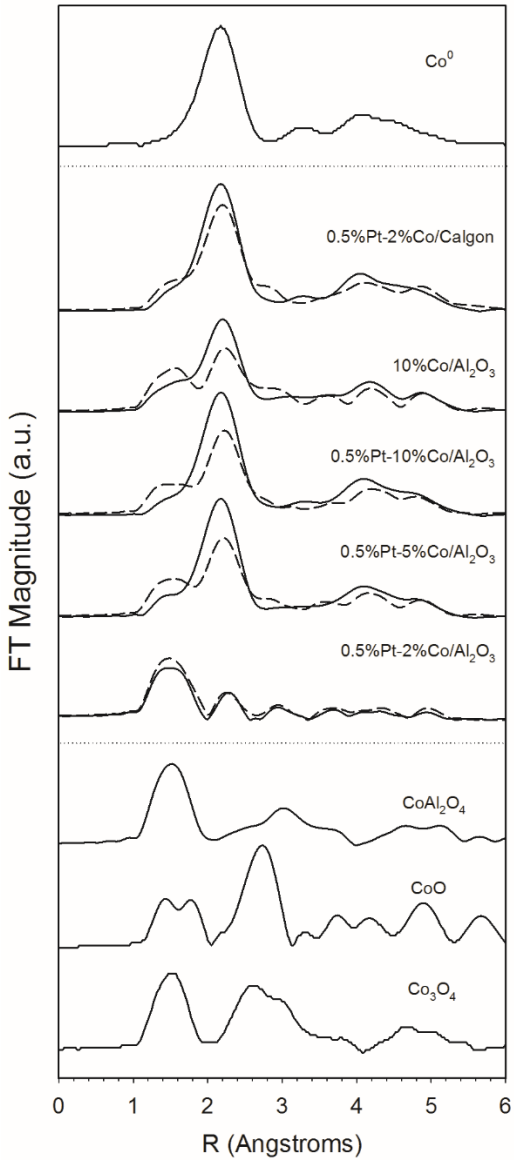

Figure 2.8.—The k^1-Weighted Fourier transform magnitude of Co K-edge EXAFS spectra of reference compounds, catalyst samples after reduction (solid line), and catalyst samples after exposure to the onset of the FTS conditions mimicking 50% CO conversion (dashed line).

TABLE 2.5.—RESULTS OF EXAFS FITTING FOR DATA ACQUIRED NEAR THE Co K-EDGE FOR CATALYST AFTER ACTIVATION AND AT THE ONSET OF FTS. THE FITTING RANGES WERE APPROXIMATELY $\Delta k = 2\text{-}14$ Å^{-1} AND $\Delta R = 1.25 – 2.7$ Å, $S_0^2 = 0.9$

Catalyst	Condition	$N_{Co\text{-}O}$	$R_{Co\text{-}O}$	$N_{Co\text{-}Co}$	$R_{Co\text{-}Co}$	e_0 (eV)	σ^2 (Å^2)	r-factor
Co^0 foil	-	-	-	12 (set)	2.486 (0.0063)	6.576 (0.772)	0.00665 (0.00047)	0.02
0.5%Pt-5%Co/Al_2O_3	Reduced	0.69 (0.11)	2.026 (0.0135)	5.24 (0.14)	2.495 (0.0037)	7.093 (0.460)	0.00538 (0.00057)	0.018
	FTS	1.55 (0.20)		3.53 (0.35)				
0.5%Pt-10%Co/Al_2O_3	Reduced	0.18 (0.08)	2.020 (0.0292)	5.80 (0.26)	2.495 (0.0030)	7.323 (0.375)	0.00600 (0.00044)	0.017
	FTS	1.34 (0.36)		3.83 (0.60)				
10%Co/Al_2O_3	Reduced	0.88 (0.11)	2.022 (0.0128)	4.48 (0.33)	2.503 (0.0044)	8.431 (0.498)	0.00603 (0.00073)	0.02
	FTS	1.75 (0.20)		3.08 (0.38)				
0.5%Pt-2%Co/Calgon carbon	Reduced	0.22 (0.11)	1.992 (0.0402)	5.76 (0.34)	2.493 (0.0040)	7.096 (0.510)	0.00554 (0.00058)	0.02
	FTS	0.97 (0.42)		4.71 (0.71)				

The EXAFS spectrum of 0.5%Pt-2%Co/Al_2O_3 reveals that Co-O coordination dominates in this catalyst even after reduction. After switching to FTS conditions, the peak tentatively assigned to Co-O appears to be slightly more intense. At higher Co loadings of 5% and 10%Co in Pt promoted Co/Al_2O_3 more pronounced Co-Co metal coordination peaks and less Co-O coordination is obtained, especially in 0.5%Pt-10%Co/Al_2O_3, after activation. On the other hand, after FTS conditions, the peak ascribed to Co-Co metal coordination decreased with an apparent increase in Co-O coordination. To quantify the changes in coordination numbers and place the tentative peak assignments on a firmer footing, EXAFS fitting was performed by using the f.c.c. Co metal model and CoO as references (Figure 2.9(A)) with the assumption of Co-Co and Co-O first shell coordination being included in the fitting. Good fits were achieved, as shown in Figure 2.9(B) and (C), with numeric fitting results being displayed in Table 2.5. It is observed that after reduction 0.5%Pt-10%Co/Al_2O_3 has a higher Co-Co coordination number than 0.5%Pt-5%Co/Al_2O_3 (5.80 vs. 5.24), while after exposure to FTS conditions Co-O bond coordination was higher for the 0.5%Pt-5%Co/Al_2O_3 catalyst (1.34 vs. 1.55). It is suggested that the lower the Co loading, the more susceptible the smaller Co^0 particles are to reoxidation (i.e., in this case 3.4 vs. 5.3 nm in 0.5%Pt-5%Co/Al_2O_3 and 0.5%Pt-10%Co/Al_2O_3, respectively). As expected, 10%Co/Al_2O_3 catalyst without Pt promoter contains more Co-O and less Co-Co coordination compared to 0.5%Pt-10%Co/Al_2O_3, as shown qualitatively in Figure 2.8 and Figure 2.9(C) and (D) with fitting parameters quantified in Table 2.5. Considering the 0.5%Pt-2%Co/Calgon catalyst, due to the weak interaction between Co and carbon support, Co-Co and Co-O coordination were close to those of the more highly loaded 0.5%Pt-10%Co/Al_2O_3 catalyst after activation, the latter support providing a much strong interaction. The EXAFS results demonstrate that Co-Co metal coordination decreases while Co-O increases for all of the research catalysts upon exposure to FTS at useful conversions, indicating that a fraction of tiny crystallites is readily oxidized by FTS conditions at the onset stage. This is likely due to tiny cobalt crystallites (i.e., < 2 to 4.1 nm) present in the catalyst that, from the standpoint of thermodynamics, favor oxidation (Ref. 82).

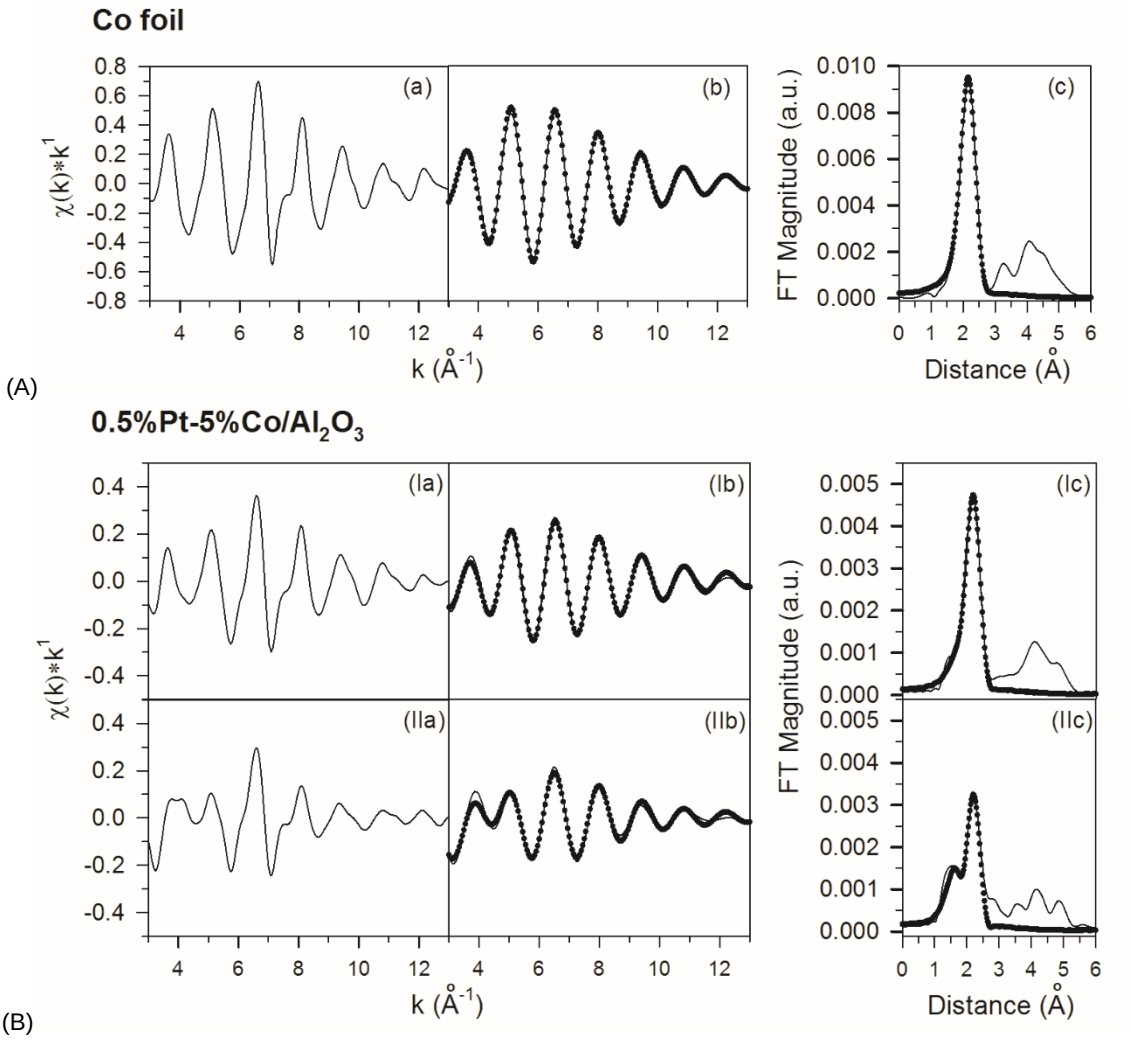

Figure 2.9.—The results of EXAFS fittings: (a) unfiltered k^1-weighted $\chi(k)$ spectra; (b) filtered k^1-weighted $\chi(k)$ spectra (solid line) and resulting of fitting (filled circles); (c) k^1-weighted Fourier transform magnitude spectra (solid line) and resulting fitting (filled circles) over the first coordination shell of Co central atom, of (A) Co^0 foil reference and catalysts; (B) 0.5%Pt-5%Co/Al_2O_3, (C) 0.5%Pt-10%Co/Al_2O_3, (D) 10%Co/Al_2O_3, and (E) 0.5%Pt-2%Co/Calgon, at (I) after activation in H_2 and at (II) the onset of FTS at condition simulating 50% CO conversion.

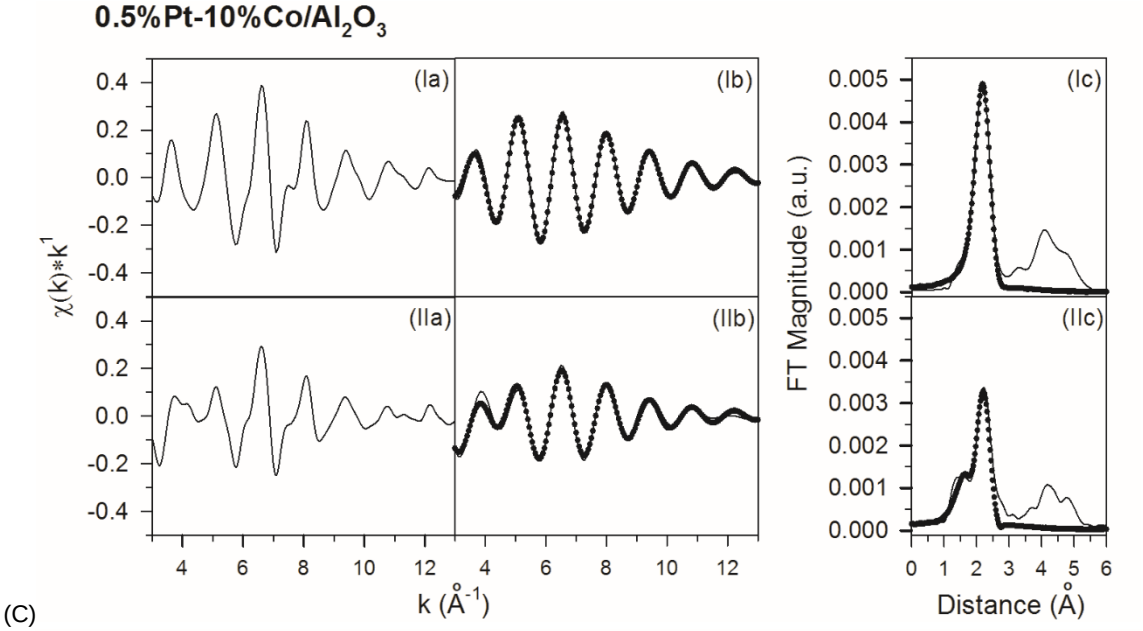

(C)

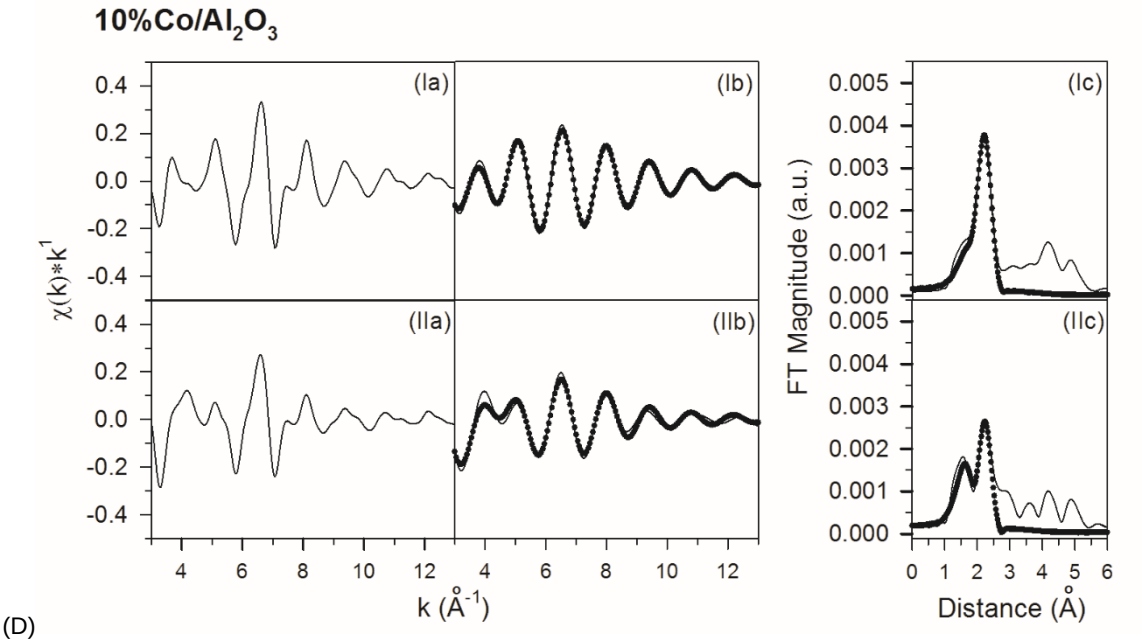

(D)

Figure 2.9.—Continued.

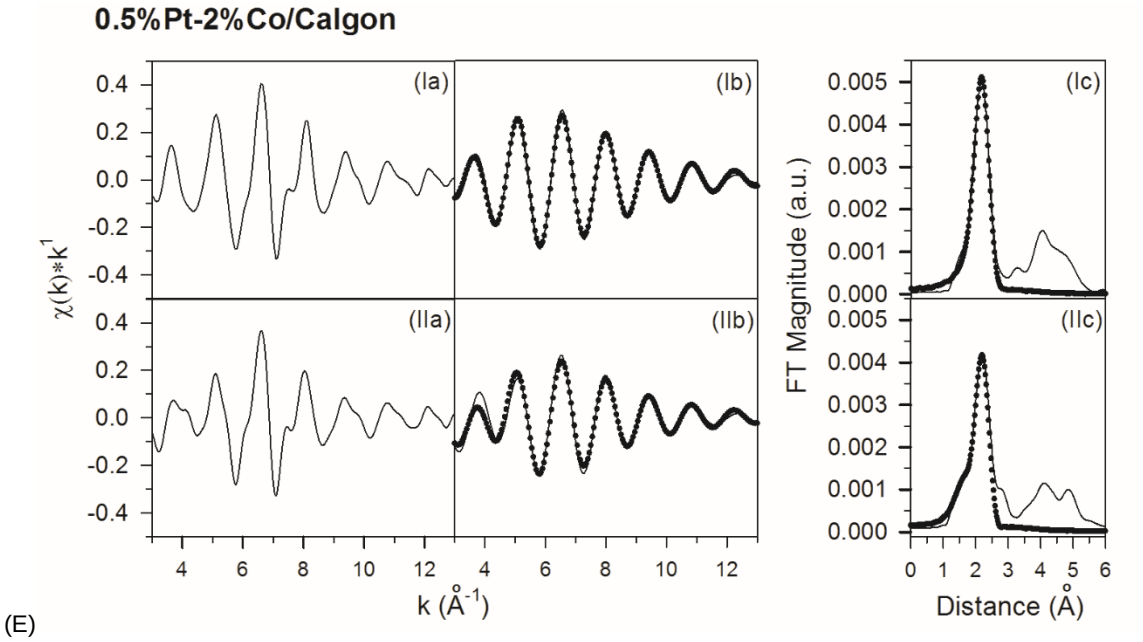

(E)

Figure 2.9.—Concluded.

2.2.4 Conclusions

It should be recognized in using FT research catalysts containing a low Co content with high Co dispersion that the oxidation of a fraction of tiny Co crystallites occurs at the onset of FTS conditions at meaningful CO conversions. Tiny Co crystallites are susceptible to oxidation regardless of support type (i.e., even for Co supported on Calgon carbon, which displays a weak interaction), as demonstrated by XANES/EXAFS results. This source of CoO, along with residual unreduced CoO following activation, would likely contribute to the complex sintering mechanism involving agglomeration and net reduction of CoO, as well as Co aluminate formation, during FTS as a function of time on-stream. Thus, tiny Co^0 crystallites should be avoided during preparation, as they contribute to catalyst deactivation.

Appendix

As of July 9, 2014, the following manuscripts were generated as a result of this project:

1. Jermwongratanachai, T.; Jacobs, G.; Ma, W.; Shafer, W.D.; Gnanamani, M.K.; Gao, P.; Kitiyanan, B.; Davis, B.H.; J.L.S. Klettlinger; Yen, C.H.; Cronauer, D.C.; Kropf, A.J.; Marshall, C.L., "Fischer-Tropsch synthesis: comparisons between Pt and Ag promoted Co/Al_2O_3 catalysts for reducibility, local atomic structure, catalytic activity, and oxidation-reduction cycles," *Applied Catalysis A: General* **464-465** (2013) 165-180.
2. Ma, W.; Jacobs, G.; Sparks, D.E.; Spicer, R.L.; Davis, B.H.; Klettlinger, J.L.S.; Yen, C.H., "Fischer-Tropsch synthesis: Kinetics and water effect study over $25\%Co/Al_2O_3$ catalysts," *Catalysis Today* **228** (2014) 158-166.
3. Ma, W.; Jacobs, G., Das, T.K., Masuku, C.M.; Kang, J.; Pendyala, V.R.R., Davis, B.H.; Klettlinger, J.L.S.; Yen, C.H. "Fischer-Tropsch synthesis: Kinetics and water effect on methane formation over $25\%Co/\gamma\text{-}Al_2O_3$ catalyst," *Industrial & Engineering Chemistry Research* **53** (2014) 2157-2166.
4. Ma, W.; Jacobs, G.; Gao, P.; Jermwongratanachai, T.; Shafer, W.D.; Pendyala, V.R.R.; Chia H. Yen; Jennifer L.S. Klettlinger; Davis, B.H., "Fischer-Tropsch synthesis: pore size and Zr promotional effects on the activity and selectivity of $25\%Co/Al_2O_3$ catalysts," *Applied Catalysis A: General* **475** (2014) 314-324.
5. Pendyala, V.R.R.; Jacobs, G.; Ma, W.; Klettlinger, J.L.S.; Yen, C.H.; Davis, B.H., "Fischer-Tropsch synthesis: effect of catalyst particle (sieve) size range on activity, selectivity, and aging of a Pt promoted Co/Al_2O_3 catalyst," *Chemical Engineering Journal* **249** (2014) 279-284.

References

1. G. Jacobs, T.K. Das, Y.-Q. Zhang, J. Li, G. Racoillet, B.H. Davis, Appl. Catal. A: General 233 (2002) 263.
2. T. Ressler, J. Synchrotron Rad. 5 (1998) 118.
3. G. Jacobs, Y. Ji, B.H. Davis, D.C. Cronauer, A.J. Kropf, C.L. Marshall, Appl. Catal. A: General 333 (2007) 177.
4. W. Ma, G. Jacobs, Y. Ji, T. Bhatelia, D.B. Bukur, S. Khalid, B.H. Davis, Top. Catal. 54 (2011) 757.
5. G. Jacobs, J.A. Chaney, P.M. Patterson, T.K. Das, B.H. Davis, Appl. Catal. A: General 264 (2004) 203.
6. G. Jacobs, M.C. Ribeiro, W. Ma, Y. Ji, S. Khalid, P.T.A. Sumodjo, B.H. Davis, Appl. Catal. A: General 361 (2009) 137.
7. G.P. Huffman, N. Shah, J. Zhao, F.E. Huggins, T.E. Hoost, S. Halvorsen, J.G. Goodwin, Jr., J. Catal. 151 (1995) 17.
8. J. Li, X. Zhan, Y.-Q. Zhang, G. Jacobs, T.K. Das, B.H. Davis, Appl. Catal. A: General 228 (2002) 203.
9. G. Jacobs, T.K. Das, P.M. Patterson, J. Li, L. Sanchez, B.H. Davis, Appl. Catal. A: General 247 (2003) 335.
10. G. Jacobs, T.K. Das, P.M. Patterson, M. Luo, W.A. Conner, B.H. Davis, Appl. Catal. A: General 270 (2004) 65.
11. J.L.V. R.L. Espinoza, P.J. van Berge, F.H. Bolder, US Patent, 5,733,839 (1998).
12. P.J. Van Berge, S. Barradas, J. Van De Loodsrecht, J.L. Visagie, Advances in the cobalt catalyzed Fischer-Tropsch synthesis, Erdoel Erdgas Kohle, 117 (2001) 138-142.
13. P. Arnoldy, J.A. Moulijn, Temperature-programmed reduction of CoO AI2O3 catalysts, Journal of Catalysis, 93 (1985) 38-54.
14. S.T. Christensen, J.W. Elam, F.A. Rabuffetti, Q. Ma, S.J. Weigand, B. Lee, S. Seifert, P.C. Stair, K.R. Poeppelmeier, M.C. Hersam, M.J. Bedzyk, Controlled growth of platinum nanoparticles on strontium titanate nanocubes by atomic layer deposition, Small, 5 (2009) 750-757.
15. T.K. Das, G. Jacobs, P.M. Patterson, W.A. Conner, J. Li, B.H. Davis, Fischer-Tropsch synthesis: Characterization and catalytic properties of rhenium promoted cobalt alumina catalysts, Fuel, 82 (2003) 805-815.
16. A.M. Hilmen, D. Schanke, A. Holmen, TPR study of the mechanism of rhenium promotion of alumina-supported cobalt Fischer-Tropsch catalysts, Catalysis Letters, 38 (1996) 143-147.
17. G. Jacobs, J.A. Chaney, P.M. Patterson, T.K. Das, J.C. Maillot, B.H. Davis, Fischer-Tropsch synthesis: Study of the promotion of Pt on the reduction property of Co/Al2O3 catalysts by in situ EXAFS of Co K and Pt LIII edges and XPS, Journal of Synchrotron Radiation, 11 (2004) 414-422.
18. G. Jacobs, T.K. Das, Y. Zhang, J. Li, G. Racoillet, B.H. Davis, Fischer–Tropsch synthesis: support, loading, and promoter effects on the reducibility of cobalt catalysts, Applied Catalysis A: General, 233 (2002) 263-281.
19. A. Kogelbauer, J.G. Goodwin Jr, R. Oukaci, Ruthenium promotion of Co/Al2O3 Fischer-Tropsch catalysts, Journal of Catalysis, 160 (1996) 125-133.
20. M. Rønning, D.G. Nicholson, A. Holmen, In situ EXAFS study of the bimetallic interaction in a rhenium-promoted alumina-supported cobalt Fischer-Tropsch catalyst, Catalysis Letters, 72 (2001) 141-146.
21. D. Schanke, S. Vada, E.A. Blekkan, A.M. Hilmen, A. Hoff, A. Holmen, Study of Pt-Promoted Cobalt CO Hydrogenation Catalysts, Journal of Catalysis, 156 (1995) 85-95.
22. S. Vada, A. Hoff, E. ÅdnaneS, D. Schanke, A. Holmen, Fischer-Tropsch synthesis on supported cobalt catalysts promoted by platinum and rhenium, Topics in Catalysis, 2 (1995) 155-162.
23. G. Jacobs, M.C. Ribeiro, W. Ma, Y. Ji, S. Khalid, P.T.A. Sumodjo, B.H. Davis, Group 11 (Cu, Ag, Au) promotion of 15%Co/Al2O3 Fischer–Tropsch synthesis catalysts, Applied Catalysis A: General, 361 (2009) 137-151.
24. J.F. Weaver, J.-J. Chen, A.L. Gerrard, Oxidation of Pt(111) by gas-phase oxygen atoms, Surface Science, 592 (2005) 83-103.
25. K.M. Cook, S. Poudyal, J.T. Miller, C.H. Bartholomew, W.C. Hecker, Reducibility of alumina-supported cobalt Fischer–Tropsch catalysts: Effects of noble metal type, distribution, retention, chemical state, bonding, and influence on cobalt crystallite size, Applied Catalysis A: General, 449 (2012) 69-80.

26. L. Guczi, D. Bazin, I. Kovács, L. Borkó, Z. Schay, J. Lynch, P. Parent, C. Lafon, G. Stefler, Z. Koppány, I. Sajó, Structure of Pt-Co/Al2O3 and Pt-Co/NaY bimetallic catalysts: Characterization by in situ EXAFS, TPR, XPS and by activity in Co (carbon monoxide) hydrogenation, Topics in Catalysis, 20 (2002) 129-139.
27. A. Kuzmin, G. Dalba, P. Fornasini, F. Rocca, O. Šipr, X-ray absorption spectroscopy of strongly disordered glasses: Local structure around Ag ions in g- Ag2O•nB2O3, Physical Review B - Condensed Matter and Materials Physics, 73 (2006).
28. A.E. N.N. Greenwood, Chemistry of the Elements, (1997) 1116.
29. T. Redjala, H. Remita, G. Apostolescu, M. Mostafavi, C. Thomazeau, D. Uzio, Bimetallic Au-Pd and Ag-Pd clusters synthesised by γ or electron beam radiolysis and study of the reactivity/structure relationships in the selective hydrogenation of buta-1,3-diene, Oil and Gas Science and Technology, 61 (2006) 789-797.
30. M. Jacoby, Chem. Eng. News, 79 (2001) 33-38.
31. T. Ressler, WinXAS97, Version 1.0 (1997).
32. B.R. Newville, D. Haskel, E.A. Stern, Y. Yacoby, Physica B, 208/209 (2005) 154.
33. J.J. Rehr, R.C. Albers, S.I. Zabinsky, High-order multiple-scattering calculations of x-ray-absorption fine structure, Physical Review Letters, 69 (1992) 3397-3400.
34. B. Ravel, ATOMS: Crystallography for the X-ray absorption spectroscopist, Journal of Synchrotron Radiation, 8 (2001) 314-316.
35. G. Jacobs, Y. Zhang, T.K. Das, J. Li, P.M. Patterson, B.H. Davis, Deactivation of a Ru promoted Co/Al2O3 catalyst for FT synthesis, in: G.W.R. J.J. Spivey, B.H. Davis (Eds.) Studies in Surface Science and Catalysis, Elsevier, 2001, pp. 415-422.
36. G. Jacobs, Y. Ji, B.H. Davis, D. Cronauer, A.J. Kropf, C.L. Marshall, Fischer–Tropsch synthesis: Temperature programmed EXAFS/XANES investigation of the influence of support type, cobalt loading, and noble metal promoter addition to the reduction behavior of cobalt oxide particles, Applied Catalysis A: General, 333 (2007) 177-191.
37. D.C. Cronauer, J.W. Elam, A.J. Kropf, C.L. Marshall, P. Gao, S. Hopps, G. Jacobs, B.H. Davis, Fischer–Tropsch Synthesis: Preconditioning Effects Upon Co-Containing Promoted and Unpromoted Catalysts, Catalysis Letters, 142 (2012) 698-713.
38. W.-J. Wang, Y.-W. Chen, Influence of metal loading on the reducibility and hydrogenation activity of cobalt/alumina catalysts, Applied Catalysis, 77 (1991) 223-233.
39. B.A. Sexton, A.E. Hughes, T.W. Turney, An XPS and TPR study of the reduction of promoted cobalt-kieselguhr Fischer-Tropsch catalysts, Journal of Catalysis, 97 (1986) 390-406.
40. K. Kinoshita, Differential thermal analysis of PtO2/carbon, Thermochimica Acta, 20 (1977) 297-308.
41. J.C.J. Bart, Adv. in Catal. 34 (1986) 203-297.
42. T. Bunluesin, R.J. Gorte, G.W. Graham, Studies of the water-gas-shift reaction on ceria-supported Pt, Pd, and Rh: Implications for oxygen-storage properties, Applied Catalysis B: Environmental, 15 (1998) 107-114.
43. D.C. Grenoble, M.M. Estadt, D.F. Ollis, The chemistry and catalysis of the water gas shift reaction. 1. The kinetics over supported metal catalysts, Journal of Catalysis, 67 (1981) 90-102.
44. C.M. Kalamaras, G.G. Olympiou, A.M. Efstathiou, The water-gas shift reaction on Pt/γ-Al2O3 catalyst: Operando SSITKA-DRIFTS-mass spectroscopy studies, Catalysis Today, 138 (2008) 228-234.
45. A.A. Phatak, N. Koryabkina, S. Rai, J.L. Ratts, W. Ruettinger, R.J. Farrauto, G.E. Blau, W.N. Delgass, F.H. Ribeiro, Kinetics of the water–gas shift reaction on Pt catalysts supported on alumina and ceria, Catalysis Today, 123 (2007) 224-234.
46. G. Jacobs, B.H. Davis, Surface interfaces in low temperature water-gas shift: The metal oxide synergy, the assistance of co-adsorbed water, and alkali doping, International Journal of Hydrogen Energy, 35 (2010) 3522-3536.
47. A. Borodziński, G.C. Bond, Selective hydrogenation of ethyne in ethene-rich streams on palladium catalysts, Part 2: Steady-state kinetics and effects of palladium particle size, carbon monoxide, and promoters, Catalysis Reviews - Science and Engineering, 50 (2008) 379-469.

48. R.L. Espinoza, J.L. Visagie, P.J. van Berge, F.H. Bolder, US Patent 5,733,839 (1998).
49. G. Jacobs, T.K. Das, Y.-Q. Zhang, J. Li, G. Racoillet, B.H. Davis, Appl. Catal. 233 (2002) 263-281.
50. B. Jongsomjit, J. Panpranot, J.G. Goodwin, Jr., J. Catal. 215 (2003) 66-77.
51. T. Ressler, J. Synchrotron Rad. 5 (1998) 118.
52. B. Ravel, J. Synchrotron Rad. 8 (2001) 314.
53. M. Newville, B. Ravel, D. Haskel, J. J. Rehr, E. A. Stern, Y. Yacoby, Physica B 208-209 (1995) 154.
54. M. Newville, B. Ravel, D. Haskel, J. J. Rehr, E. A. Stern, Y. Yacoby, Physica B 208-209 (1995) 154.
55. G. Jacobs, Y. Ji, B.H. Davis, D.C. Cronauer, A.J. Kropf, C.L. Marshall, Appl. Catal. A: General (2007) 177-191.
56. Haifeng Xiong, Yuhua Zhang, Kongyong Liew, Jinlin Li Journal of Molecular Catalysis A: Chemical 231 (2005) 145–151.
57. Ma, W.; Jacobs, G.; Keogh, R.A.; Bukur, D.B.; Davis, B.H., "Fischer-Tropsch synthesis: Effect of Pd, Pt, Re, and Ru noble metal promoters on the activity and selectivity of a 25%Co/Al2O3 catalyst," Applied Catalysis A: General 437-438 (2012) 1-9.
58. G. Jacobs, M.C. Ribeiro, W. Ma, Y. Ji, S. Khalid, P.T.A. Sumodjo, B.H. Davis, Group 11 (Cu, Ag, Au) promotion of 15%Co/Al2O3 Fischer–Tropsch synthesis catalysts, Applied Catalysis A: General, 361 (2009) 137-151.
59. Wenping Ma, Gary Jacobs, Yaying Ji Tejas Bhatelia , Dragomir B. Bukur , Syed Khalid, Burtron H. Davis Top Catal (2011) 54:757–767
60. E. Iglesia, Appl. Catal. A: General 161 (1997) 59.
61. Andreas Feller, Michael Claeys, and Eric van Steen Journal of Catalysis 185, 120–130 (1999)
62. Ishimura, Yoshimasa; Fukushima, Takakazu; Ozaki, Atsumu, 1981, J. the Research Institute for Catalysis Hokkaido University, 28(3): 209-214
63. Transition Metal Oxides Surface Chemistry and Catalysis – H.H. Kung 1989, pp136-146 Elsevier science publishers B.V. P.O. box 211 1000 AE Amsterdam, The Netherlands.
64. M.E. Dry, Catal. Today 6 (1990) 183.
65. I. Wender, Fuel Proc. Tech. 48 (1996) 189.
66. E. Iglesia, Appl. Catal. A 161 (1997) 59.
67. R.C. Reuel, C.H. Bartholomew, J. Catal. 85 (1984) 78.
68. A. Barbier, A. Tuel, I. Arcon, A. Kodre, G.A. Martin, J. Catal. 200 (2001) 106.
69. G.L. Bezemer, J.H. Bitter, H.P.C.E. Kuipers, H. Oosterbeek, J.E. Holewijn, X. Xu, F. Kapteijn, A.J. Van Dillen, K.P. De Jong, J. Am. Chem. Soc. 128 (2006) 3956.
70. Ø. Borg, P.D.C. Dietzel, A.I. Spjelkavik, E.Z. Tveten, J.C. Walmsley, S. Diplas, S. Eri, A. Holmen, E. Rytter, J. Catal. 259 (2008) 161.
71. B.G. Johnson, C.H. Bartholomew, D.W. Goodman, J. Catal. 128 (1991) 231.
72. S.-W. Ho, M. Houalla, D.M. Hercules, J. Phys. Chem. 94 (1990) 6396.
73. C. Moreno-Castilla, F. Carrasco-Marin, J. Chem. Soc., Faraday Trans. 91 (1995) 3519.
74. A.Y. Khodakov, A. Griboval-Constant, R. Bechara, V.L. Zholobenko, J. Catal. 206 (2002) 230.
75 C.M. Lok, Stud. Surf. Sci. Catal. 147 (2004) 283.
76. R.L. Espinoza, J.L. Visagie, P.J. van Berge, F.H. Bolder, US Patent (1998) 5,733,839.
77. G. Jacobs, T.K. Das, Y. Zhang, J. Li, G. Racoillet, B.H. Davis, Appl. Catal. A: Gen. 233 (2002) 263–281.
78. G. Jacobs, Y. Zhang, T.K. Das, J. Li, P.M. Patterson, B.H. Davis, Deactivation of a Ru promoted Co/Al2O3 catalyst for FT synthesis, in: G.W. Roberts, B.H. Davis (Eds.), Stud. in Surf. Sci. Catal., 139, Elsevier, Amsterdam, The Netherlands, 2001, pp. 415–422
79. Jacobs, G, Patterson, PM, Zhang, YQ, Das, TK, Li, J, Davis, BH (2002) Appl Catal A Gen 233:215
80. Tsakoumis, NE, Rønning, M, Borg, Ø, Rytter, E, Holmen, A (2010) Catal Today 154:162
81. Jacobs, G, Das, TK, Zhang, Y, Li, J, Racoillet, G, Davis, BH (2002) Appl Catal Gen 233:263
82. van Steen, E, Claeys, M, Dry, ME, van de Loosdrecht, J, Viljoen, EL, Visagie, JL (2005) J Phys. Chem. B 109:3575

83. Jacobs, G, Das, TK, Patterson, PM, Li, J, Sanchez, L, Davis, BH (2003) Appl Catal A: Gen 247:335
84. Sirijaruphan, A, Horváth, A, Goodwin Jr, JG, Oukaci, R (2003) Catal Lett 91:89
85. Moodley, DJ, Saib, AM, van de Loosdrecht, J, Welker-Nieuwoudt, CA, Sigwebela, BH, Niemantsverdriet, JW (2011) Catal Today 171:192
86. Das, TK, Jacobs, G, Patterson, PM, Conner, WA, Li, J, Davis, BH (2003) Fuel 82:805
87. Jacobs, G, Ji, Y, Patterson, PM, Das, TK, Luo, M, Davis, BH (2006) AIChE Annual Meeting, San Francisco, CA, Nov. 12-17, 2006
88. Jacobs, G, Patterson, PM, Das, TK, Luo, M, Davis, BH (2004) Appl Catal A: Gen 270:65
89. Storsater, S, Borg, O, Blekkan, E, Holmen, A (2005) J Catal 231:405
90. Saib, AM, Moodley, DJ, Ciobîcă, IM, Hauman, MM, Sigwebela, BH, Weststrate, CJ, Niemantsverdriet, JW, van de Loosdrecht, J (2010) Catal Today 154:271
91. Li, J, Jacobs, G, Das, TK, Zhang, Y-Q, Davis, BH, Appl Catal A: Gen 236:67
92. Li, J, Zhan, X, Zhang, Y, Jacobs, G, Das, TK, Davis, BH (2002) Appl Catal A: Gen 228:203
93. Saib, AM, Borgna, A, van de Loosdrecht, J, van Berge, PJ, Niemantsverdriet, JW (2006) Appl Catal. A: Gen 312:12
94. van de Loosdrecht, J, Balzhinimaev, B, Dalmon, JA, Niemantsverdriet, JW, Tsybulya, SV, Saib, AM, van Berge, PJ, Visagie, JL (2007) Catal Today 123:293
95. Fischer, BC N, Feltes, TE, van Steen, E, Claeys, M, Syngas Convention 2012, Apr. 1-4, 2012, Cape Town, South Africa.
96. Feltes, T, Fischer, N, Claeys, M, 10th Nat Gas Conv Symp, Mar 2-7, 2013, Doha, Qatar.
97. Rønning, M, Tsakoumis, NE, Voronov, A, Johnsen, RE, Norby, P, van Beek, W, Borg, Ø, Rytter, E, Holmen, A (2010) Catal Today 155:289
98. van Steen, E, Claeys, M, Visagie, J, van de Loosdrecht, J, 22nd North American Meeting of The Catalysis Society, Jun. 5-10, 2011, Detroit, MI, USA.
99. Emmett, PH, Brunauer, S, Teller, E (1938) JACS 60:309
100. Barrett, EP, Joyner, LG, Halenda, PP, (1951) JACS 73:373
101. Jacobs, G, Ji, Y, Davis, BH, Cronauer, DC, Kropf, AJ, Marshall, CL (2007) Appl Catal A: Gen 333:177
102. Wang, W-J, Chen, Y-W (1991) Appl Catal. 77:223
103. Guczi, L, Bazin, D, Kovács, I, Borkó, L, Schay, Z, Lynch, J, Parent, P, Lafon, C, Stefler, G, Koppány, Z, Sajó, I, (2002) Top Catal. 20:129
104. Jacobs, G, Chaney, JA, Patterson, PM, Das, TK, Maillot, JC, Davis, BH (2004) J Synchrotron Rad 11:414
105. Zayat, M., Levy, D., Chem Mat (2000) 12:2763
106. Bazin, D, Kovács, I, Guczi, L, Parent, P, Laffon, C, de Groot, F, Ducreux, O, Lynch, J (2000) J Catal. 189:456
107. Hilmen, AM, Schanke, D, Hanssen, KF, Holmen, A (1999) Appl Catal A: Gen 186:169
108. van Berge, PJ, van de Loosdrecht, J, Barradas, S, van der Kraan, AM (2000) Catal. Today 58:321